



National Library
of Canada

Acquisitions and
Bibliographic Services Branch

395 Wellington Street
Ottawa, Ontario
K1A 0N4

Bibliothèque nationale
du Canada

Direction des acquisitions et
des services bibliographiques

395, rue Wellington
Ottawa (Ontario)
K1A 0N4

Your file *Votre référence*

Our file *Notre référence*

NOTICE

The quality of this microform is heavily dependent upon the quality of the original thesis submitted for microfilming. Every effort has been made to ensure the highest quality of reproduction possible.

If pages are missing, contact the university which granted the degree.

Some pages may have indistinct print especially if the original pages were typed with a poor typewriter ribbon or if the university sent us an inferior photocopy.

Reproduction in full or in part of this microform is governed by the Canadian Copyright Act, R.S.C. 1970, c. C-30, and subsequent amendments.

AVIS

La qualité de cette microforme dépend grandement de la qualité de la thèse soumise au microfilmage. Nous avons tout fait pour assurer une qualité supérieure de reproduction.

S'il manque des pages, veuillez communiquer avec l'université qui a conféré le grade.

La qualité d'impression de certaines pages peut laisser à désirer, surtout si les pages originales ont été dactylographiées à l'aide d'un ruban usé ou si l'université nous a fait parvenir une photocopie de qualité inférieure.

La reproduction, même partielle, de cette microforme est soumise à la Loi canadienne sur le droit d'auteur, SRC 1970, c. C-30, et ses amendements subséquents.

UNIVERSITY OF ALBERTA

CAPABILITIES AND LIMITATIONS OF CUTANEOUS RECORDINGS OF
GASTRIC ELECTRICAL ACTIVITY

BY

MARTIN PAVLOV MINTCHEV

A thesis submitted to the Faculty of Graduate Studies and Research in partial
fulfillment of the requirements for the degree of Doctor of Philosophy

DEPARTMENT OF ELECTRICAL ENGINEERING
EDMONTON, ALBERTA

Spring 1994



National Library
of Canada

Acquisitions and
Bibliographic Services Branch

395 Wellington Street
Ottawa, Ontario
K1A 0N4

Bibliothèque nationale
du Canada

Direction des acquisitions et
des services bibliographiques

395, rue Wellington
Ottawa (Ontario)
K1A 0N4

Your file *Votre référence*

Our file *Notre référence*

The author has granted an irrevocable non-exclusive licence allowing the National Library of Canada to reproduce, loan, distribute or sell copies of his/her thesis by any means and in any form or format, making this thesis available to interested persons.

L'auteur a accordé une licence irrévocable et non exclusive permettant à la Bibliothèque nationale du Canada de reproduire, prêter, distribuer ou vendre des copies de sa thèse de quelque manière et sous quelque forme que ce soit pour mettre des exemplaires de cette thèse à la disposition des personnes intéressées.

The author retains ownership of the copyright in his/her thesis. Neither the thesis nor substantial extracts from it may be printed or otherwise reproduced without his/her permission.

L'auteur conserve la propriété du droit d'auteur qui protège sa thèse. Ni la thèse ni des extraits substantiels de celle-ci ne doivent être imprimés ou autrement reproduits sans son autorisation.

ISBN 0-612-11301-9

Canada

UNIVERSITY OF ALBERTA

RELEASE FORM

NAME OF THE AUTHOR: Martin Pavlov Mintchev

TITLE OF THESIS: Capabilities and Limitations of Cutaneous Recordings of Gastric
Electrical Activity

DEGREE: Doctor of Philosophy

YEAR THIS DEGREE GRANTED: 1994

Permission is hereby granted to the University of Alberta Library to reproduce single copies of this thesis and to lend or sell such copies for private, scholarly or scientific research purposes only.

The author reserves all other publication rights in association with the copyright in the thesis, and except as hereinbefore provided neither the thesis nor any substantial portion thereof may be printed or otherwise reproduced in any material form whatever without the author's prior written permission.

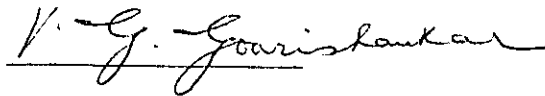
M. P. Mintchev

Sofia 1504, Panaiot Volov Str. No.1, Bulgaria

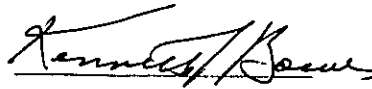
29 03 1994.

UNIVERSITY OF ALBERTA
FACULTY OF GRADUATE STUDIES AND RESEARCH

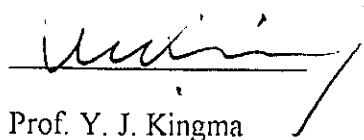
The undersigned certify that they have read, and recommend to the Faculty of Graduate Studies and Research for acceptance, a thesis entitled **Capabilities and Limitations of Cutaneous Recordings of Gastric Electrical Activity** submitted by **Martin Pavlov Mintchev** in partial fulfillment of the requirements for the degree of **Doctor of Philosophy in Electrical Engineering**.



Dr. V. G. Gourishankar



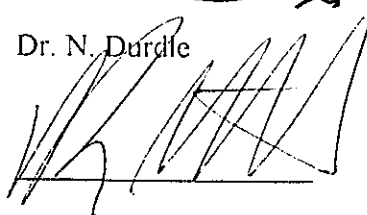
Dr. K. L. Bowes



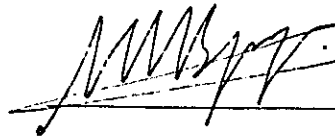
Prof. Y. J. Kingma



Dr. N. Durdle



Dr. R. Rajotte



Dr. N. Spyrou

12. 04. 1994

To my son Paul:

Върви, народе възродени
към светли бъднини върви !
С книжовността - тази сила нова
съдбата си ти поднови.

Химн на Св.св. Кирил и Методиѝ.

Go, revived people,
go towards a bright future !
With the science - this new power
reshape your own destiny.

Hymn of Sts. Cyril and Methodius

ABSTRACT

The goal of this research was to improve clinical usefulness of cutaneous recordings of gastric electrical activity (electrogastrograms, EGG) by exploring their capabilities and limitations using computer modeling and analysis. Previous studies reported abnormalities in electrogastrographic signals in a variety of clinical conditions. However, the diagnostic value of electrogastrography is still in question mainly because only qualitative methods of evaluation were used. The developed methodology utilized computer modeling to gather more information about the nature of gastric electrical signals and suggested amplification, electrode configuration, and quantitative evaluation procedures based on this new knowledge. The evaluation procedures were clinically tested. First, a computer-based model of the electrical field produced by the human stomach was developed. The results from the modeling helped for a better understanding of the internal and cutaneous patterns of gastric electrical activity and the interrelations between cutaneous and internal signals. With the model fast and efficient simulations of hundreds of expensive, time-consuming and some times technically impossible experiments were performed. The new knowledge helped to determine appropriate electrode configurations and to design a specialized electrogastrographic amplifier. Using modern digital signal processing procedures, the accuracy of electrogastrographic signals was reexamined. The frequency of these signals was found to be the only reliable parameter for clinical applications. Gastric electrical frequencies extracted from multichannel electrogastrograms of healthy volunteers were subjected to various methods of evaluation. Two criteria for normality were established based solely on the frequency dynamics during the whole experiment. These two criteria were tested in a clinical study of patients with various gastrointestinal complaints. The groups of patients studied included subjects with partial gastrectomies, postoperative patients, patients with implanted serosal electrodes, etc. With the proposed quantitative method of evaluation, electrogastrography was used

as a clinical test. The results from this test were related to the results from the internal recordings of gastric electrical activity (for the patients with implanted serosal electrodes) or to the previously established clinical condition of the patient. It has been clearly demonstrated that electrogastrograms, when evaluated objectively, can provide a valuable clinical information. One of the major advantages of the proposed method is that its reliability will grow with the technological development.

ACKNOWLEDGEMENT

The author would like to express his gratitude to the members of his supervisory committee: Prof. Y.J. Kingma, Dr. K.L. Bowes and Dr. V.G. Gourishankar for their guidance and help.

The study was supported in part by a grant from the Medical Research Council of Canada.

LIST OF SYMBOLS, NOMENCLATURE AND ABBREVIATIONS

AC - alternating current
BMI - body mass index
CMRR - common-mode rejection ratio
cpm - cycles per minute
DAC - digital to analog converter
DC - direct current
DFT - discrete Fourier transform
DHT - discrete Hartley transform
DSP - digital signal processing
dB/oct - decibels per octave
EGG - electrogastrography
EKG - electrocardiography
FET - field emission transistor
FIR - finite impulse response
FHT - fast Hartley transform
FFT - fast Fourier transform
FT - force transducers
GEA - gastric electrical activity
ILP - intraluminal pressure
LDB - long distance bipolar
MMC - migrating myoelectric complex
pdf - probability density function
SDB - short distance bipolar

TABLE OF CONTENTS

INTRODUCTION	1
CHAPTER 1. Electrical phenomena in the human stomach.	4
1.1. The anatomy of the stomach	5
1.2. Gastric electrical signals and their relation to contractile activity of the stomach	8
1.3. Gastric electrical activity recorded "in vivo" with implanted electrodes	11
1.4. Electrogastrography	14
CHAPTER 2. Conoidal dipole model of gastric electrical activity	17
2.1. Main concepts in modeling of gastric electrical activity	18
2.2. Mathematical model	22
2.2.1. Main equation of the model	22
2.2.2. Area of the annular band	23
2.2.3. Dipole density	27
2.2.4. Distance to the point of interest	27
2.3. Results	30
2.3.1. Testing the model	31
2.3.2. Study of electrode distance in bipolar recordings	31
2.3.3. Study of electrode surface area	34
2.3.4. Effect of increased distance between an electrode and the field source	35
2.4. Discussion	37
CHAPTER 3. Amplification of gastric electrical signals	39
3.1. Amplifier requirements	40
3.1.1. Flexible frequency range	40
3.1.2. Wide range of gains	41
3.1.3. Differential input	41
3.1.4. High input impedance	43
3.1.5. Galvanic isolation	43
3.1.6. High common-mode rejection ratio (CMRR)	44
3.1.7. Low noise	45
3.1.8. Good offset compensation	47
3.2. The input stage of an isolated EGG amplifier	47
3.3. Programmable gain and offset compensation	49
3.4. Block and circuit diagrams of the isolated EGG amplifier	51
3.5. Performance characteristics of the GEA amplifier	52

CHAPTER 4. Methods for analysis of gastric electrical activity	55
4.1. Information extracted from gastric electrical activity	56
4.1.1. Migrating myoelectrical complex and contractions	56
4.1.2. Electrical coupling between different parts of the stomach	56
4.1.3. Gastric electrical frequency	57
4.2. Methods to assess the migrating myoelectrical complex and contractions	57
4.2.1. Building the MMC from serosal SDB electrodes	57
4.2.2. Quantitative assessment of EGG amplitudes	60
4.2.3. Other methods to assess contractions and MMC	60
4.3. Methods to assess electrical coupling	61
4.3.1. Visual analysis of the time shifts between different channels	61
4.3.2. Analysis of the time shifts using crosscorrelation	62
4.3.3. Analysis of the waveform of EGG	64
4.4. Methods to assess gastric electrical frequency.....	64
4.4.1. Quantitative visual analysis	64
4.4.2. Frequency analysis and time-frequency plots	65
4.4.3. Statistical evaluation of time-frequency plots	78
4.5. Digital filtering of GEA	80
4.5.1. Frequency-sampling filters	80
4.5.2. Adaptive filters	80
 CHAPTER 5. Accuracy of EGG	 84
5.1. Introduction	85
5.1.1. Frequency	85
5.1.2. Amplitude	86
5.1.3. Phase lag	86
5.1.4. Wave form	86
5.2. Methods	87
5.2.1. Subjects	87
5.2.2. Frequency	89
5.2.3. Amplitude	89
5.2.4. Phase lag	90
5.2.5. Wave form	91
5.3. Results	92
5.3.1. Frequency	92
5.3.2. Amplitude	95
5.3.3. Phase lag	99
5.3.4. Wave form	100
5.4. Discussion	101
 CHAPTER 6. Derivation of an objective method for clinical study of EGG	 104
6.1. Introduction	105

6.2. Methods	105
6.3. Results	107
6.3.1. Statistical evaluation of time-frequency plots	107
6.3.2. Impact of the overlap	109
6.3.3. Criterion for stability	111
6.3.4. Criterion for coupling	112
6.4. Discussion	113
CHAPTER 7. Clinical EGG study	114
7.1. Introduction	115
7.2. Possible patterns of gastric electrical abnormalities as seen from EGG	115
7.2. Subjects and settings	117
7.3. Results	118
7.3.1. Comparison between internal and cutaneous recordings in the two postoperative patients	118
7.3.2. Patients with partial gastrectomy	124
7.3.3. Ileus patients	124
7.3.4. Patients with idiopathic constipation	125
7.3.5. Patients with other gastrointestinal complaints	125
7.4. Study of the abnormal EGG patterns	126
7.4.1. Abnormal electrical activity - pattern 2	126
7.4.2. Abnormal electrical activity - pattern 4	130
7.4.3. Abnormal electrical activity - pattern 6	132
7.4.4. Abnormal electrical activity - other patterns	135
7.5. Discussion	135
REFERENCES	137
APPENDIX	147

LIST OF FIGURES

- Figure 1.1.** *Macroscopic anatomy of the stomach*.....5
- Figure 1.2.** *Structure of Gastric Muscularis: A -- the longitudinal layer (the area where the longitudinal fibers split is marked with a black circle); B - the circular layer; C - the oblique layer*.....6
- Figure 1.3.** *Cross section of gastric wall*.....7
- Figure 1.4.** *Electrical and contractile activity of gastric smooth muscle cell*.....9
- Figure 1.5.** *Intracellular (A, B) and extracellular (C, D) electrical activity (ECA and ERA). The distance between the cells A and B is approximately 2.5 mm in distal direction. The biphasic signal E is the difference between C and D*..... 13
- Figure 1.6.** *Long distance bipolar (LDB) signals are obtained when the distance between the extracellular bipolar electrodes is greater than 2 cm*.....14
- Figure 1.7.** *Typical electrogastrographic (EGG) signal recorded bipolarly using a pair of standard electrocardiographic (EKG) electrodes 4 cm apart. Only ECA can definitely be recognized*..... 16
- Figure 2.1.** *Human stomach represented as a truncated conoid in the spherical system of coordinates O, R . A sample band of depolarized cells is shown along with a magnified section depicting the perpendicularly-oriented to conoidal axis dipoles (below right)*....21

Figure 2.2. *Stereometry of the truncated conoid used for derivation of the equations of the model.....29*

Figure 2.3. *Simulated short distance (2.5 mm) bipolar serosal recordings in the area of the greater (Channel 1) and lesser (Channel 2) curvatures in the distal corpus, and respective recordings from an actual experiment performed on a patient (Channels 3 and 4).....32*

Figure 2.4. *Simulated short distance bipolar serosal recordings in the area of the greater (Channel 1) and lesser (Channel 2) curvatures in the antrum, and respective recordings from an actual experiment performed on a patient (Channels 3 and 4).....33*

Figure 2.5. *Effect of gradual increment of the distance between serosal bipolar electrodes in simulated experiments. The initial inter electrode distance of 0.5 cm (Channel 1) was successively increased with 0.5 cm. In all recordings positive electrode was placed in the proximal antrum, while negative electrode was moved towards terminal antrum.....34*

Figure 2.6. *Effect of gradual increment of electrode surface on GEA wave shape in simulated experiments (A). Electrode diameter was increased from 2.5 mm (Channel 1) to 6.5 mm (Channel 2), and to 1.0 cm (Channel 3). Distance between the electrode centers was kept 4 cm. The signal in Channel 3 resembled the wave form of cutaneous EGG (B).....36*

Figure 3.1. *Simplified diagram of the input stage of the amplifier.....48*

Figure 3.2. *Digitally controlled four-pole low-pass filter.....49*

Figure 3.3. *Cascaded programmable amplifiers with an automatic offset compensation circuit.....50*

Figure 3.4. *Block diagram of an isolated GEA amplifier. The shadow area is the isolated section.....52*

Figure 3.5. *Bode plots of the GEA preamplifier adjusted for EGG. The shadow area is the pass band. Note that the overall phase is inverted by 180 degrees.....54*

Figure 4.1. *SDB signal divided into three zones: A - the zone of ECA; B - the quiescent zones; C - the zone of spikes.....58*

Figure 4.2. *Block-diagram of an algorithm for counting ECA and ECA with spikes from SDB recordings (A), and a typical canine MMC obtained using this algorithm (B). All four phases of the MMC are clearly seen.....59*

Figure 4.3. *Simulated electrically coupled SDB signals recorded from proximal (A) and distal (B) antrum. The lines connecting the peaks of ECA remained parallel even when a minor frequency irregularity occurred between the third and the fourth wave.....61*

Figure 4.4. *Block-diagram of an algorithm to calculate gradient plots.....65*

Figure 4.5. *One-hour three dimensional plot of a sine wave signal which changes its frequency from 0.05 Hz to 0.06 Hz after the first half hour of recording. The frequency window is 0.01-0.16 Hz.....75*

Figure 4.6. Time-frequency plot extracted from the three dimensional plot shown on Fig. 4.5. with frequency scale in cycles per minute (cpm). The moment of the change in frequency is clearly seen..... 77

Figure 4.7. Block diagram of an adaptive filter. Recorded signal d is considered a superposition of the primary signal s and the noise n_0 , which are not correlated. The reference signal n_1 is a noise, correlated with n_0 . The objective of the filtering process is to extract the primary signal s81

Figure 4.8. A modified adaptive filter for EGG. The noise n_1 is obtained from the recorded signal d using a band reject filter.....83

Figure 5.1. Gastric electrical signals obtained with SDB electrodes (top), LDB electrodes (center), and cutaneous electrodes (bottom) during the first postoperative day of the patient. Rhythm irregularities are clearly seen..... 93

Figure 5.2. Human gastric electrical signals obtained with SDB electrodes (left, A), LDB electrodes (left, B) and cutaneous electrodes (left, C) and their respective power spectra (right, A-C).....94

Figure 5.3. Two-hour (1 hour fasting and 1 hour postprandial) three-dimensional plots of LDB signal (A) and cutaneous EGG (B) of the patient. Power spectra are calculated from successive 4.27-minute intervals without overlapping. Postprandial increment in the frequency is seen in both channels..... 94

Figure 5.4. Relationship between gastric contractions and changes in EGG amplitude in normal volunteers: (A) incidence of increased EGG amplitudes during gastric contractions and (B) incidence of gastric contractions during increased EGG amplitudes.....95

Figure 5.5. Incidence of gastric contractions when (Left) SDB channels displayed spikes; (Center) Increased signal amplitude was observed in LDB channels; and (Right) Increased signal amplitude was observed in EGG recordings.....96

Figure 5.6. Effect of gastric distention on incidence of increased EGG signal amplitudes.....96

Figure 5.7. Signals recorded from nondistended (top) and distended (bottom) canine stomach with force transducers (1, 2), SDB electrodes (3, 4), LDB electrodes (5, 6) and cutaneous electrodes (7, 8). Gastric distention after blocking the mechanical activity with atropine and glucagon led to significant increment in the cutaneous but not internal recordings.....97

Figure 5.8. Mechanical activity of the stomach (top) and EGG (bottom) before any blocking of contractile activity (a) and after that (b). The moment of distention is marked with an arrow. A significant increase of EGG amplitude is clearly seen.....98

Figure 5.9. Time shifts between pairs of SDB (top), LDB (middle) and EGG (bottom) channels. SDB and LDB pairs were implanted in proximal and distal antrum. EGG electrodes were overlying the LDB ones.....99

Figure 5.10. *A typical gradient plot of multichannel EGG recorded from a volunteer. Only a slight predominance of the descending arms was noted..... 101*

Figure 6.1. *Typical time-frequency plots obtained for each EGG channel recorded from a healthy volunteer..... 108*

Figure 6.2. *Probability density functions of the points that built up the time-frequency plots of Fig. 6.1. Maxima coincided at 3.047 cpm, but some other frequencies were also present..... 109*

Figure 6.3. *Time-frequency plot obtained with 75% overlap from the same set of EGG data used to obtain the time-frequency plots shown on Fig. 6.1..... 110*

Figure 6.4. *Probability density functions of the time-frequency plots obtained with 75% overlap were narrower than these shown on Fig. 6.2. Coincidence of their maxima was more evident..... 111*

Figure 7.1. *Four-minute combined recording of SDB (1, 2 and 3), LDB (4 and 5) and EGG (6-8) channels from the female patient. Regular gastric frequency and electrical coupling were clearly seen..... 119*

Figure 7.2. *Typical time-frequency plots recorded from the female patient..... 120*

Figure 7.3. *Probability density functions obtained from the time-frequency plot on Fig.7.2. All maxima coincided in the normal frequency range..... 121*

Figure 7.4. *SDB channels recorded from the male patient showed consistent frequency irregularities as well as electrical uncoupling..... 122*

Figure 7.5. *Typical time-frequency plots recorded from the male patient..... 122*

Figure 7.6. *Probability density functions obtained from the time-frequency plot on Fig. 7.5. The maxima did not coincide..... 123*

Figure 7.7. *Unstable time-frequency plots recorded from a patient with abnormal gastric electrical activity (Pattern 2)..... 128*

Figure 7.8. *Probability density functions calculated from the time-frequency plots of different EGG channels. The maxima did not coincide in the normal frequency range..... 129*

Figure 7.9. *Time-frequency plots recorded from patient with abnormal gastric electrical activity (Pattern 4)..... 131*

Figure 7.10. *Probability density functions calculated from the time-frequency plot on Fig. 7.9. Note that the maxima coincided, but outside the normal frequency range..... 132*

Figure 7.11. *Time-frequency plots recorded from patient with abnormal gastric electrical activity (Pattern 6)..... 133*

Figure 7.12. *Probability density functions calculated from the time-frequency plots on Fig. 7.11. The maxima did not coincide well..... 134*

LIST OF TABLES

Table 2.1. <i>Relationship between stomach parameters measured from average human and mathematically calculated values using model approximations.....</i>	<i>25</i>
Table 5.1. <i>Recognition of changes in gastric electrical frequency by different recording methods.....</i>	<i>92</i>
Table 5.2. <i>Quantitative study of GEA waveform.....</i>	<i>100</i>
Table 6.1. <i>Electrode combinations used for different EGG channels. Electrode 1 was the most proximal, Electrode 5 - the most distal.....</i>	<i>106</i>
Table 6.2. <i>Basic averages obtained from the time-frequency plot on Fig.6.1. Only one EGG channel showed standard deviation higher then 0.450 cpm.....</i>	<i>108</i>
Table 6.3. <i>Basic averages of the time-frequency plots shown on Fig. 6.3. Channel 5 showed excellent stability.....</i>	<i>110</i>
Table 7.1. <i>Number of patients with identical or similar complaints.....</i>	<i>118</i>
Table 7.2. <i>Basic averages of the time-frequency plots from Fig. 7.2. Only one channel was out of the range of stability.....</i>	<i>123</i>
Table 7.3. <i>Basic averages of the time-frequency plot on Fig.7.5. Standard deviations of all EGG channels were out of the normal range.....</i>	<i>127</i>

Table 7.4. *Quantitative comparison between abnormal (Pattern 2) and total number of patients with identical or similar complaints.....127*

Table 7.5. *Basic averages obtained from a patient with abnormal gastric electrical activity (Pattern 2). Only 2 EGG channels were within the normal frequency range..... 129*

Table 7.6. *Quantitative comparison between abnormal (Pattern 4) and total number of patients with identical or similar complaints..... 130*

Table 7.7. *Basic averages obtained from a patient with abnormal gastric electrical activity (Pattern 4)..... 131*

Table 7.8. *Quantitative comparison between abnormal (Pattern 6) and total number of patients with identical or similar complaints..... 133*

Table 7.9. *Basic averages obtained from a patient with abnormal gastric electrical activity (Pattern 6). More than 3 EGG channels exhibited stability, but outside the normal frequency range..... 134*

INTRODUCTION

The electrical activity of the stomach, its interrelations with gastric motor function, and its role in gastric motility disorders has been the research focus of many scientists in this century. The works of Alvarez (1, 2, 3), Alvarez and Mahoney (4, 5) and others (6, 7, 8) in the early 1920s paved the way for decades of research in this area.

While a great deal of attention has been directed at understanding the electrophysiological processes in the stomach *in vitro* (outside the living organism), significant efforts have also been devoted to studying these phenomena *in vivo* (within the living organism).

Gastric electrical abnormalities recorded *in vivo* with electrodes implanted on the stomach wall can be related to certain gastric motility disorders (9, 10, 11, 12). However, such techniques are rarely used because they are invasive and uncomfortable (10, 11, 12).

Cutaneous recordings of gastric electrical activity (GEA), known as electrogastrography (EGG), would seem to be an avenue for the non-invasive assessment of gastric motility. Although Alvarez recorded electrogastrographic signals in 1921 (2), only recently has the technique shown practical promise. EGG has been introduced into several gastrointestinal motility laboratories in North America, Europe, Japan and Australia. Unfortunately, the diagnostic value of this method is still in question and much new knowledge is required before clinical disorders can be related to EGG signals with any certainty (10).

The objective of this work is to be able to facilitate utilization of the EGG as an objective non-invasive diagnostic tool to detect gastric motility disorders.

The first important step towards realizing the above objective is a better understanding of the electrical field produced by the human stomach and the transformation of the GEA from an intracellular signal into the EGG.

This new knowledge would help to determine the requirements for suitable electrode configurations and amplifiers which would ensure reliable and stable recordings of the EGG.

Once the signal is acquired and stored the focus could turn to signal processing procedures and visualization techniques that would extract any valuable diagnostic information which EGG signals contain.

Finally, studies on animals, normal subjects and on patients should be performed to validate the methodology and to define the patterns of normal and abnormal EGG.

CHAPTER ONE

ELECTRICAL PHENOMENA IN THE HUMAN STOMACH.

1.1. THE ANATOMY OF THE STOMACH.

The main function of the stomach is to process and transport food. After feeding, the contractile activity of the stomach helps to mix, grind and eventually evacuate small portions of chyme into the small bowel (12), while the rest of the chyme is mixed and ground.

Anatomically, the stomach can be divided into three major regions: fundus (the most proximal), corpus and antrum (Fig.1.1). Histologically, the fundus and corpus are hardly separable. In the antral area, the density of the smooth muscle cells increases (11).

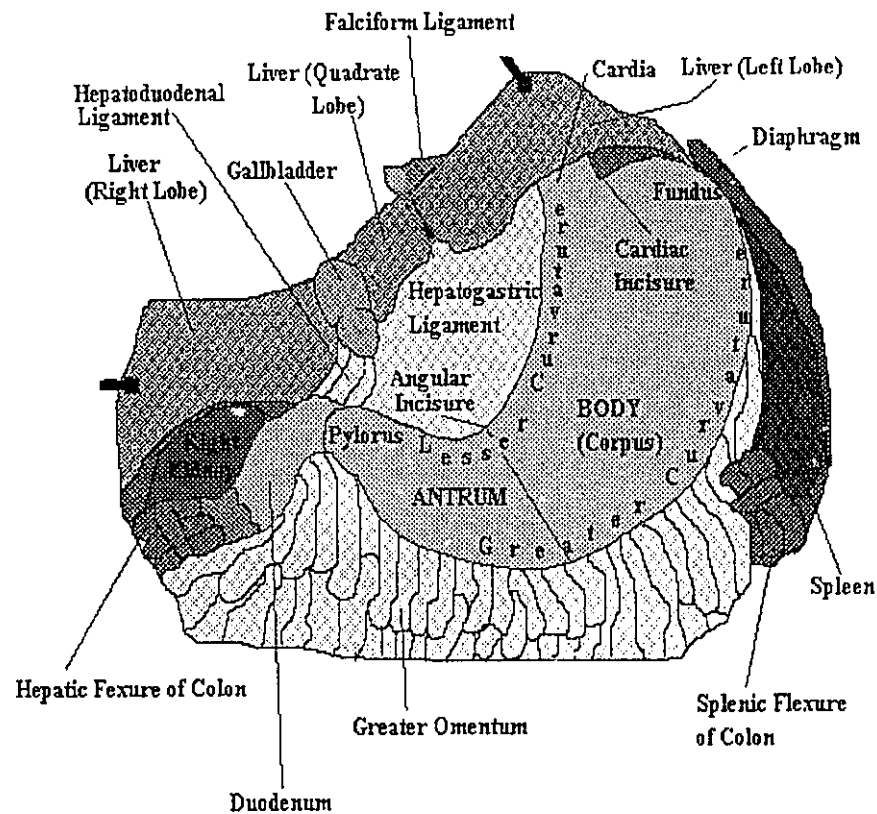


Figure 1.1. Macroscopic anatomy of the stomach.

The gastric wall, like the wall of most other parts of the digestive canal, consists of three layers: the mucosal (the innermost), the muscularis and the serosal (the outermost). The mucosal layer itself can be divided into three layers: the mucosa (the epithelial lining of the gastric cavity), the muscularis mucosae (low density smooth muscle cells) and the submucosal layer (consisting of connective tissue interlaced with plexi of the enteric nervous system). The second gastric layer, the muscularis, can also be divided into three layers: the longitudinal (the most superficial), the circular and the oblique (Fig.1.2). The longitudinal layer of the muscularis can be separated into two different categories: a longitudinal layer that is common with the esophagus and ends in the corpus, and a longitudinal layer that originates in the corpus and spreads into the duodenum.

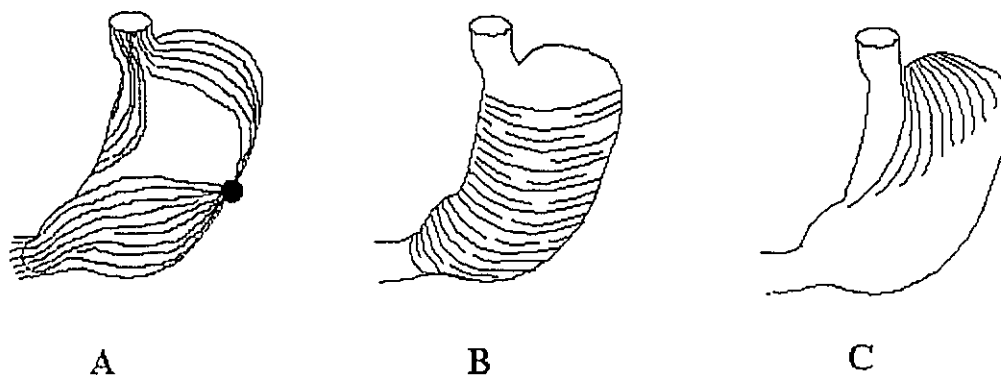


Figure 1.2. *Structure of Gastric Muscularis: A -- the longitudinal layer (the area where the longitudinal fibers split is marked with a black circle); B - the circular layer; C - the oblique layer.*

The area in the corpus around the greater curvature, where the split of the longitudinal layers takes place, is considered to be anatomically correlated with the origin of gastric electrical activity (11). The circular layer of the muscularis is continuous with the circular layer of the esophagus, but is absent in the fundus (12). The thickness of the circular layer increases in the antrum and especially in the pyloric sphincter (9). It does not continue into the duodenum. The oblique layer of the muscularis is clearly seen in the fundus and near the lesser curvature of the corpus, but the oblique fibers disappear distally (towards the antrum). The outermost main layer is the serosa (Fig. 1.3).

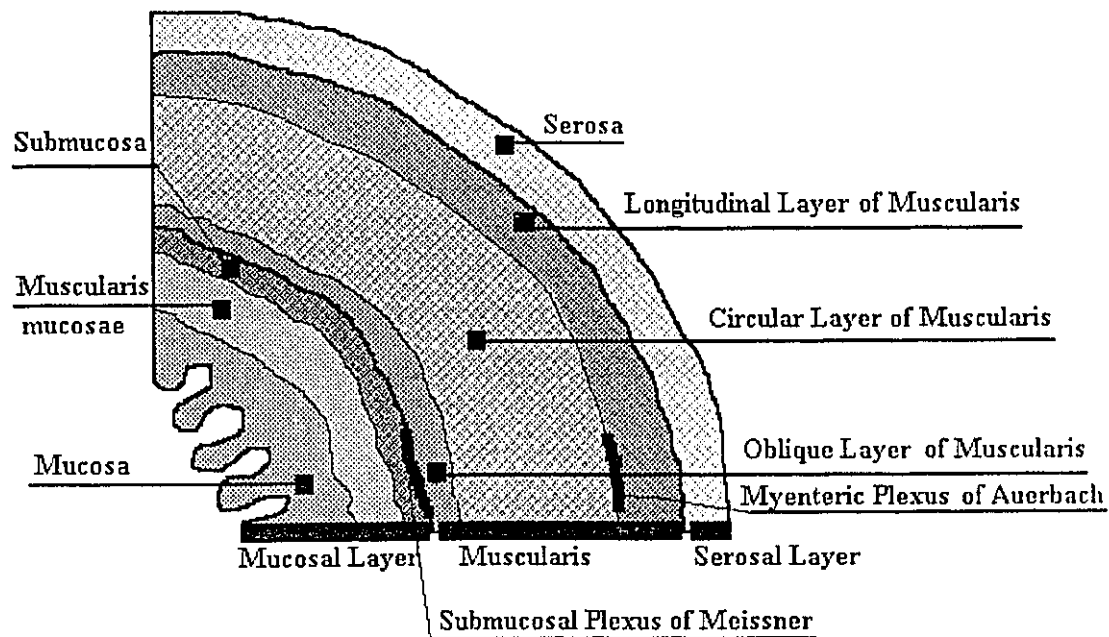


Figure 1.3. Cross section of gastric wall.

Nerve plexi provide the interface between the mucosa and the muscularis, as well as between the longitudinal and circular layers of the muscularis (9, 12).

1.2. GASTRIC ELECTRICAL SIGNALS RECORDED "IN VITRO" AND THEIR RELATION TO CONTRACTILE ACTIVITY OF THE STOMACH.

Intracellular electrical and contractile activity of smooth muscle fibers has been studied by many investigators (13, 14, 15). There is a general agreement regarding the relationship between these two phenomena.

Many different terms have been used to describe gastric electrical activity: "slow potential", "slow wave", "initial potential", "control potential", "spiking", etc. In 1975 Sarna et al. (16) introduced a new terminology, that was adopted by the majority of the research groups working in the field. This terminology will be strictly followed in the present study.

Gastric electrical activity recorded in vitro is divided in two major types: Electrical Control Activity (ECA) and Electrical Response Activity (ERA).

It has been shown (17, 18) that intracellular electrical depolarization due to spontaneous ionic exchange through the membrane precedes contraction of the gastric smooth muscle fiber. However, not all depolarizations are followed by contractile activity (18). This is an important difference between cardiac muscle fibers and gastric smooth muscle cells. The two different types of electrical activity, ECA and ERA, are clearly recognized in the cells of the distal two-thirds of the stomach (Fig. 1.4.).

Many studies have attempted to determine histologically the origin of GEA in the stomach (19, 20, 21). It is definitely known, that smooth muscle cells of the fundus do not have the electrical and contractile behavior described above. Weber and Kohatsu (22) and Kelly and Code (23) pointed out as a possible origin of gastric electrical activity an area in the corpus along the greater curvature where the longitudinal muscle fibers that continue into the duodenum originate. This concept is rejected by many who feel that the longitudinal layer in the stomach is integral with no area of split in the longitudinal fibers (24).

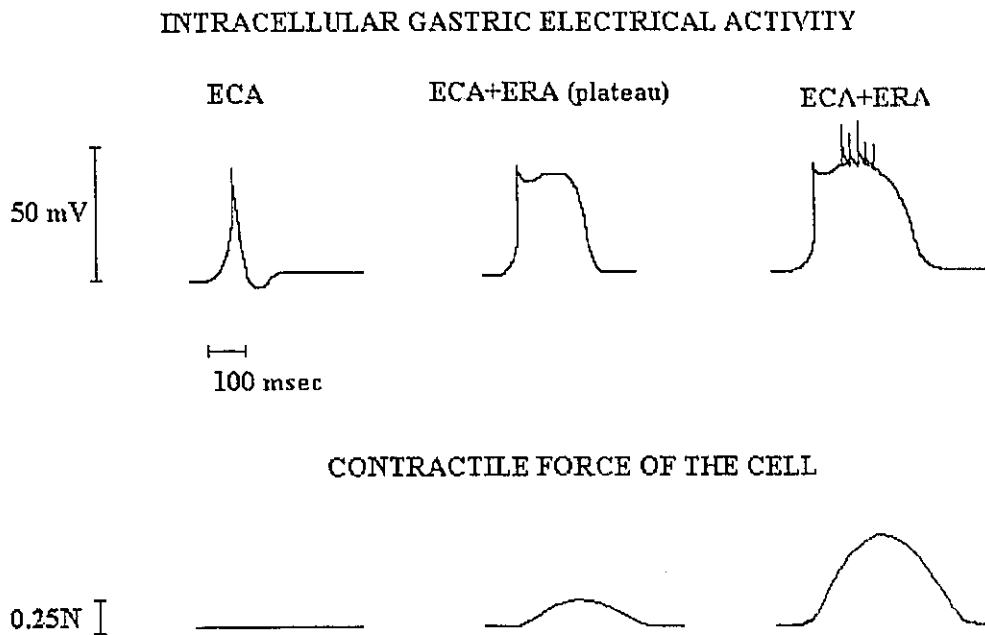


Figure 1.4. *Electrical and contractile activity of gastric smooth muscle cell.*

The mechanism of propagation of gastric electrical activity from one cell to another is still unknown. There is no doubt that regardless of the exact mechanism of propagation, there is a full electrical coupling of different parts of the normal stomach, in other words there are well defined temporal and spatial rules that regulate the propagation of gastric electrical activity. The nature of this regulation is not entirely known (25).

ECA is considered to be the initial rapid depolarization of the cell and is a necessary, but not a sufficient condition for contraction to occur. It is periodic by nature, with a period of about 20 seconds (or frequency of 3 cycles per minute, cpm). Only the appearance of the plateau of the ERA, the second type of activity, and eventually the second component of the ERA, the spikes that are superimposed over the plateau of the

ERA, indicate that contraction will follow. It is clear, that ERA itself is separated into two components: plateau and spikes. These components are not independent. Spike bursts cannot exist without the plateau, while the opposite can happen, the plateau of ERA might follow ECA without any spikes. The force of contraction that will follow in that case, however, will not be higher than 0.25 N. The presence of spikes indicates that a contraction with greater strength is expected. ECA is always present in the stomach, while ERA with its component(s) manifests itself occasionally (12, 16, 17).

Most authors (20, 21, 24) relate the occurrence of ERA to the injection of Ca^{2+} ions into the smooth muscle cell. They point out that the plateau of ERA is possibly related to the opening of the so called "slow Calcium channels" of the cell membrane, while the spikes are produced after the injection of Ca^{2+} ions through the "fast Calcium channels". There are some suggestions also that similarly to the ECA, the first component of ERA, the plateau, is always present in the stomach, but it has to reach a certain threshold level for contraction to occur (14, 15).

During the gastric fasting state, Code and Marlett (26) pointed out that GEA can display the features of the so called Migrating Myoelectrical Complex (MMC), a phenomenon initially described by Szurszewski in the small bowel (27). The MMC can be separated into four phases: quiescent phase 1, when only ECA is present; transitional phase 2, when cycles of ECA without any ERA are mixed with cycles in which both ECA and ERA are present; phase 3, during which ECA is always followed by ERA with its two components (in other words, spike activity is always superimposed on the plateau of ERA); and transitional phase 4, very similar to phase 2. The total duration of all four phases is about 1.5 - 2 hours, the active phase 3 usually lasts 10 - 18 minutes. After feeding, the pattern of MMC changes probably because the stomach becomes active until it empties (28). The fasting pattern of MMC returns 6 - 8 hours after feeding. Although the strength of contractile activity varies postprandially, quiescent periods are not observed in normal subjects (28).

In all in vitro measurements of GEA, special methods of recording with microelectrodes are used. These experiments are quite complicated and are performed under special laboratory conditions (11, 12, 14, 15).

1.3. GASTRIC ELECTRICAL ACTIVITY RECORDED "IN VIVO" WITH IMPLANTED ELECTRODES.

The relationship between extracellular and intracellular recordings of gastric electrical activity is a complex and controversial issue (29, 30, 38). The approach followed in this study is to consider one isolated cell as a monopole, i.e. a single (point) source or sink of current within a conducting medium. The cell culture from which an extracellular recording is considered a current dipole (combination of a current source and a current sink). The potential V_m produced by the monopole can be given with (38):

$$V_m = I_0 / (4\pi \cdot \sigma \cdot r) = i / (4\pi \cdot \sigma) \quad [1.1]$$

where I_0 is the current of the source, σ is the conductivity of the medium through which the current is flowing, $i = I_0/r$, and r is the distance between the monopole and the measuring point. The potential V produced by a current dipole (combination of a current source and a current sink, for example current flows out of the membrane of a cell at one point, and back in at another one nearby) in a conductive medium is expressed with:

$$V = [I_0 / (4\pi\sigma)] \cdot \left[\frac{\partial}{\partial d} (1/r) \right] \cdot d = [d \cdot \left(\frac{\partial i}{\partial d} \right)] / (4\pi \cdot \sigma) \quad [1.2]$$

where d is the displacement of the current source caused by the dynamics of the depolarization wave. This equation indicates that V can be considered differentiated with respect to V_m . The problem is that this differentiation is not versus time, but versus d ,

which is the displacement of the current source. Ultimately, d is a function of time, but this does not mean that the extracellular signal can be considered a true time derivative of the intracellular one. In fact, it can be concluded that the waveform of the extracellular signals differ from the one of the intracellular, which is related in part to the fact that the depolarization wave in the living tissues is not static. Equation [1.1] indicates that the extracellular potential would repeat the waveshape of the intracellular one only if the cell is considered isolated from the outside world. This assumption is entirely hypothetical and has only a theoretical rather than a practical value. In the real situation, i.e. when a group of cells are considered a current dipole situated in a conductive medium, the extracellular potential would have, in general, different waveshape than the intracellular one (see equation [1.2]). Some authors claim that extracellular waveshape resembles the waveshape of the first derivative of the intracellular signals (29, 30). Smout (12) and other European authors (11, 14) recorded monopolarly the extracellular voltage with implanted serosal electrodes and speculated that it is also inverted with respect to the intracellular potential. It should be mentioned, however, that it is quite difficult to determine the extracellular waveform experimentally mainly because of the so called "injury potential" (29). This potential is a result of damaging the cells by the extracellular electrode. The "injury" can make the transmembrane resting potential in the affected area close to zero (this potential is normally negative), and permeability to ions may become very high.

The intracellular electrode configuration is monopolar, while the extracellular signals are recorded using both monopolar or bipolar recording techniques. Additional change in the waveform can be expected if the recording technique (monopolar or bipolar) is altered. When recording bipolarly with the extracellular serosal electrodes (usually implanted stainless steel or silver needles) about 2.5 mm apart along the longitudinal axis, the recorded signal represents the difference between the two extracellular signals. If the waveform of the extracellular signals was found to be close to the waveform of the first

derivative of a typical intracellular signal, the waveform of these bipolar signals can be estimated with the second derivative of the intracellular signal.

The pattern of this signal is shown on Fig. 1.5. In this study the abbreviation SDB (short distance bipolar) will be used for this type of recording.

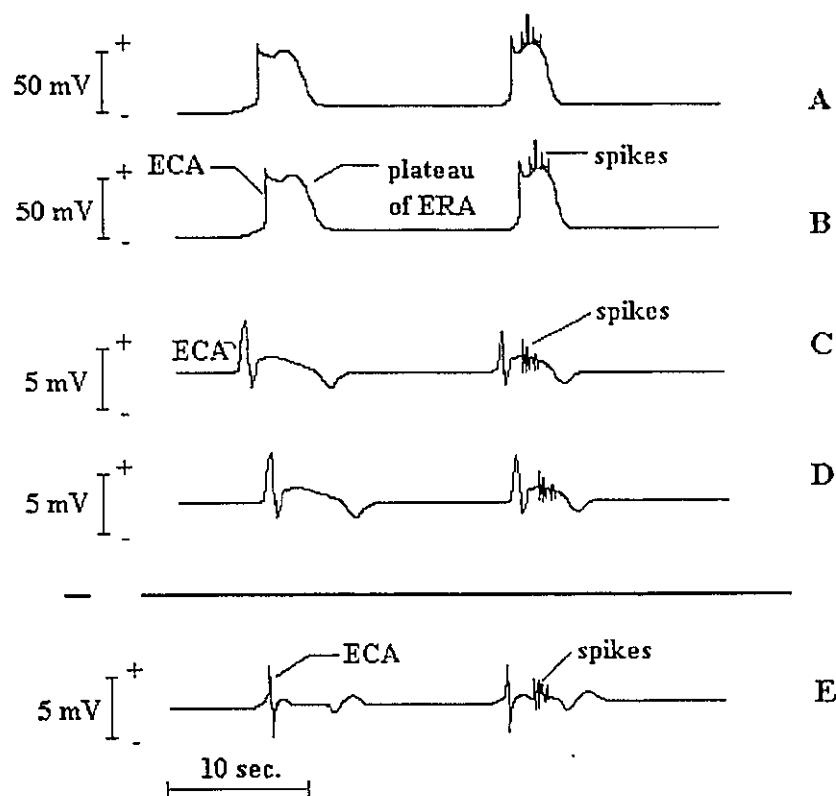


Figure 1.5. Intracellular (A, B) and extracellular (C, D) electrical activity (ECA and ERA). The distance between the cells A and B is approximately 2.5 mm in distal direction. The biphasic signal E is the difference between C and D.

An increase of the distance between the two extracellular electrodes would change the waveform of the recorded signal dramatically (Fig. 1.6). The term LDB (long distance bipolar) will be used for these recordings.

The relationship between the waveform of the signal and the electrode configuration will be discussed in more detail when modeling of the electrical field produced by the stomach is described.

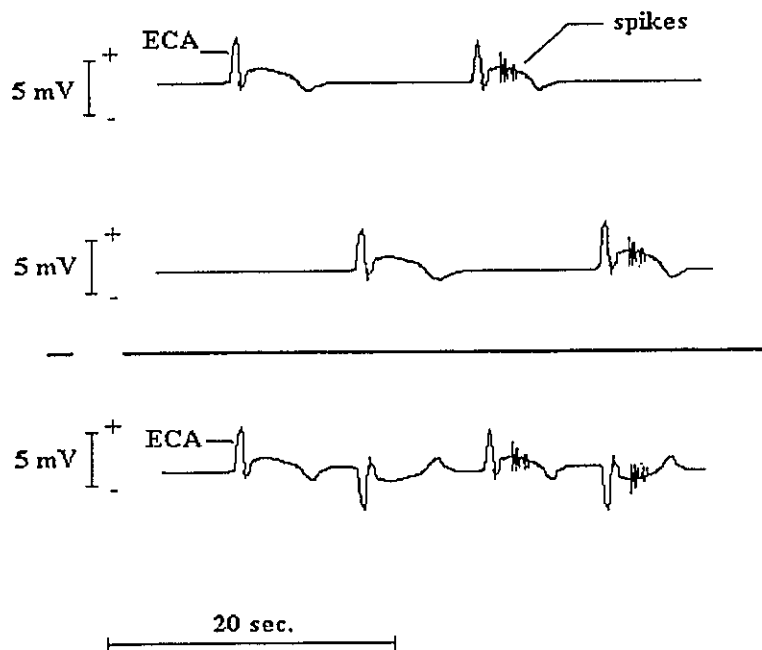


Figure 1.6. Long distance bipolar (LDB) signal is obtained when the distance between the extracellular bipolar electrodes is greater than 2 cm. Note that the signal has two waves in the 20-second interval.

In SDB recordings, the plateau of ERA is hardly recognizable, but spikes are well grouped following the successive biphasic ECAs. On the contrary, in LDB recordings one can easily miss spikes, but the plateau level is recognized better. Of course the ideal technique would be to record monopolarly a signal that is close to the first derivative of the intracellular gastric electrical signal. Unfortunately, many noise components, that would be rejected as common mode signals with the bipolar recording technique, would now pass the input stage of the amplification system and the signal-to-noise ratio would

become worse. That is why bipolar recordings are more popular when studying extracellular GEA.

1.4. ELECTROGASTROGRAPHY.

In some early studies of gastric electrical activity, the term "electrogastrography" (EGG) was used for any extracellular recordings performed in vivo (3, 7, 8). This term is, however, now used almost exclusively for cutaneous recordings of gastric electrical activity obtained with abdominal electrodes (9, 10, 11, 17).

Depending on the electrode configuration bipolar EGG could be SDB or LDB. Standard electrocardiographic (EKG) electrodes arranged in different configurations on the abdomen are routinely used for bipolar EGG recordings in many laboratories. The radius of a standard disposable EKG electrode is about 0.5 cm. When the centers of the two cutaneous electrodes from one bipolar pair are closer than 1.5 cm no signal can be recorded even with the most recent amplification techniques, probably due to a combination of limited resolution and many external noise factors. This implies that these recordings are actually LDB (Fig. 1.7, 31).

Many different configurations of cutaneous electrodes have been suggested (9, 10, 11, 12, 17). Mirrizzi et al. (31, 32, 33) modeled the electrical field produced by the human stomach and pointed out that the optimal position of the EGG electrodes is along the projection of the stomach axis on the abdomen. This concept was also proven experimentally and has been utilized by most research centers in the world (10, 17).

If electrogastrograms are actually cutaneous LDB recordings of GEA, the first and most important restriction on the EGG recordings is imposed: cutaneous signals can provide no more information than internal LDB signals. Ideally, EGG signals should be 100% comparable to LDB recordings. However, there are three major differences between EGG and internal LDB signals:

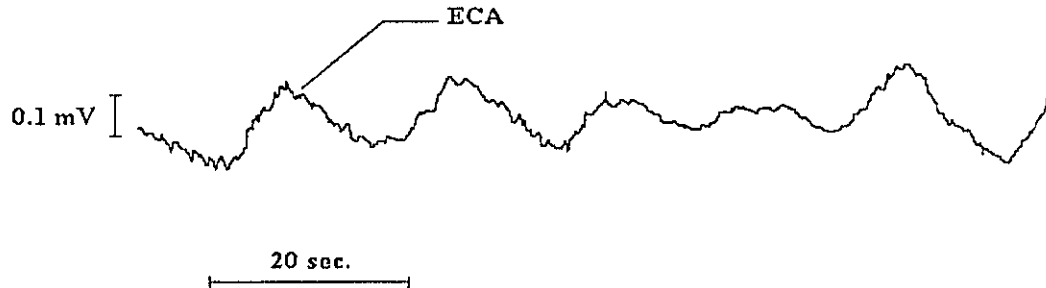


Figure 1.7. *Typical electrogastrographic (EGG) signal recorded bipolarly using a pair of standard electrocardiographic (EKG) electrodes 4 cm apart. Only ECA can definitely be recognized.*

- (a) the active surface areas of the recording electrodes (stainless steel or silver needles internally and standard EKG electrodes cutaneously) are quite different;
- (b) the distance between the source of the electrical field (the stomach) and the electrodes is much greater in EGG recordings;
- (c) external noise on the abdominal surface is much greater compared to that in internal recordings.

How these differences affect the ability of EGG to represent internal GEA is the subject of a separate chapter in this thesis.

CHAPTER TWO

**CONOIDAL DIPOLE MODEL OF GASTRIC
ELECTRICAL ACTIVITY.**

2.1. MAIN CONCEPTS IN MODELING OF GASTRIC ELECTRICAL ACTIVITY.

In the last decade there has been a substantial interest in non-invasive electrogastrography (EGG) as a possible diagnostic tool in gastroenterology. Cutaneous EGG signals from the stomach have been recorded since 1922 (3), but the poor quality of the recordings and the difference between the electrical parameters of cutaneous EGG and those of the internal gastric electrical activity (GEA) complicated clinical applications of the method (10). Mathematical modeling of the electrical phenomena that occur in the human stomach can solve some of the above problems. There are two general approaches towards this type of modeling:

- (a) "passive" models (34, 35, 36, 37), which try to represent a precise picture (map) of voltage and current distribution on the stomach surface usually by means of coupled relaxation oscillators;
- (b) "active" models (11, 32, 33) in which dipole theory is applied to describe mathematically vector characteristics of the electrical field produced by the stomach.

Using the characteristics of gastric electrical field a theoretical value for the electrical potential can be obtained at any point of interest around the stomach. Active models can be divided into two main streams themselves: models that try to represent the electrical phenomena in the stomach by means of current dipoles and models that represent the above phenomena electrostatically as a distribution of electric charge in dielectric medium. According to Plonsey and Barr (38) these two approaches could be considered dualistic.

Passive models, although reasonably accurate in representing voltages and currents on the stomach surface, cannot simulate recordings from the areas surrounding the stomach including on the abdominal surface. Therefore, for the purpose of EGG applications, active models are far more valuable. There are two known active models:

"cylindrical" (11), which is the first model to use the dipole theory, and "conical" (32, 33), which applies the "annular band" concept when describing the dipole distribution and movement. Of the two active models the latter is more related to the electrophysiological phenomena that occur in the human stomach. Some of the main concepts of this model that are widely accepted as fundamental are (32, 33) :

- (a) electrical activity originates in the mid corpus of the stomach and is present throughout the terminal antrum but is not found in the orad corpus and fundus;
- (b) the component of the stomach electrical activity known as Electrical Control Activity (ECA) is always present, i.e. it is not intermittent in time;
- (c) ECA is associated with the distal movement of a δ -wide annular band polarized by electrical dipoles pointed perpendicularly to the stomach axis;
- (d) the dipoles in the rest of the stomach have random polarization and generate null potential at every point of space;
- (e) the fundamental frequency of ECA is about 3 cycles per minute (cpm);
- (f) the propagation velocity is slow in the corpus but increases distally;
- (g) the ECA recorded from different points of the stomach wall shows a phase lag in the distal direction;
- (h) the abdominal surface can be represented by means of a surface α and is separated from the stomach by a dielectric.

Despite these important assumptions the conical model has two major disadvantages which are avoided in the proposed conoidal model.

The propagation velocity along the greater and the lesser curvature of the stomach is different, which explains the pattern of electrical coupling between different parts of the stomach (39, 40, 41). This difference could not be taken into account by the conical model.

The conical model is developed in Cartesian coordinate system, which complicates the model equations and much simplification is required to make these

equations solvable. Eventually because of these simplifications the model becomes rather cylindrical (32, 33).

Taking into account the above facts the following new concepts are considered in the proposed conoidal model:

- (i) the waveshape of gastric electrical activity as recorded in experiments *in vivo* depends on the position and configuration of the recording electrodes and is not, in general, the same as the waveshape of intracellular ECA;
- (k) normally the velocity of propagation of ECA is different along the greater and the lesser curvature of the stomach, so that the depolarization waves in the greater and lesser curvatures spread simultaneously through any radial plane perpendicular to the stomach axis despite the different route that they have to pass, i.e., there is full electrical coupling between different parts of the normal stomach;
- (l) for the purpose of this modeling, the form and the shape of the stomach is most closely represented by a truncated conoid with a finite length (Fig.2.1);
- (m) the modeling is to be done in spherical system of coordinates with no transformations into Cartesian coordinates, thus avoiding any unwanted mathematical simplifications;
- (n) using the model, researchers should be able to do fast and efficient simulation of experiments with both invasive (attached on the stomach wall) and non-invasive (placed on the abdominal wall) electrodes, and obtain a plot of the potential (when monopolar recording is simulated) or the potential difference (in the case of bipolar recording simulation) versus time;
- (o) Electrical Response Activity (ERA) could be responsible for some power changes in cutaneous EGG signals, but in general it has no significant effect on the spatial and temporal organization, frequency, velocity of propagation, waveform, phase lock, and coupling of the signals and therefore it can be ignored when modeling ECA.

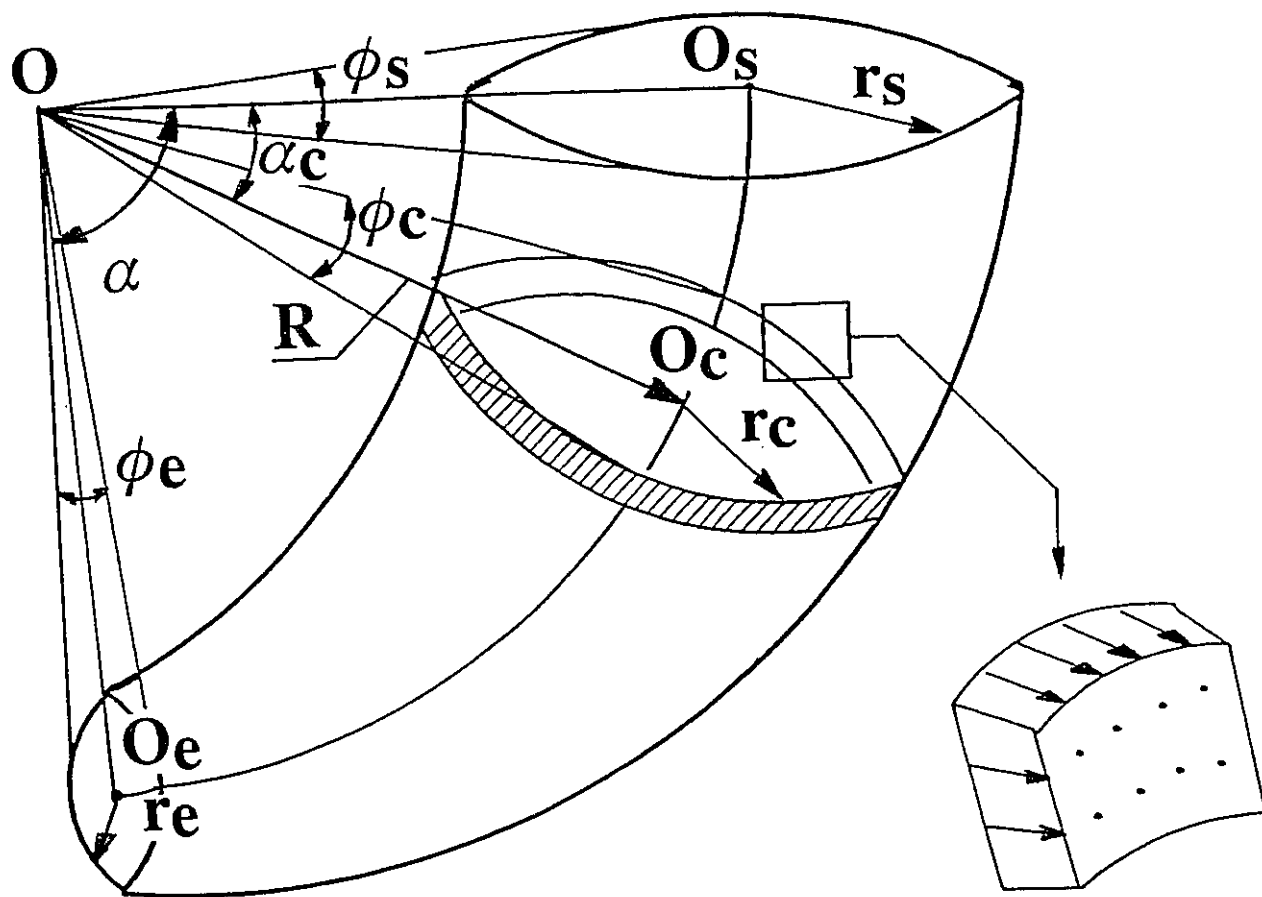


Figure 2.1. Human stomach represented as a truncated conoid in the spherical system of coordinates O , R . A sample band of depolarized cells is shown along with a magnified section depicting the perpendicularly-oriented to the conoidal axis dipoles (below right).

The main goals of this study were to develop the conoidal dipole model of gastric ECA implementing the above requirements, and to compare the signals produced by this model to the ones obtained in real in vivo experiments. A reasonably accurate model could then be used to simulate the impact of different electrode configurations and active electrode surface areas on EGG as well as to investigate the effect of gradual movement of the electrodes away from the serosa.

Previous studies had shown increased EGG amplitude postprandially, i.e. when ERA was present. A recent study (42), however, showed that stomach displacement also profoundly affects the amplitude of cutaneous EGG, and the increased postprandial amplitude might be due solely to stomach displacement or distention. Therefore, incorporating ERA in the model has more theoretical, rather than practical importance.

If the dipoles are considered a set of current sources and sinks, the assumption that they point to the center is in agreement with several studies (24, 25), which showed that the depolarization wave spreads very rapidly in circumferential direction from the longitudinal towards the circular muscle layers. Applying the principle of duality, however, in the modeling process the dipoles can be considered from an electrostatic point of view.

The assumption that electric dipoles outside the annular band of depolarized cells are oriented randomly and generate null electrical potential in each and every point in space is a simplification, which excludes from consideration the influence of other electrical phenomena i.e., the electrical fields created by the heart and the gut, the polarization phenomena related to the ion transport in areas surrounding the stomach, the distortions due to the contact between the electrodes and body tissues, noise in the amplifiers etc. In reality all of the above mentioned factors influence the recordings and affect the signal-to-noise ratio, but they do not change the electrophysiological phenomena that occur in the stomach itself.

2.2. MATHEMATICAL MODEL.

2.2.1. MAIN EQUATION OF THE MODEL.

Figure 2.1 represents the truncated conoid in a spherical system of coordinates with center O , angles α and ϕ and radius-vector \mathbf{R} . The conoid is limited by the circles (O_s, r_s) and (O_e, r_e) . When the electric field is created by a band of dipoles pointing to the center, the potential V_Q at a given point Q , situated at a vector distance ρ from an infinitesimal area segment of the band dS is (38):

$$V_Q = [1/4 \pi \epsilon] \int [(\mathbf{D} \cdot \rho) / \rho^3] dS \quad [2.1]$$

(S)

where S is the area of the δ wide annular polarized band, \mathbf{D} is the vector of the dipole density of that band and ρ is the vector distance between the point of interest and the infinitesimal area segment dS , situated on the polarized band (Fig. 2.1).

In this study the width δ was considered to be 2 mm. This assumption (used also by Mirrizzi et al.) is based on the fact that if the extracellular electrodes are separated more than 2.5 mm in real recordings from humans, a gap between the two phases of the signal is usually evident, while if the distance is smaller than 2 mm the potential dynamics recorded from either electrode is the same and no signals are recorded (11). However, the model must allow for calculations with greater δ , if desired.

The modeling is based on equation [2.1]. It is clear, that appropriate expressions for \mathbf{D} , ρ , S and dS are to be derived so that this area integral is solvable.

2.2.2. AREA OF THE ANNULAR BAND.

The polarized band can be considered as built from circles $[O_c(\alpha_c, \phi_c), r_c(\alpha_c, \phi_c)]$ (see Fig.2.1). The area of this band then can be expressed as:

$$S = 2 \pi \delta r(t) \quad [2.2]$$

where r represents the radii of the circles that build up the band. Obviously, r can be expressed as a function of the central angle α , which itself is a function of time. Table 2.1 (based in part upon the published literature, and in part on independent expert evaluation) shows that an exponential approximation of this function fits best the initial values measured from an average human:

$$r(\alpha) = 0.04026 - 0.001263 \cdot \exp(-\alpha) - 0.017321 \cdot \alpha \quad [2.3]$$

The expression for dS can be easily obtained also as a function of α :

$$dS = 2\pi\delta[dr(\alpha)/d\alpha]d\alpha \quad [2.4]$$

The angle α is a function of time. This function can be obtained indirectly, considering the velocity of propagation of the depolarization wave. This velocity has been investigated by several authors (11, 12, 37, 39). Many different values were suggested in different points along the greater and lesser curvature. However, there is a general agreement in the literature, that the velocity increases exponentially towards the pylorus.

Table 2.1. *Relationship between stomach parameters measured from average human and mathematically calculated values using model approximations.*

t [s]	V [cm/s] calculated	V [cm/s] average human	l(t) [cm] calculated	α [degrees] calculated	r [cm] calculated	r [cm] average human	ϕ [degrees] calculated
0	0.250	0.250	0.000	0.000	3.90	3.90	45.90
1	0.424		0.342	1.959	3.82	3.81	44.91
2	0.546		0.832	4.767	3.76	3.76	44.17
3	0.631		1.420	8.153			
4	0.690		2.081	11.946			
5	0.732		2.790	16.025	3.45	3.53	
6	0.759		3.542	20.305			39.26
7	0.779		4.311	24.717	3.19	3.10	
8	0.793		5.102	29.232			
9	0.803		5.912	33.804			
10	0.809	0.810	6.731	38.428	2.80	2.80	32.52
11	0.814		7.513	43.080			
12	0.817		8.331	47.761	2.71	2.73	
13	0.820		9.155	52.454			
14	0.821		9.976	57.158			
15	0.822		10.791	61.822	2.11	2.17	25.06
16	0.823		11.623	66.577			
17	0.824		12.434	71.046	1.85	1.96	20.97
18	0.824		13.212	75.687			
19	0.824		14.092	80.729			
20	0.825	0.825	15.000	85.943	1.40	1.40	16.09

Familoni et al. (39) compared the velocities of propagation in the areas of greater and lesser curvatures of the distal corpus, the proximal antrum and the distal antrum. For the purpose of this modeling the velocity along the stomach axis should be considered. It can be estimated, that it is the average between the respective velocities along the greater and lesser curvatures. This assumption leads to the following three values: 0.25 cm/s for the distal corpus, 0.810 cm/s for the proximal antrum and 0.825 cm/s in the distal antrum. The following system with three unknowns has to be solved with respect to a, b and c:

$$\begin{aligned} a + b &= 0.0025 \\ a + b \cdot \exp(10 \cdot c) &= 0.00810 \\ a + b \cdot \exp(20 \cdot c) &= 0.00825 \end{aligned} \quad [2.5]$$

This system has only one real set of solutions: $a = 0.00825$, $b = -0.00575$ and $c = -0.362$, which gives the following expression for the velocity of propagation (in m/sec):

$$v(t) = 0.00825 - 0.00575 \cdot [\exp(-0.362 \cdot t)] \quad [2.6]$$

If $l(t)$ represents the curve $0_s 0_c$ (see Fig. 1), then

$$l(t) = \int_0^t v(t) dt \quad [2.7]$$

After a substitution of [2.6] in [2.7] and solving the integral the result is:

$$l(t) = 0.00825 \cdot t + 0.158 \cdot [\exp(-0.362 \cdot t) - 1] \quad [2.8]$$

which is equal to 0 for $t = 0$ sec, and 15 cm for $t = 20$ sec. From anatomical point of view a length of 0.15 m for the stomach axis is quite reasonable. The relation between the angle α and $l(t)$ is given with:

$$\alpha(t) = l(t)/R \quad [2.9]$$

Thus the function $\alpha(t)$ is defined, which itself helps to define the expression for $r(t)$ from [2.3] and [2.9].

Angle ϕ is also a function of time, related to the change of the radius r with

$$\phi(t) = 2.\arcsin [r(t)/R] \quad [2.10]$$

Since the function $r(t)$ is already known, it is not difficult to calculate the set of values for $\phi[r(t)]$ and show that a linear approximation for the angle $\phi(t)$ would be appropriate:

$$\phi(t) = - 1.5t + 46, \text{ [degrees]} \quad [2.11]$$

2.2.3. DIPOLE DENSITY.

The relationship between the vector of the dipole density \mathbf{D} and the vector of the equivalent dipole moment \mathbf{P} was previously described (32, 33) as :

$$\mathbf{D} = \mathbf{P}/ S \quad [2.12]$$

The value for $|\mathbf{P}| = 2.2 \times 10^{-6}$ C.m was suggested in (32, 33) along with the assumption that it is constant because the charge distribution on each side of the polarized cell is approximately equal and the amount of the polarized cells in the band remains the same

regardless of the current angle α . Note that with the decrement of the area S in distal direction, the dipole density increases.

2.2.4. DISTANCE TO THE POINT OF INTEREST.

Vector ρ represents the vector from the infinitesimal area dS of the band to the point of interest Q , in which the potential is to be obtained. This vector is a function of angles α and ϕ . To derive this function some geometrical relations are to be described (Fig. 2.2) and the initial position of the annular band is considered. The point of interest Q is defined as $Q(OQ, \alpha_C, \phi_C)$, and the initial circle of the annular dipole band is (O_S, α_S, ϕ_S) . The current location of the infinitesimal area dS is labeled with L . The length ρ can be obtained from the triangle LOQ as:

$$\rho = [OL^2 + OQ^2 - 2 \cdot OL \cdot OQ \cdot \cos(\angle LOQ)]^{1/2} \quad [2.13]$$

The triangle $OO_S L$ gives:

$$OL = [R^2 + r^2 - 2 \cdot R \cdot r \cdot \cos(\angle OO_S L)]^{1/2} \quad [2.14]$$

Angle $\angle OO_S L$ is related to the current angle ϕ_S with:

$$\phi_S = \arcsin [\sin(\angle OO_S L) \cdot r_S / OL] \quad [2.15]$$

On the other hand it can be shown that

$$\cos(\angle LOQ) = \cos(\phi_S - \phi_C) \cdot \cos(\alpha_C - \alpha_S) \quad [2.16]$$

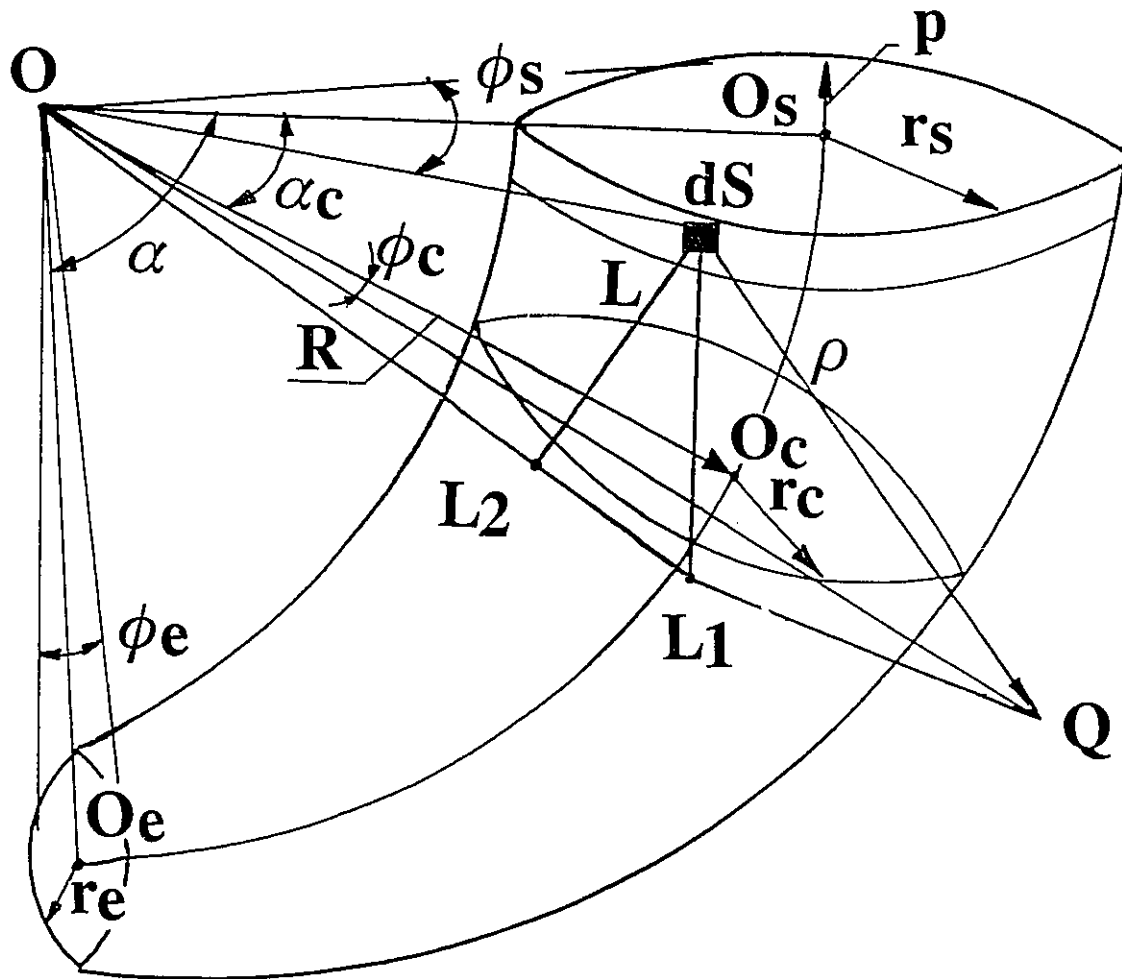


Figure 2.2. Stereometry of the truncated conoid used for derivation of the equations of the model.

where α_s, ϕ_s represent the angle coordinates of the current band that is to be considered. For the purpose of simplicity the initial position of the band is chosen. From expressions [11 - 14] one can conclude that

$$\rho = [OL^2 + OQ^2 - 2 \cdot OL \cdot OQ \cdot \cos(\phi_s - \phi_c) \cdot \cos(\alpha_c - \alpha_s)] \quad [2.17]$$

Along with the length of vector ρ , $\cos(\mathbf{P}, \rho)$ has to be determined. Both the conoid axis $O_s O_e$ (or its extension) and the plane $OO_s O_e$ are always perpendicular to the plane $OO_c Q$. Let LL_2 be the perpendicular to the plane $OO_c Q$ and let LL_1 be the perpendicular to the line OL in the plane OLL_2 . From triangle $L_1 QL$ it is obvious that

$$\cos(L_1 LQ) = (LL_1^2 + LQ^2 - L_1 Q^2) / (2 \cdot LL_1 \cdot LQ) \quad [2.18]$$

and also

$$-\cos(L_1 LQ) = \cos(\pi - L_1 LQ) = \cos(\mathbf{P}, \rho) \quad [2.19]$$

Considering that

$$LL_1 = OL \cdot \text{tg}(\alpha_c)$$

$$LQ = \rho$$

$$L_1 Q = [OL_1^2 + OQ^2 - 2 \cdot OL_1 \cdot OQ \cdot \cos(\phi_s - \phi_c)]^{1/2} \quad [2.20]$$

after an obvious substitution (OL has already been determined and OQ is known) the final expression becomes :

$$\cos(\mathbf{P}, \rho) = -\{[OL \cdot \text{tg}(\alpha_c)]^2 + \rho^2 - OQ^2 + 2 \cdot OQ \cdot OL \cdot \cos(\phi_s - \phi_c)\} / \{2 \cdot OL \cdot \text{tg}(\alpha_c) \cdot \rho\} \quad [2.21]$$

All necessary variables in equation [2.1] are now expressed as functions of the two angles $\alpha_c(t)$ and $\phi_c(t)$. The so obtained equation for the potential V_Q at the point of interest Q is solvable by a digital computer using the well-known Simpson formula (44).

2.3. RESULTS.

The model has been incorporated into a computer program (TURBOC++, Borland, 1990) that shows a picture of a truncated conoid (the stomach) on the screen and allows the user to place monopolar or bipolar electrodes simulating real experiments. The output of the program MODEL plots the dynamics of the potential or the potential difference (depending on the chosen electrode configuration) calculated after the simulation. When doing cutaneous simulations the abdomen is represented as a plane on which the stomach is projected.

2.3.1. TESTING THE MODEL.

Four pairs of short distance bipolar (SDB) needle electrodes were chronically implanted on the gastric serosa of a patient with suspected gastric motility disorder in the areas of the distal corpus and the antrum along the greater and the lesser curvatures using a technique described before (42).

The obtained recordings were compared with the results from the simulation with the program MODEL initially for the mid-corpus electrode pairs (Fig. 2.3) and after that for the antral pairs (Fig. 2.4).

The high cut-off frequency for the real recordings was 0.53 Hz (time constant 0.3 s) to prevent external noise. This relatively large time constant affected the sharpness of the edges of the obtained waves without significantly influencing the test results.

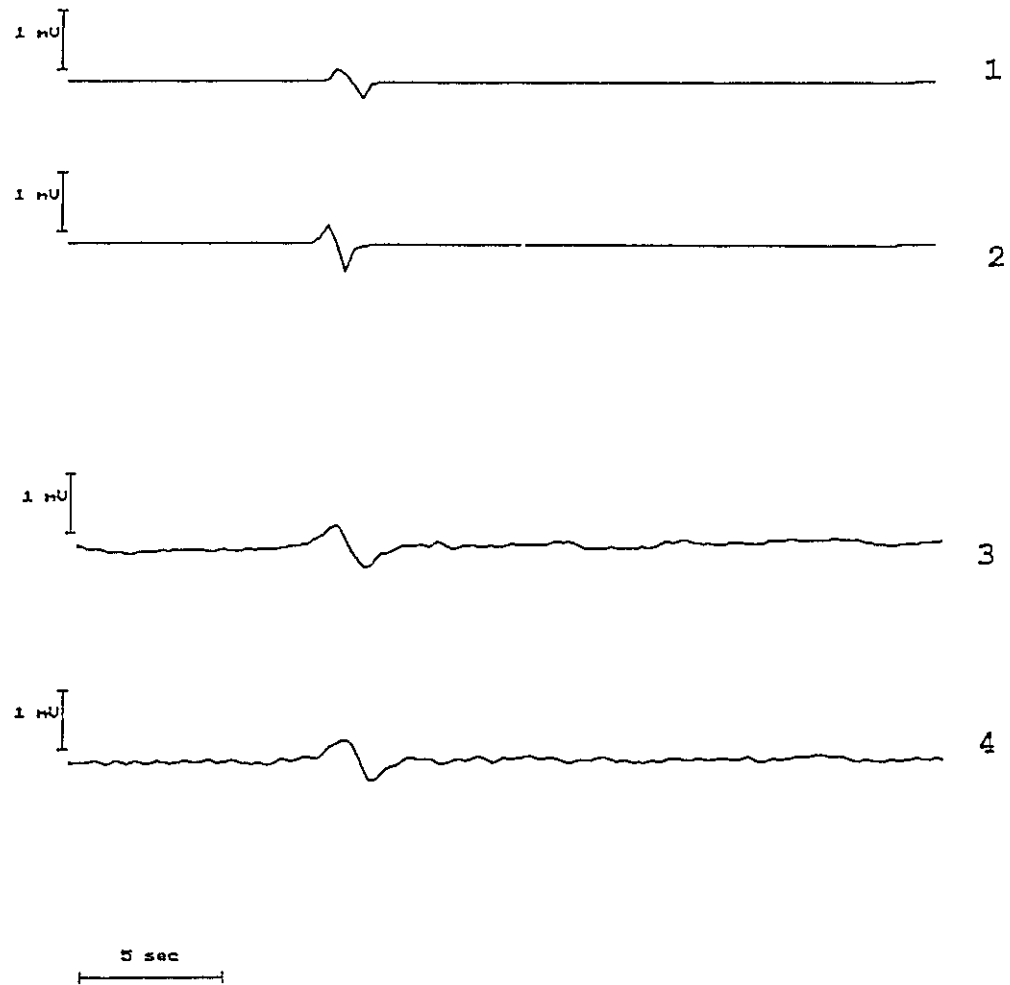


Figure 2.3. Simulated short distance (2.5 mm) bipolar serosal recordings in the area of the greater (Channel 1) and lesser (Channel 2) curvatures in the distal corpus, and respective recordings from an actual experiment performed on the patient (Channel 3 and 4).

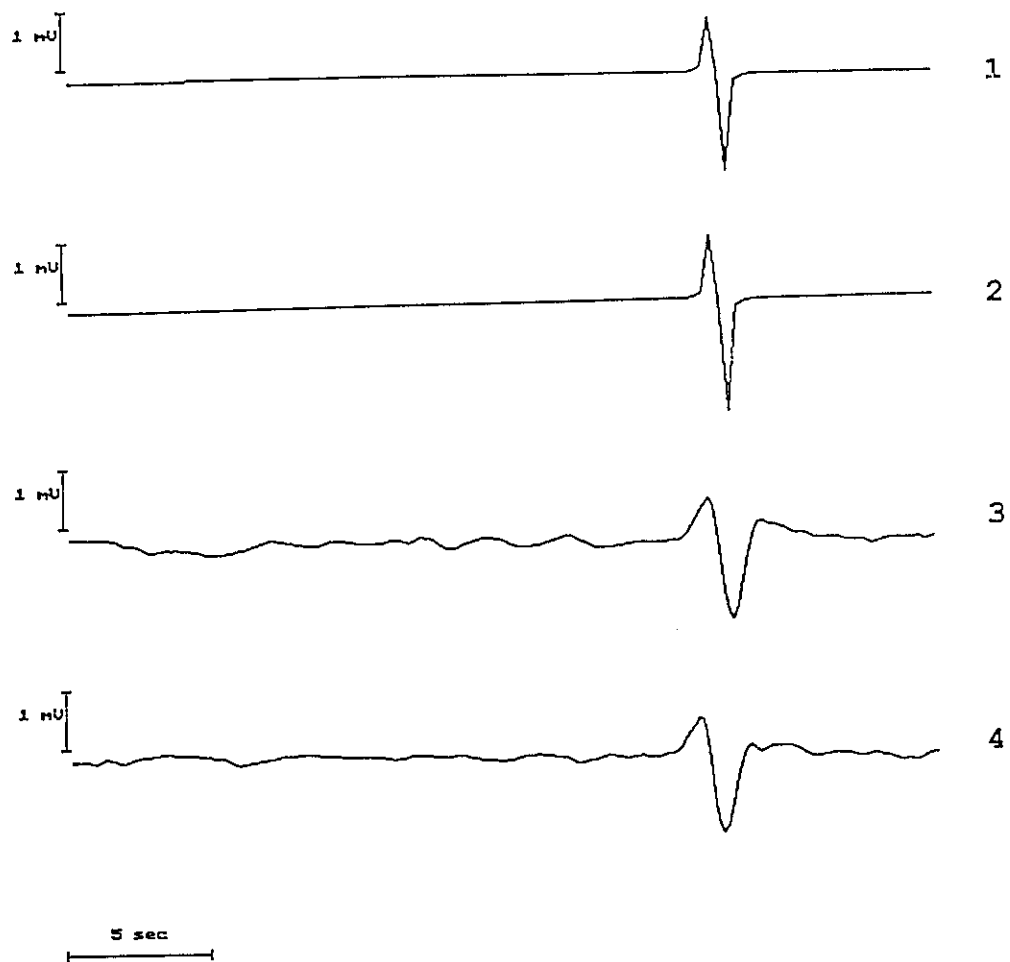


Figure 2.4. *Simulated short distance bipolar serosal recordings in the area of the greater (Channel 1) and lesser (Channel 2) curvatures in the antrum, and respective recordings from an actual experiment performed on the patient (Channel 3 and 4).*

Comparing the results from the tests with those from the computer model it can be suggested that the model represented relatively well stomach anatomy and electrophysiology and could be used as a tool for better understanding the parameters of human electrogastrographic signals.

2.3.2. STUDY OF THE ELECTRODE DISTANCE IN BIPOLAR RECORDINGS.

A simple example of the usefulness of the model could be a study of the effects of electrode distance on GEA recordings. Figure 2.5 represents a simulation of an experiment with implanted bipolar electrodes in the antral area with a distance varying from 5 mm to 2 cm.

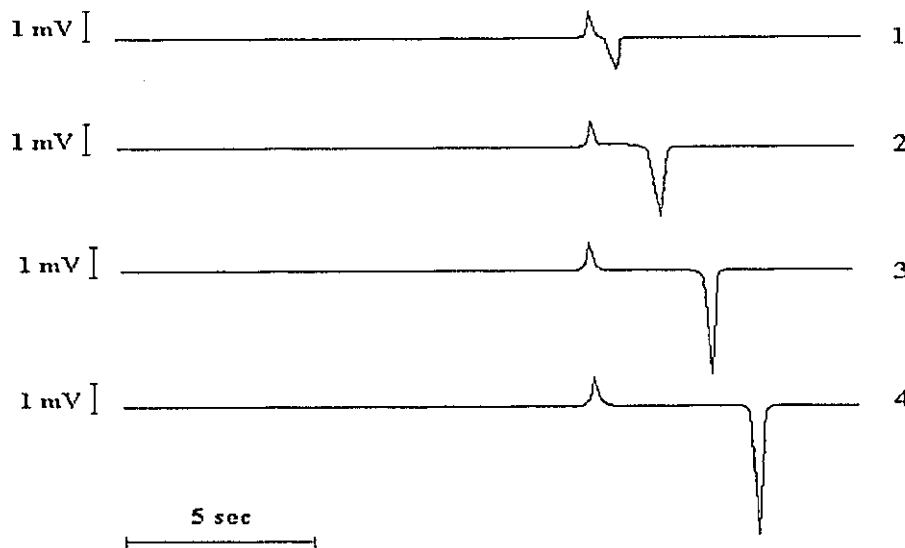


Figure 2.5. *Effect of gradual increment of the distance between serosal bipolar electrodes in simulated experiments. The initial inter electrode distance of 0.5 cm (Channel 1) was successively increased with 0.5 cm. In all recordings positive electrode was placed in the proximal antrum, while negative electrode was moved towards terminal antrum.*

Increasing the electrode distance increased the gap between the two potentials changing the obtained voltage from the well-known biphasic signal to a signal with relatively narrow frequency spectrum. The closer the electrode was placed to the terminal antrum, the higher the amplitude of the obtained potential was; this also contributed to the waveshape change.

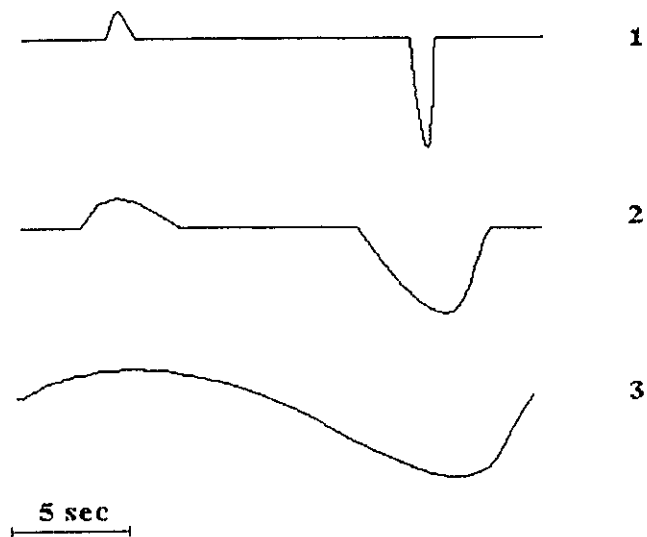
2.3.3. STUDY OF THE ELECTRODE SURFACE AREA.

In the previous section the potential V at a point of interest Q was investigated. Converted into a real experiment this means that the measuring electrode had an extremely small surface area, which could be a reasonable assumption, provided serosal needle electrodes were used. When an experiment with wider electrodes was modeled, one more integration over the electrode surface area was required.

Figure 2.6 shows the impact of increased electrode surface area on simulated experiments with antral long distance bipolar (LDB) electrodes. The electrode diameter was increased gradually from 2.5 mm to 1 cm. The greater the electrode surface, the closer to a sine wave the signal became, i.e. the spectrum of the signal became narrower. Increment of the electrode surface area increased the averaging effect upon the obtained potentials, and changed the waveshape of the obtained signal gradually transforming it to a signal with significantly fewer frequency components.

2.3.4. EFFECT OF INCREASED DISTANCE BETWEEN AN ELECTRODE AND THE FIELD SOURCE.

The electrostatic approach (38) leads to equation [2.1] which suggests that the following two factors would influence the signal when the distance between the electrode (the point of interest Q) and the source of the electrical field changes:



A



B

Figure 2.6. *Effect of gradual increment of electrode surface on GEA wave shape in simulated experiments (A). Electrode diameter was increased from 2.5 mm (Channel 1) to 6.5 mm (Channel 2), and to 1.0 cm (Channel 3). Distance between the electrode centers was kept 4 cm. The signal in Channel 3 resembled the wave form of cutaneous EGG (B).*

(a) the cosine of the angle between the vector of the equivalent dipole moment P and the vector distance ρ from the infinitesimal area dS of the δ -wide band to the point of interest Q ;

(b) the magnitude of vector ρ .

Considering that vector \mathbf{P} is always perpendicular to the radial plane of the current ring of depolarized cells, one can easily see that moving the electrode (the point of interest) away from the serosa (or mucosa) would bring the cosine of the angle (\mathbf{P} , ρ) close to zero. In addition, the increment of magnitude of vector ρ contributes to a further parabolic reduction of the potential at the point of interest Q . Therefore, when measuring the EGG the best approach would be to reduce the distance between the serosa and the abdomen. This distance is less in thin people, and that is possibly why some success was reported in recording time shifts (phase lags) between different cutaneous EGG channels from thin volunteers (41).

Another approach to reduce the distance ρ and the angle (\mathbf{P} , ρ) would be to distend the stomach. Unfortunately, stomach distention changes the conditions under which the stomach operates and this affects the parameters of cutaneous gastric electrical activity (42). However, stomach distention may be the only way to get reliable information from cutaneous EGG signals, because a distended stomach would be closer to the recording abdominal electrodes. This could help to overcome the negative effect of obesity on EGG.

2.4. DISCUSSION.

Although always questionable, modeling of bioelectrical phenomena, if done properly, can be valuable not only in theoretical studies but also as a tool that replaces the need for expensive and some times very uncomfortable experiments. Mirrizzi et al. (1985, 1986; 32, 33) made a significant step in modeling of the stomach electrical field, proposing

their "truncated cone" model. Unfortunately no further improvements or clinical tests of this model were published.

The methodology followed in this study was not only to create the new, "truncated conoid" model based on the electrostatic approach, but also to implement it for theoretical assessment of the correlation between the obtained biovoltages, different electrode positions and different electrode surfaces. In that aspect this type of modeling is quite convenient, because with the recent computer technology it allows almost immediate results after the electrode parameters and positions are determined by the investigator. The following main conclusions could be suggested as a result from this study.

Different electrode configurations have profound impact on GEA signals. Increment of the distance between individual electrodes in bipolar recordings and increment of the electrode surface area make the spectra of the recorded signals narrower.

Moving electrodes away from the stomach dramatically reduces the signal-to-noise ratio and one way to improve it is with gastric distention. Additional simulations can be performed with the model to examine quantitatively this effect, but it can be estimated that the decay in the amplitude is reversely proportional to the square of the distance between the electrodes and the stomach (providing the electrodes are with one and the same active surface area).

A high quality GEA amplifier with flexible frequency characteristics is required when attempts are made to obtain the cutaneous EGG, especially when electrodes with smaller active surface area are to be used.

The proposed model can be a useful testbed for many other simulations. For example, uncoupling or irregularities can be simulated by changing the way the depolarization ring propagates in order to study how these two phenomena are recorded with different electrode configurations.

CHAPTER THREE

AMPLIFICATION OF GASTRIC ELECTRICAL SIGNALS

3.1. AMPLIFIER REQUIREMENTS.

Although gastric electrical activity, which manifests itself as biovoltages, has been recorded for many decades, no special attention has been devoted to the problem of its proper amplification. The preferred approach was empirical modification of cut-off frequencies of all-purpose multichannel amplification units for the needs of gastric electrical signals (11, 17, 45). Because of the fact that this approach usually provides results, the problem has not been addressed until recently.

3.1.1. FLEXIBLE FREQUENCY RANGE.

The results from the previous chapter clearly indicate that the more similar cutaneous recordings are to the signals recorded invasively, the better the chances are for the useful clinical application of EGG. A well designed amplifier might record cutaneous LDB or even SDB gastric electrical signals comparable to the internal ones. The fact that today the EGG is recorded only with the a LDB configuration using standard EKG electrodes with a large active surface area, does not necessarily mean that this is the only possible EGG waveform. Signals with different waveforms have, in general, frequency spectra with different bandwidths even if their periods are the same (42). Therefore, if different electrode configurations or/and active surface areas are to be used, different low-pass and high-pass cut-off frequencies of the bandpass characteristic of the amplifier should be available. Whatever the waveform of the GEA signal is, its period of repetition is about 3 cpm, but variations from about 2 cpm (bradygastria) to 9 cpm (severe tachygastria) can be expected. Internal SDB signals can contain higher harmonics up to 4-5 Hz (11, 42), while the information from EGG signals is concentrated primarily in the fundamental (17, 40, 42, 45).

3.1.2. WIDE RANGE OF GAINS.

In the next chapter special attention will be devoted to the importance of the EGG amplitude. Here it should be mentioned, that the GEA amplitude is also dependent on the interelectrode distance and electrode active surface area. Cutaneous signals become weaker as the distance between the stomach and the abdominal electrodes becomes greater (e.g. in obese patients), when the distance between the electrodes in one bipolar pair is less, or when the recording electrodes have smaller active surface area. A peak-to-peak amplitude range between 0.01 and 0.5 mV can be expected for EGG. The amplitude range for invasively recorded GEA signals is 0.1-10 mV (9, 12). This implies that a wide range of gains is necessary.

3.1.3. DIFFERENTIAL INPUT.

It was pointed out earlier that monopolar recordings of gastric electrical activity are rarely used, because the monopolar GEA signal is superimposed upon a higher amplitude EKG, respiration and motion artifacts, etc., all of which would be amplified. Therefore, differential input is preferred when amplifying GEA. Fortunately, high-quality instrumentation amplifiers are now available to meet these requirements. These instrumentation amplifiers are usually DC coupled, which means that the signal is not high-pass filtered before the next amplification stage. This contradicts the need to get as much gain as possible as soon as possible and thus eliminate the negative impact of the noises in the next amplifier stages (46, 47). A major problem for a high gain of the differential input stage is the polarization voltages of the electrodes (48, 49, 50). Although Ag-AgCl electrodes are deemed to be non-polarizable (48), it is worthwhile to reexamine their behavior in the the infralow frequency range.

The impedance of a standard Ag-AgCl electrode was studied by Lenhart (52). It can be expressed by an equivalent resistor R and capacitor C connected in parallel. Their values are functions of the frequency f and could be estimated as: (52):

$$\begin{aligned} R &= 2.5 \cdot 10^3 \cdot f^{-0.39}, \Omega \\ C &= 90.4 \cdot 10^{-6} \cdot f^{-0.6}, \text{ F} \end{aligned} \quad [3.1]$$

For frequencies in the range 0.02-0.1 Hz the equivalent impedance of the electrodes alone can reach $10\text{k}\Omega$. In addition, the impedance of the skin and skin-electrode contact is also quite large in this low frequency range.

Huhta and Webster (50) as well as Metting van Rijn et al. (49) studied the interference currents through the patient's body in bioelectric measurements. They pointed out that there are three types of interference currents to be considered:

1. Interference currents through the body;
2. Interference currents into the amplifier;
3. Interference currents into the measurement cables.

The interference currents through the body are caused by the capacitances between the patient, the power lines and earth, and have a typical peak-to-peak value of $0.5 \mu\text{A}$ (49). A portion of these currents can flow through the neutral electrode thus causing a potential difference between the average potential of the body and the amplifier common: the common-mode voltage.

When doing an isolated bioelectric measurement, the capacitances between the isolated ground and mains and the isolated and non-isolated grounds are the major sources of the interference currents into the amplifier. These capacitances should be made as small as possible, to reduce the negative impact of these currents, portion of which flows through the neutral electrode contributing to the common-mode voltage.

The interference currents into the cables have a typical value of 10 nA peak-to-peak and flow through the recording electrodes and the electrode-skin impedance associated with them (49). This can potentially produce a relatively large differential voltage and saturate the input stage. The problem can be addressed by connecting a simple passive RC network at each input with the input impedance of each of the operational amplifiers serving as R. This would provide the low cut-off frequency of the whole system converting it to an AC amplifier. However, in case of accidental saturation of the input stage (for example due to motion artifacts) there is not a low-resistance path available for discharge of these capacitors except through the patient. The discharge can take minutes after removing the overload conditions (53). Van Heuningen et al. (53) suggested a frequency dependent negative feedback as a possible solution for this problem. They pointed out that the suggested circuit can handle time constants up to 1000 s. In this design, the differential amplifier of the standard instrumentation circuit used at the input is fed back by an integrator.

3.1.4. HIGH INPUT IMPEDANCE.

The electrode-skin interface has a complex impedance between $1\text{k}\Omega$ and $1\text{M}\Omega$ at frequencies up to 50-60 Hz (48, 49, 54). It increases in the infralow (0.01 - 1 Hz) frequency range. This impedance depends on the skin condition and its preparation, the equivalent impedance of the electrodes, the fat volume underneath the skin layer and the distance between the source of the electrical field and the electrodes. An increase of the electrode-skin impedance is to be expected when recording in the infralow frequency range, because the capacitive component would be great. A high input impedance would prevent the formation of voltage dividers between the electrode-skin impedance and the input of the amplifier. That is why as a general rule the input impedance of a biomedical amplifier should be as high as possible (46, 47).

3.1.5. GALVANIC ISOLATION.

Galvanic isolation between input and output is a must for any electrophysiological measurements in vivo. The primary reason for this is patient safety (53, 49). Leakage currents from the mains which flow into the body through the amplification system can cause fibrillation of the heart (50, 53, 54). Currents even as low as 10 μA could be dangerous. For all equipment in contact with the patient, not only must the case be electrically grounded, but connections to the patient must have very low current flowing through them (54). In galvanically isolated systems, there is a danger of undesired connections between the isolated and non-isolated grounds. Therefore, the general requirement is to separate physically the two grounds as much as possible (50, 50).

The absence of leakage currents also diminishes the unwanted line voltage input to the amplifier through the electrodes (53).

3.1.6. HIGH COMMON-MODE REJECTION RATIO (CMRR).

The signals $s_1(t)$ and $s_2(t)$ in each of the active inputs of an instrumentation amplifier are entirely differential at the moment T if

$$s_1(T) - s_2(T) = (V_{cc+} + V_{cc-})/2 \quad [3.2]$$

where V_{cc+} and V_{cc-} are the supply voltages of the amplifier. Modern differential amplifiers can easily provide common-mode rejection ratios (CMRR) higher than 100 dB. However, this feature alone does not ensure high CMRR for the whole amplification system. There are two possibilities for common-mode signals to go through despite the high CMRR of the input stage: because of the limited common-mode rejection ratio (CMRR) of the stage itself, and due to a partial transformation of the common-mode

signal into a differential at the input. While the first factor is rather technological, the conversion of the input common-mode signal into differential can be controlled. This conversion is due to the fact that ideal symmetry at the two active inputs of the differential amplifier cannot be provided. The more inputs the amplification system has the worse the symmetry problem gets, because it becomes more difficult to match them all. Since the differential input impedances of the instrumentation amplifiers can be matched quite precisely, the greatest unbalance in the equivalent input impedance comes from the electrode-skin contact and the cables. High input impedance, skin conditioning, galvanic isolation, appropriate cable shielding and driving the shields to the isolated ground or to the common-mode signal can increase CMRR by reducing the differences in the equivalent input impedances thus providing better input symmetry (50, 51, 53). In some cases, driving the body to the common-mode voltage gives very good results (50, 51, 55).

3.1.7. LOW NOISE.

There are three major sources of noise in amplification systems for electrophysiological measurements:

- (a) noise of the operational amplifiers E_{Oa} ;
- (b) thermal noise from the electrodes, cables and passive components E_t ;
- (c) noise introduced by the power supply E_p .

These noises are nearly random in nature and determine the ultimate lower limit of signal-handling capability of the amplifier (46).

The equivalent noise E_{Oa} of a differential operational amplifier can be separated into thermal (or Johnson) noise, voltage (flicker or 1/f) noise e_n , and current (or shot) noise i_{n+} and i_{n-} . It can be expressed with [46]:

$$E_{Oa} = \{[2.e_n^2 + 2.(i_{n+}.R_s)^2 + 2.(i_{n-}.R_e)^2 + 8KTR_s].BW\}^{1/2} \quad [3.3]$$

where R_s is the source impedance, R_e is the equivalent impedance at the negative input, K is Boltzmann's constant, T is the temperature in degrees/Kelvin, and BW is the frequency bandwidth in which the noise has been measured. An estimate of the noise of OPA404 (quad high precision FET operational amplifier, Burr Brown) in the bandwidth of 0.01 - 5 Hz with a source impedance of $1M\Omega$ (worst case scenario) shows that E_{Oa} would vary in the range of 0.02-0.35 μV (rms).

Thermal noise from the electrodes, cables and passive components is more difficult to assess because many of the impedances are unknown. It can be estimated by

$$E_t = \{(8KTR_e)+(8KTR_c)+\sum(4KTR_j)\}^{1/2} \quad [3.4]$$

where R_e is the equivalent resistance of the electrodes, R_c is the resistance of the cables, and R_j are the resistors in the amplifier. It is clear, that since the resistance of the cables is very low, major contributors to the noise are the electrodes and the resistors on the printed circuit board. This noise can exceed 0.1 μV only if a great number of resistors are used in the printed circuit board of the amplifier.

Whatever power supply is used, it introduces additional noise in the amplification system (46, 49, 50). Modern isolation amplifiers usually have built-in isolated power supply, i.e. they are internally powered. Isolation amplifiers with a modest cost would have relatively big ripple current and voltage associated with the isolated power supply. A typical example is Burr-Brown ISO 107 which is recommended for biomedical applications, but has voltage ripples from the power supply in the range of 60 mV (peak-to-peak).

This discussion clearly indicates that the power supply is the major source of noise in amplification systems with galvanic isolation. There are two ways of addressing this problem:

- (a) filtering the high-frequency ripple according to the recommendations of the manufacturer;
- (b) synchronizing the ripples so that they become common-mode signal before the next stage of the amplifier.

While the first option is obvious, the second option implies that two synchronized isolation amplifiers (one for each input) would be required for each channel and the instrumentation amplifier would be in the non-isolated part of the circuit. This would almost double the cost of the device.

3.1.8. GOOD OFFSET COMPENSATION.

Although most of the high-quality instrumentation and operational amplifiers have laser-trimmed offset, in an amplification system with multiple stages and built-in active filters some offset voltage is to be expected. In the modern systems the offset is automatically compensated to provide better output range for the amplified signals.

3.2. INPUT STAGE OF THE ISOLATED GEA AMPLIFIER.

Many of the above stated requirements for the GEA amplifier are to be met at the input of the amplification system. In fact, the input stage of a differential amplifier determines the CMRR and the input impedance of the whole system (46, 47, 53). In this study the solution for the input stage proposed by Van Heuningen et al. (53) was utilized for the gastric electrical signals. The frequency-dependent negative feedback was implemented on the differential operational amplifier of the monolithic instrumentation amplifier after the galvanic isolation (Fig. 3.1). Two synchronized isolation amplifiers were connected as buffers in the isolated part. Their common power supply was used to supply the two input FET operational amplifiers, which had a gain of 10. A quad (four-in-

package) operational amplifier OPA404 was used, so one of the two amplifiers left was used to drive the shielding of the cables to the isolated ground. Appropriate shielding of the active inputs was also provided to ensure better symmetry.

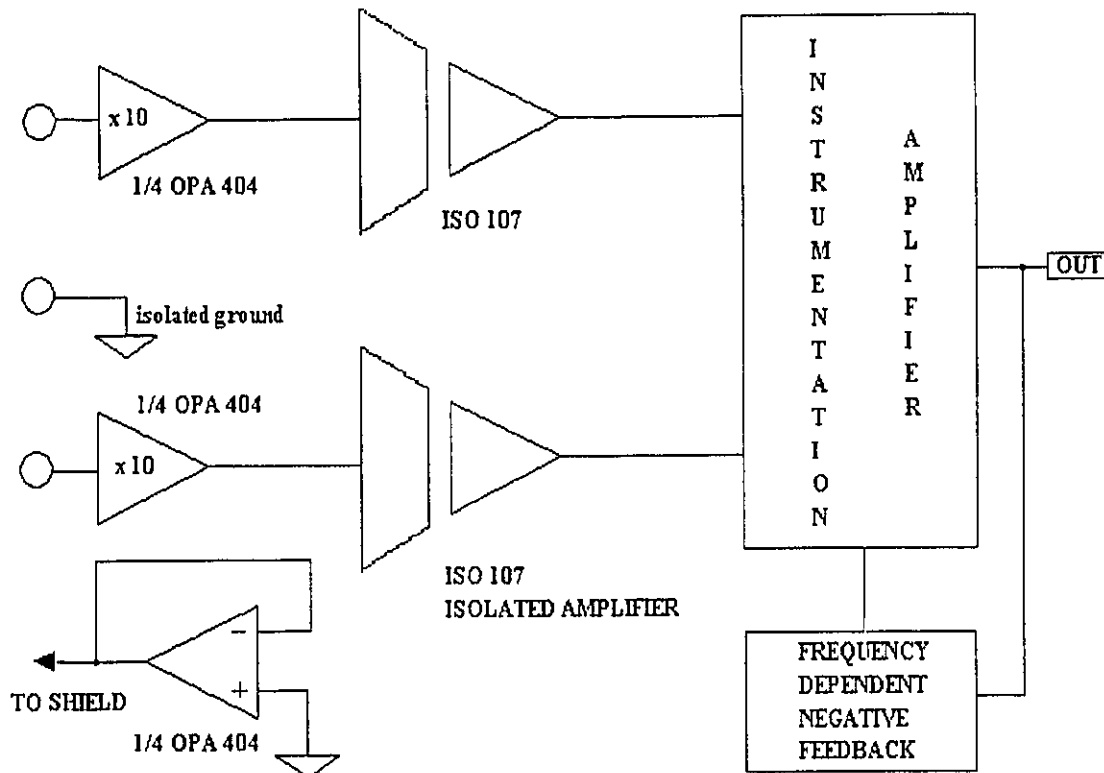


Figure 3.1. Simplified diagram of the input stage of the amplifier.

A possibility for easy on-line change of the cut-off frequencies as well as computer control via software accessible registers should be provided if the requirements for a flexible frequency range are to be met. It is important to use active filters with monotonic frequency and phase characteristics (for example Butterworth filters) in order to avoid the negative impact of non-linear phase responses. Ripples in the phase characteristic of the amplifier can lead to misinterpretation of the recorded time shifts between different GEA

channels. An example of a digitally controlled 4-pole low-pass filter which follows the input stage is shown on Fig 3.2.

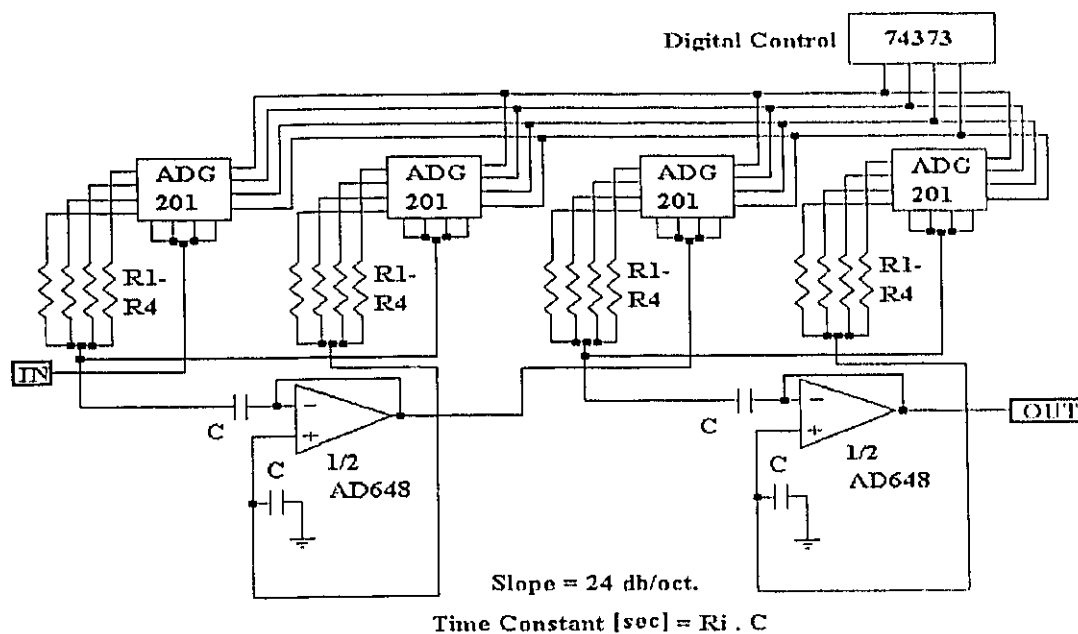


Figure 3.2. Digitally controlled four-pole low-pass filter.

3.3. PROGRAMMABLE GAIN AND OFFSET COMPENSATION.

Computer controlled gain is relatively easy to realize with the new integrated circuit technology. The problem is how to cover wider range of gains. This is usually achieved by cascading several programmable operational amplifiers (56).

Automatic offset compensation is still a problem in any computerized amplification system (46). The problem can be solved using an analog or digital compensation circuit.

When doing an analog compensation, the input is short-circuited and the measured offset is stored in a holding capacitor. The stored value of the offset is later applied during the recording to the positive input of the programmable amplifier instead of grounding it.

When using digital compensation, the offset is assessed similarly, but it is then converted to its digital value and returned back to analog by a digital-to-analog converter (DAC). The DAC output is applied to the positive input of the programmable amplifier.

Both approaches have advantages and disadvantages. The major drawback of the analog approach is the leakage current of the holding capacitor, which prevents the offset voltage to be held unchanged indefinitely. However, this can be overcome with an appropriate compensation circuit (Fig. 3.3).

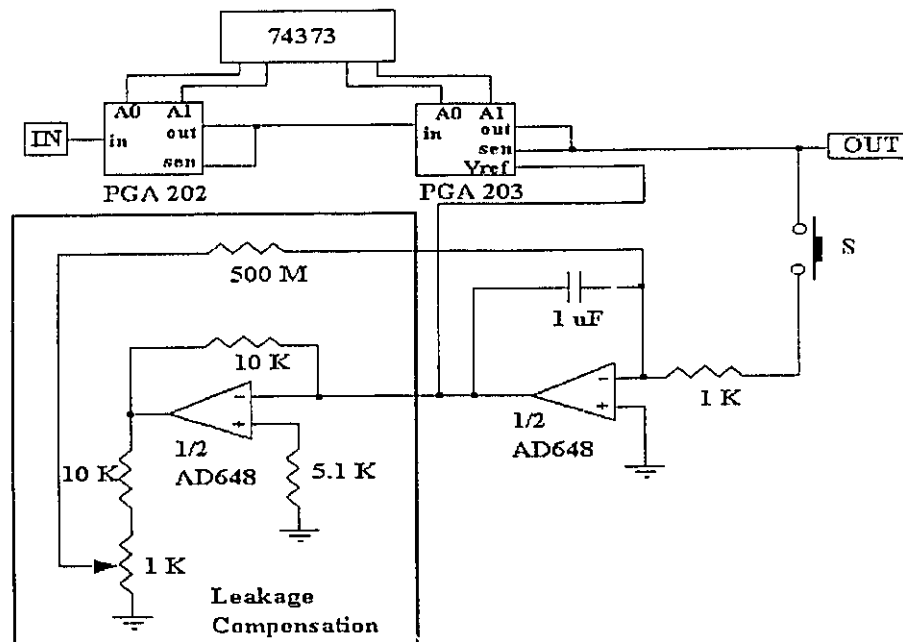


Figure 3.3. Cascaded programmable amplifiers with an automatic offset compensation circuit.

The holding problem is avoided in the digital alternative, but the finite resolution of the digital-to-analog converter often makes the compensation voltage different from the real offset. To achieve good offset compensation in the microvolt range using the digital approach at least a 16-bit DAC would be required.

In this study the analog approach is preferred because of its simplicity and modest cost. Good shielding around the active inputs of the programmable amplifier used for offset compensation is provided.

3.4. BLOCK AND CIRCUIT DIAGRAMS OF THE GEA AMPLIFIER.

The block diagram of the isolated GEA amplifier (Fig 3.4) contains several major blocks:

- (a) isolated input stage with a circuit for driving the shielding;
- (b) instrumentation amplifier with computer controlled frequency dependent negative feedback (high-pass filter);
- (c) computer controlled low-pass filter;
- (d) cascaded programmable amplifiers;
- (e) automatic offset compensation.

The circuit diagram of the amplifier is given in Appendix 1. The isolated EGG amplifier utilizes two non-inverting FET amplifiers with a gain of 10 (U1a, U1b) on each of the two inputs. The amplifier outputs are then applied to a differential amplifier made up of two unity gain ISO 107s (U2a & b) and a monolithic instrumentation amplifier (INA 101) with a gain of 10 (U3), thus providing an overall gain of 100. U1c drives all shielding to isolated common. A single-pole high pass filter (U4) implements the idea of frequency dependent negative feedback and provides filtering of the input signal with a cutoff frequency of 0.015, 0.029, 0.5, or 1.6 Hz selected by the appropriate setting of the analog switches (U20).

The output of the INA 101 is applied to a variable four-pole low-pass filter (U5) which filters the signal with a cutoff frequency of either 0.1, 0.5, 2, or 3.4 Hz selected by the appropriate setting of the analog switches (U6-9).

The filtered signal is then applied to a programmable gain block (U11 & 12) with a gain varying from +1 to +8000 by powers of 2 up to 8 (PGA203) and powers of 10 up to 1000 (PGA202). The value of the low and high-pass cutoff frequencies, as well as the gain, are determined by bits loaded into U18 and U19 by a software accessible register.

The auto-offset group is made up of an integrator (U13b) and a leakage current compensator (U13a). This block is toggled active and inactive by the switch S1.

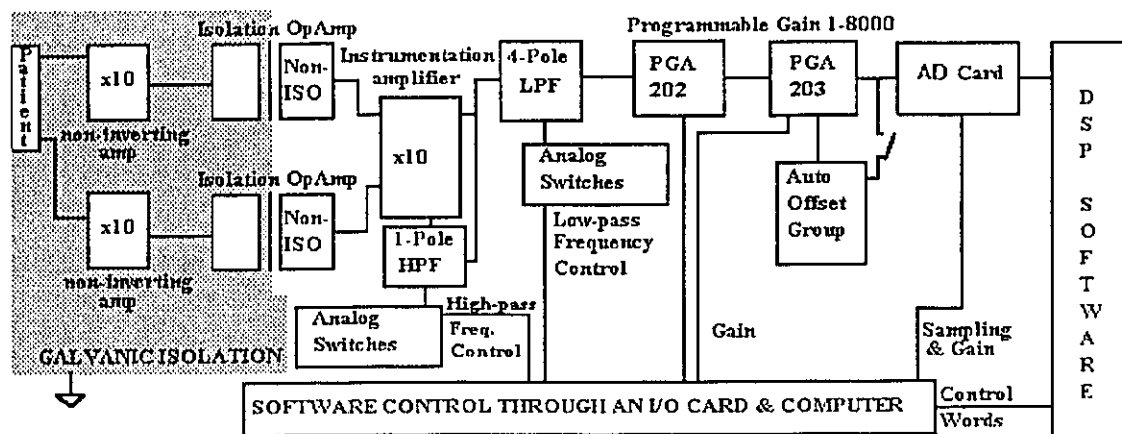


Figure 3.4. Block diagram of an isolated GEA amplifier. The shadow area is the isolated section.

3.5. PERFORMANCE CHARACTERISTICS OF THE GEA AMPLIFIER.

The effective CMRR of the designed multichannel GEA amplifier was measured as the ratio between the input and output voltage when the input was short-circuited. The input voltage varied between -6 and +6 V. The measured CMRR was between 80 and 85 dB depending on the amplitude of the input common-mode signal.

Jung (46) points out that the noise of an amplifier system can be measured by connecting the input to a defined source resistance, and measuring the output rms noise in a defined bandwidth using different gains. The noise at the output of the EGG amplifier referred to the input (i.e. with the gain considered) in the widest frequency range (5 Hz) was in the range of 20 μV rms. The following equation is recommended (47) to assess the noise:

$$E_{\text{rms}} = \{(E_{\text{amp}}^2) \cdot \text{BW}\}^{1/2} = 20 \mu\text{V} \quad [3.5]$$

In the 1 Hz bandwidth the equivalent noise can be estimated to about 9-10 μV rms, which is somewhat high. However, the fact that this is a prototype must be taken into account. An implementation of the amplifier in factory conditions would probably improve its noise performance because the input symmetry and the synchronization of the two isolation amplifiers would be better.

Another way of assessing the noise is to measure it at the output of the amplifier when the inputs are short-circuited. The result of the measurement is then divided by the gain. Using this approach the measured noise was in the range of 12-16 μV peak-to-peak.

Input impedance of the system corresponds to the input impedance of OPA404 which is in the range of several $\text{G}\Omega$.

The galvanic isolation cannot be provided by the isolation amplifiers alone. At the present time the requirements of Canadian Standard Association are that the short-circuited input should provide isolation up to 2500 V (rms). Despite the fact that ISO 107 have above 2500 V (rms) isolation capabilities, the panel-mount couplers, potentiometers, switches, etc. should also have similar characteristics. There should be enough physical separation between isolated and nonisolated parts of the printed circuit board as well.

Figure 3.5 shows the Bode plots of the bandpass GEA amplifier adjusted for standard EGG recordings. Since the high-pass filter is a single-pole integrator in the negative feedback of the instrumentation amplifier INA101 (slope 6 dB/oct), and the low-

pass filter is 4-pole (slope 24 dB/oct), the frequency characteristic is asymmetric. The phase characteristic is relatively linear and smooth in the EGG frequency range. These results were obtained using the simulation software Electronic Workbench (Toronto, Ont., 1990).

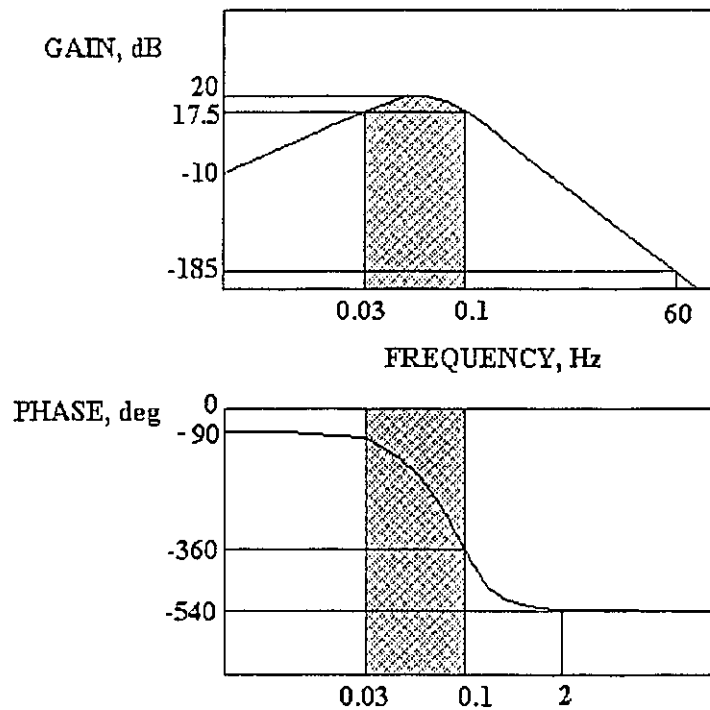


Figure 3.5. Bode plots of the GEA preamplifier adjusted for EGG. The shadow area is the pass band.

Note that the overall phase is inverted by 180 degrees.

CHAPTER FOUR

**METHODS FOR ANALYSIS OF GASTRIC
ELECTRICAL ACTIVITY.**

4.1. INFORMATION EXTRACTED FROM GASTRIC ELECTRICAL ACTIVITY.

4.1.1. MIGRATING MYOELECTRICAL COMPLEX AND CONTRACTIONS.

It was pointed out earlier (see Chapter 1) that spikes indicate the presence of gastric contractions. In experiments in vivo, spikes are best seen in serosal SDB recordings, and this is the most reliable method of assessing contractions from gastric electrical signals (11, 12, 42). As a direct consequence of that a histogram of the Migrating Myoelectrical Complex (MMC) can be built from SDB recordings. Each value in this histogram represents the ratio between the number of ECA waves followed by spikes, and the total number of ECA waves in a certain time interval (usually 2 minutes). Whether contractions can be reliably assessed from LDB and EGG recordings is subject of a separate chapter in this thesis.

4.1.2. ELECTRICAL COUPLING BETWEEN DIFFERENT PARTS OF THE STOMACH.

Electrical activity in the normal stomach has a firm temporal organization. While the velocity of propagation from the distal corpus to the terminal antrum can differ individually, it has been shown that corresponding ECAs recorded from different areas of a normal stomach maintain a consistent time shift between them. This phenomenon has been called *electrical coupling* (12, 43). Even in cases of significant frequency irregularities, the pattern of electrical coupling in the stomach may be preserved (43). Normal electrical coupling between different parts of the stomach corresponds to a distal direction of propagation of gastric electrical and contractile activity (41, 43, 57):

Electrical coupling can easily be studied invasively with a set of serosal SDB electrode pairs implanted in the areas of interest (42, 43). Although LDB signals cover greater stomach areas, they can also be used to assess electrical coupling (42).

A recent study (41) reported that the direction of propagation could be assessed from EGG recordings as well. In another study, analysis of the EGG waveform has been suggested as an indirect method for non-invasive assessment of direction of propagation of GEA (39). However, a comparative frequency study of SDB and EGG signals to objectively prove these assumptions has not been done.

4.1.3. GASTRIC ELECTRICAL FREQUENCY.

The frequency of GEA can be assessed by all recording techniques, but with different degrees of reliability. It could be very informative in identifying gastric electrical irregularities, which are believed to be related to irregularities in contractile activity (17, 39). Some investigators assume that tachygastria (gastric electrical signals with frequencies above 4 cpm) and bradygastria (below 2.25 cpm) could be related to certain gastric motility disorders (11, 17). Biphasic serosal SDB signals have very well defined time characteristics and are very reliable in assessing frequency (39, 42). It has been suggested that EGG signals can also show gastric electrical irregularities (9, 11, 39, 42, 43, 45). However, the relationship between EGG frequency and gastric electrical frequency obtained from SDB recordings has not been sufficiently explored.

4.2. METHODS TO ASSESS THE MIGRATING MYOELECTRICAL COMPLEX (MMC) AND CONTRACTIONS.

4.2.1. BUILDING THE MMC FROM SEROSAL SDB RECORDINGS.

The biphasic shape of Electrical Control Activity (ECA) in SDB recordings of GEA is very well defined both in terms of amplitude and duration when appropriate amplification bandwidth is used (Fig.4.1). Each ECA wave is surrounded with quiescent intervals in which no spikes or remnants of the plateau of ERA are recorded. Spikes, on the other hand, usually have less power and are packed between consecutive ECA waves. This makes both ECA and spikes easily identifiable and therefore automatic computation of the MMC from serosal SDB recordings is relatively easy. A block-diagram of an algorithm to do that and a sample canine MMC obtained with it are shown in Fig.4.2.

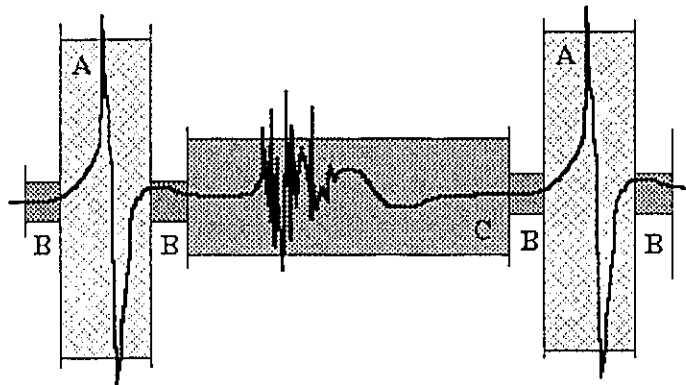
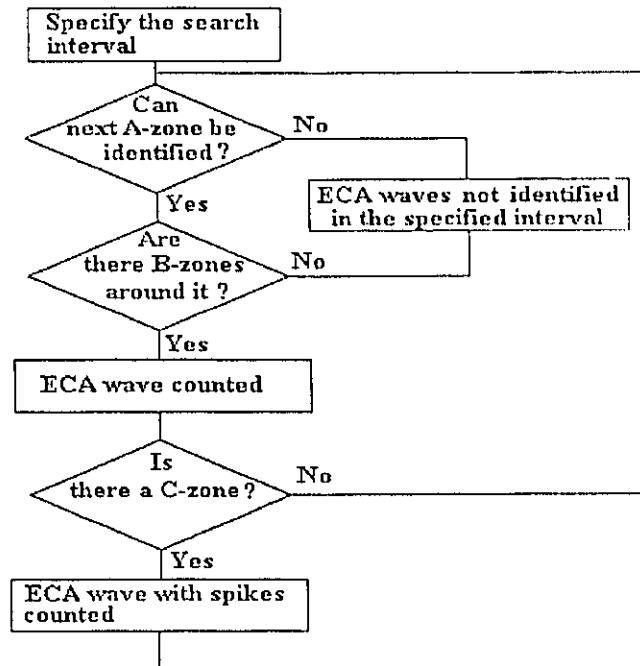
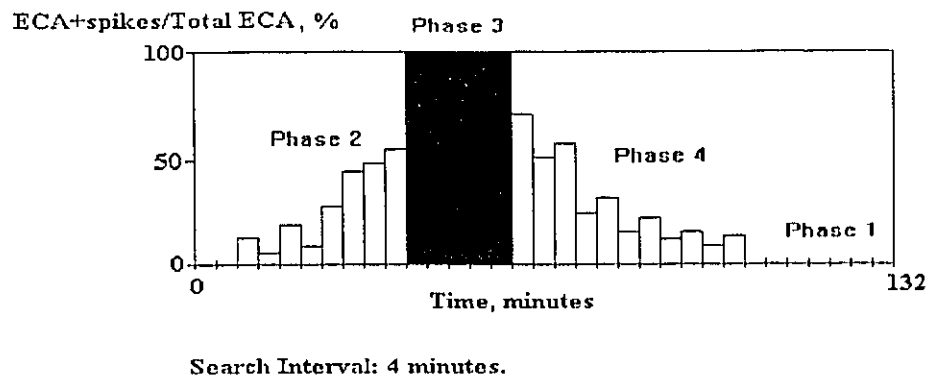


Figure 4.1. SDB signal divided into three zones: A - the zone of ECA; B - the quiescent zones; C - the zone of spikes.



A

CANINE MIGRATING MYOELECTRICAL COMPLEX



B

Figure 4.2. Block-diagram of an algorithm for counting ECA and ECA with spikes from SDB recordings (A), and a typical canine MMC obtained using this algorithm (B). All four phases of the MMC are clearly seen.

4.2.2. QUANTITATIVE ASSESSMENT OF EGG AMPLITUDES.

Many authors (9, 11, 12, 14, 45) believe that the appearance of spikes in internal recordings of GEA corresponds to an increased EGG amplitude, i.e. gastric contractions can be assessed by amplitude analysis of EGG.

Changes in EGG amplitudes are relatively easy to follow in the time domain, if the electrodes are positioned properly and the amplifier has an adequate bandwidth. Usually the average of the absolute values of all amplitudes is calculated. EGG amplitude is considered increased if it exceeds 25% of this average (42).

The dynamics of EGG amplitudes can also be assessed in the frequency domain (10). This will be subject of special attention in this chapter when frequency analysis is discussed.

4.2.3. OTHER METHODS TO ASSESS CONTRACTIONS AND MMC.

The most reliable method to measure contractions is with implanted serosal force transducers (FT; 58, 59). Such recordings show MMC directly without any need for processing. The method is invasive and is usually used on unconscious dogs.

In humans, contractions can be assessed indirectly by measuring changes in gastric intraluminal pressure (ILP, 60). This is usually done by means of special manometric tubes introduced orally and perfused with water. Once in the stomach, the intraluminal tube assembly is connected externally to a pneumo-hydraulic system (Arndorfer pump). Thus the pressure transducer records the changes in the stomach pressure only.

Although less reliable than FT, ILP measurements are widely used, because they are less harmful for the patient. The Migrating Myoelectric Complex can be recognized in the time domain ILP recordings.

Similarly to the changes in EGG amplitudes, the amplitude changes recorded using both ILP and FT methods can be assessed quantitatively by calculating the average of the absolute values of all amplitudes and taking 25% of this average as a threshold level of recognition (42).

4.3. METHODS TO ASSESS ELECTRICAL COUPLING.

4.3.1. VISUAL ANALYSIS OF THE TIME SHIFTS BETWEEN DIFFERENT CHANNELS.

This is the simplest way of assessing electrical coupling and is illustrated on Fig.4.3. As long as the lines that connect the corresponding waves remain parallel, the coupling is intact.

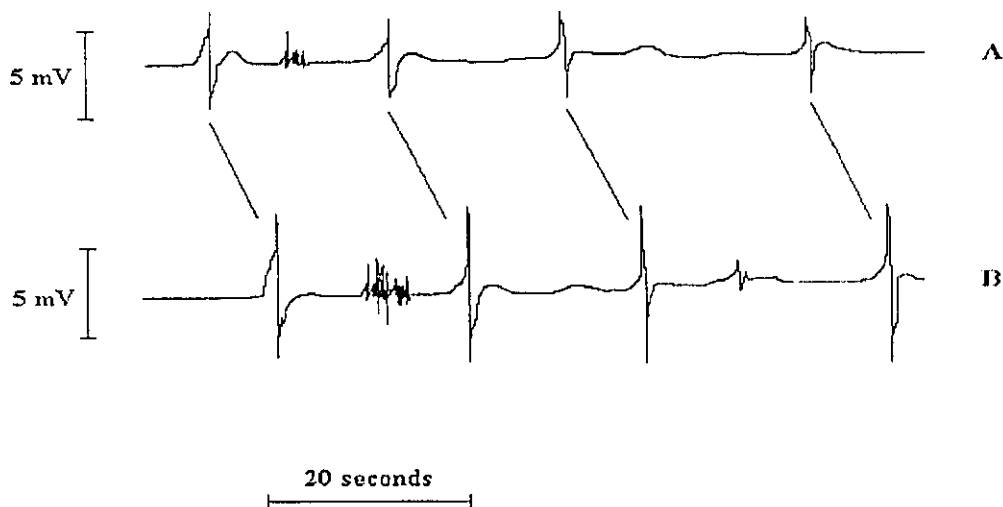


Figure 4.3. Electrically coupled SDB signals from proximal (A) and distal (B) antrum. The lines connecting the peaks of ECA remained parallel even when a minor frequency irregularity occurred between the third and the fourth wave.

4.3.2. ANALYSIS OF THE TIME SHIFTS USING CROSSCORRELATION.

Correlation between two groups of data means that they change with respect to each other in a structured way. If, for example, signal a always increases and decreases, as signal b increases and decreases for a certain amount of time, then x and y are positively correlated in this time interval (61). When the signals are two sets of N digital numbers (e.g. two digitized sine waves), the correlation coefficient r_{xy} between them can be calculated with the following equation:

$$r_{xy} = \frac{\sum \{ [x(n) - Mn_x] \cdot [y(n) - Mn_y] \}}{\sqrt{\{ \sum [x(n) - Mn_x]^2 \cdot \sum [y(n) - Mn_y]^2 \}}} \quad [4.1]$$

where Mn_x and Mn_y are the mean values of signal x and signal y respectively, and all summations are from 0 to N-1.

If signal x is an N-point sine wave with period T and amplitude A, and signal y is an N-point cosine wave with the same period and amplitude as the signal x (i.e. the phase lag between the two signals is 90 degrees), the correlation coefficient between them will be 0. However, these signals have strong interrelation. Practically, the only difference between them is the phase lag (time shift). On!, shifting the signals with respect to each other can produce a correlation coefficient different than 0.

The cross-correlation function is formed from successive values of the correlation coefficient taken at time shifts of 0, 1, 2, 3 and so on, data sample intervals (61):

$$r_{xy}(k) = \frac{\sum \{ [x(n) - Mn_x] \cdot [y(n+k) - Mn_y] \}}{\sqrt{\{ \sum [x(n) - Mn_x]^2 \cdot \sum [y(n) - Mn_y]^2 \}}} \quad [4.2]$$

where $k = 0, 1, 2, \dots, N-1$ represents the time shifts. It is obvious that the crosscorrelation function of two shifted signals with similar periods is also periodic. It is also well known

(see Challis and Kitney, 61) that the phase lag (time shift) between the two signals is coded as the time shift from $k=0$ to the first local maximum of the crosscorrelation function.

Equation [4.2] looks somewhat strange for greater values of k and n , because the index $k+n$, the signal y might exceed $N-1$. There are two ways of handling this problem.

When linear crosscorrelation is to be calculated, all values for the signal y when the indexes are outside the range $(0, N-1)$ are considered 0. The method is called zero-padding (61, 62, 63, 64, 65). The crosscorrelation sequence has a length of $2N-1$ samples.

Circular crosscorrelation considers the signal y to be symmetrical and continuous outside the index range $(0, N-1)$. The crosscorrelation sequence in that case has length N .

Both methods produce different results, which are illustrated in the following two examples based on simple numerical sequences (65):

(a) linear correlation:

$$\{1\ 1\ 0\ 0\} \otimes \{1\ 3\ 3\ 1\} = \{1\ 4\ 6\ 4\ 1\ 0\ 0\}$$

(b) circular correlation:

$$\{1\ 1\ 0\ 0\} \otimes \{1\ 3\ 3\ 1\} = \{2\ 4\ 6\ 4\}$$

It is crucial to use linear correlation when processing non-periodic signals, because if circular crosscorrelation is used the signals would artificially be made periodic (61, 65). GEA signals, however, can be considered quasi periodic, so circular crosscorrelation would be acceptable. In this study it is preferred because its sequence length is less.

The signals x and y have been analyzed in a given time interval, and only N points of each signal have been taken to calculate the crosscorrelation function between them. Consequently, the obtained function is just an estimate, based on the two given segments of the processes x and y . This affects the obtained function when calculating for greater shifts k (61). Of course, the longer the time intervals (respectively, the greater the number of points N), the better the estimate of the crosscorrelation function.

Time shifts measured from the crosscorrelation functions calculated from successive time intervals of the two studied signals can be presented as a function of the recording time in a *time shift plot*.

4.3.2. ANALYSIS OF THE WAVEFORM OF EGG.

Familoni et al. (39) suggested that EGG waveform analysis could be used for indirect assessment of direction of propagation. They pointed out that in normal subjects the descending portion of EGG waves usually dominates, which probably indicates distal direction of propagation. During periods of uncoupling the direction of propagation is disturbed. Therefore uncoupling could be reflected by a change in EGG waveform. However, no quantitative evaluation of this suggestion has been made.

The simplest method to study the dynamics of EGG waveforms in a certain time interval is to divide the number of points with smaller amplitudes than their predecessor by the number of points with greater amplitudes than their predecessor in the whole interval. A ratio greater than unity would indicate that the descending arms of the waves dominated in this interval. These ratios could be obtained for successive time intervals and arranged versus time in a *gradient plot*. The block diagram of an algorithm for a computer program that calculates these ratios and arranges them in a gradient plot is shown in Fig. 4.4.

4.4. METHODS TO ASSESS GASTRIC ELECTRICAL FREQUENCY.

4.4.1. QUANTITATIVE VISUAL ANALYSIS.

This is simply visual counting the number of waves in a certain time interval. It is quite reliable when dealing with SDB signals, but some lower amplitude or irregular LDB

and EGG waves can easily be missed. This reduces the reliability of the method in comparative studies.

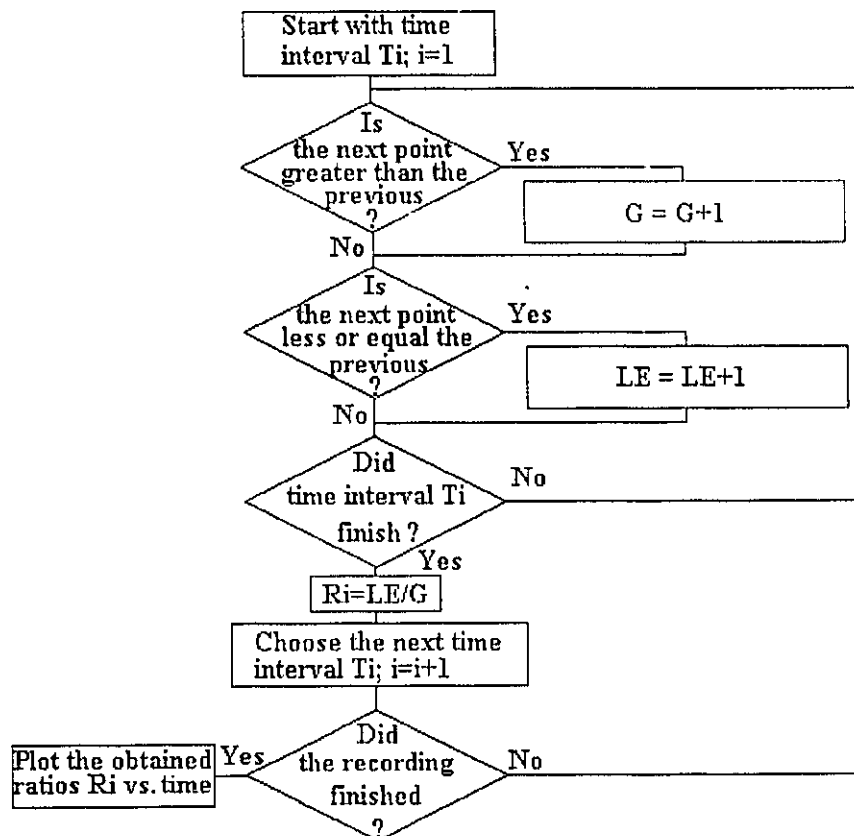


Figure 4.4. Block-diagram of an algorithm to calculate gradient plots.

4.4.2. FREQUENCY ANALYSIS AND TIME-FREQUENCY PLOTS.

While counting SDB waves in the time domain can easily be implemented by computer, a little bit more sophisticated mathematics is required for the analysis of LDB and EGG signals in the frequency domain.

Fourier Transforms.

The two Fourier transforms (64, 65) for any integrable function can be given with:

$$F(f) = \int_{-\infty}^{+\infty} V(t) \cdot e^{-j2\pi ft} dt \quad [4.3a]$$

$$V(t) = \int_{-\infty}^{+\infty} F(f) \cdot e^{j2\pi ft} df \quad [4.3b]$$

where $V(t)$ is a function in the time domain, and $F(f)$ is its image function in the frequency domain. This pair of equations converts signals that are functions of one variable (time or frequency) into functions of the other (frequency or time). The two variables are independent (63). The two transforms are not entirely similar, because of the different sign in the exponent.

It is quite clear that transforming the function (the signal) $V(t)$ from the time domain into the frequency domain to obtain $F(f)$, the integration should be done along the whole time interval in which the function $V(t)$ is defined. In general, if the function is continuous the integration is from $-\infty$ to $+\infty$. However, if the integral is to be solved practically, some real limits are required. Although these limits can be made very large, they can never reach infinity. Therefore, the obtained function $F'(f)$ when the integral is limited is an estimate of the actual function $F(f)$. The phenomenon that comes as a result of this is called "*leakage*" (64) and will be considered later.

On the other hand even if $V(t)$ is a real signal, $F(f)$ is, in general, a complex function which can be expressed as [65]:

$$F(f) = |F(f)| \cdot e^{j\phi(f)} \quad [4.4]$$

where $|F(f)|$ is the magnitude (or amplitude) spectrum of $V(t)$, and $\phi(f)$ is the phase spectrum. The square of the magnitude spectrum is known as the power spectrum. These three entities are very useful for practical evaluation of $F(f)$.

Hartley Transforms.

Recently (65, 66) a new pair of transforms was suggested as a real alternative to the complex Fourier transforms. The idea for the Hartley transforms has been suggested by Ralph Hartley in 1942, and it was more recently further by Bracewell (65). The two transforms are given by

$$H(f) = \int_{-\infty}^{+\infty} V(t) \cdot \text{cas}(2\pi ft) dt \quad [4.5a]$$

$$V(t) = \int_{-\infty}^{+\infty} H(f) \cdot \text{cas}(2\pi ft) df \quad [4.5b]$$

where $\text{cas}(x) = \cos(x) + \sin(x)$. Similarly to the Fourier transforms, these equations constitute time-to-frequency and frequency-to-time transforms. In addition, they are real and the function multiplier in the integral is the same. These two important qualities distinguish the two Hartley transforms making them easier to implement in practice with one and the same procedure. The problem is to define the relationship between the two functions $H(f)$ and $F(f)$ and respectively that between Fourier and Hartley transforms

Relationship between Fourier and Hartley Transforms.

Bracewell (65) points out that if $H(f) = E(f) + O(f)$, where $E(f)$ and $O(f)$ are the even and odd parts of $H(f)$, then:

$$E(f) = [H(f) + H(-f)]/2 = \int_{-\infty}^{+\infty} V(t) \cdot \cos(2\pi ft) dt \quad [4.6a]$$

$$O(f) = [H(f) - H(-f)]/2 = \int_{-\infty}^{+\infty} V(t) \cdot \sin(2\pi ft) dt \quad [4.6a]$$

It is then easy to notice that:

$$E(f) - j \cdot O(f) = F(f) \quad [4.7]$$

Consequently, *the Fourier transform is the even part of the Hartley transform minus j times the odd part. The Hartley transform is the real part of the Fourier transform minus the imaginary part.* It is obvious that one set of Hartley coefficients can produce one and only set of Fourier coefficients and vice versa.

Power (and respectively magnitude) spectra can easily be obtained from the Hartley transform using

$$|F(f)|^2 = [H(f)^2 - H(-f)^2]/2 \quad [4.8]$$

Phase spectrum can be found with

$$\phi(f) = \arctan[F_{\text{imag}}(f)/F_{\text{real}}(f)] = \arctan[-O(f)/E(f)] \quad [4.9]$$

Convolution and Correlation using Frequency Transforms.

The expression for the convolution of two processes, signals or functions is well known and is given with (65):

$$y(t) = \int_{-\infty}^{+\infty} x(t-\tau) \cdot z(\tau) \, d\tau \quad [4.10]$$

if $y(t)$ is subjected to the forward Fourier transform it can be shown that

$$F_y(f) = F_x(f) \cdot F_z(f) \quad [4.11]$$

which means that the convolution between two signals can be obtained simply by multiplying their images in the frequency domain and taking the inverse Fourier transform. Bracewell (65) points out that a similar expression can be obtained using the Hartley transform:

$$H_y(f) = [H_x(f) \cdot H_z(f) - H_x(-f) \cdot H_z(-f) + H_x(f) \cdot H_z(-f) + H_x(-f) \cdot H_z(f)]/2 \quad [4.12]$$

If one of the convolving functions is even (which is often the case in many filtering procedures), this expression becomes similar to [4.11], but the multiplications are real, rather than complex.

The analog version of crosscorrelation can be written as:

$$r_{xy}(t) = \int_{-\infty}^{+\infty} x(t) \cdot y(t+\tau) d\tau \quad [4.13]$$

Similar to the convolution, it can be easily proven that

$$F_r(f) = F_x^*(f) \cdot F_y(f) \quad [4.14]$$

where $F_x^*(f)$ is the complex conjugate of $F_x(f)$. The expression for the crosscorrelation in frequency domain based on Hartley transform is a matter of some sign changes in equation [4.12].

Equation [4.14] can be used as a second method to calculate crosscorrelation and respectively time shifts between different GEA channels. The image of the crosscorrelation function in the frequency domain is usually called the *cross power spectrum* [62].

Since limiting the integral of equation [4.3b] is nothing else but a time-domain multiplication of the signal with a rectangular window, the *leakage effect* mentioned before can now be redefined as the effect of convolution in the frequency domain between the desired spectrum and the spectrum of the rectangular limiting window. As a result of this convolution, spectral components would spread away from the correct frequency, resulting in an undesirable modification of the actual spectrum of the signal (62, 64). The impact of the leakage can be reduced (if it is critical to the processing procedures), using limiting windows that are not rectangular (62, 64).

Discrete Transforms.

The transition from an integral to a discrete Fourier or Hartley transforms has been discussed in many studies (61, 62, 63, 64, 65). Here, the pairs of these discrete transforms will be given, and some effects of the discretization will be discussed.

Discrete Fourier transforms (DFT) are given with (64, 65):

$$F(n) = N^{-1} \sum_{k=0}^{N-1} f(k) \cdot \exp(-j2\pi nk/N) \quad [4.15a]$$

$$f(k) = \sum_{n=0}^{N-1} F(n) \cdot \exp(j2\pi nk/N) \quad [4.15b]$$

where k is the index in time domain, and n is the index in frequency domain.

The pair of discrete Hartley transforms (DHT, 65) is:

$$H(n) = N^{-1} \sum_{k=0}^{N-1} f(k) \cdot \text{cas}(2\pi nk/N) \quad [4.16a]$$

$$f(k) = \sum_{n=0}^{N-1} H(n) \cdot \text{cas}(2\pi nk/N) \quad [4.15b]$$

One of the most important effects of sampling an analog signal is so called "aliasing". It occurs as a direct consequence of not complying with the Nyquist's (or Shannon's) sampling theorem (62, 64), which states that

$$F_s = 1/T_s \geq 2F_h \quad [4.17]$$

where F_s is the sampling frequency, T_s - the sampling interval, and F_h is the highest frequency contained in the signal. If the sampling is done ignoring equation [4.17], the high frequency components of the signal will show up on the left side of the spectrum, thus misleading the investigator that some low frequency components are present. The negative impact of this effect can be avoided by appropriate low pass filtering before the sampling, as well as by choosing an adequate sampling frequency.

One of the main properties of the discrete frequency transforms is that they repeat themselves in the frequency domain at intervals of N points. This symmetry implies that the multiplications between the functions in frequency domain will result in their circular convolution in time domain, which might not always be desired, especially when the signal is not periodic. If linear convolution is to be done, the signals in the time domain with a length of N samples each, have to be padded with zeros up to the $(2N-1)^{\text{th}}$ sample prior to the frequency conversion (see Challis and Kitney, 62).

Fast Algorithms.

To calculate the DFT (or DHT) directly is a tedious work which involves very many multiplications and thus a large amount of computer time. That is why fast algorithms have been suggested first for the DFT (62, 63, 64) and recently for the DHT (65, 66). These algorithms are known as the fast Fourier transform (FFT) and the fast

Hartley transform (FHT). There are two basic groups of algorithms, each of which decomposes the sampled signal in a particular way.

The first is based on a *decimation in frequency*, which decomposes the original signal into sections of sequential samples, until a number of two-sample signals are produced (62). For a two-sample signal the transform is very easy:

$$\begin{aligned} F(0) &= f(0) + f(1) \\ F(1) &= f(0) - f(1) \end{aligned} \quad [4.18]$$

In order that a digital signal of length N be decomposed into $N/2$ two-sample DFTs, N should be a power of 2.

The second main group of algorithms is based on *decimation in time*. The samples that form every new group of samples are not sequential, but alternate. The decomposition results again in $N/2$ pairs of samples, which are then transformed using equation [4.18].

Most FFTs require $N/2 \log_2 N$ complex multiplications and $N/2 \log_2 N$ complex additions, while DFT requires N^2 complex multiplications and $N(N-1)$ complex additions. Theoretically FHT requires the same number of operations as the FFT. However, the fact that the two Hartley transforms are identical and real gives the opportunity to cut significantly the real operating time of the transforms. Bracewell (65) points out that if Fourier coefficients are not to be computed, but instead the power spectrum is calculated directly from the Hartley coefficients using

$$|F(n)|^2 = H(n)^2 + H(N-n)^2 \quad [4.19]$$

the actual computing time is always less when using the FHT. More details can be found in Chapter 8 of Bracewell's book "The Hartley Transform" (65), where a careful comparison between the actual computing times for FFT and FHT is made.

Running Spectrum Analysis.

From the previous discussion it is quite clear that the frequency spectrum of a time segment taken from the analyzed signal represents the distribution of frequencies present in this particular segment. If the segment is very big with respect to the period of the signal and this period changes for a small amount of time within this huge time segment, it is quite possible that in frequency domain this change will not be clearly seen, especially if other noise signals are also present. Therefore, a reasonable compromise between the understandable desire to make N as big as possible (to reduce the leakage effect) and the above considerations should be made. It has been widely accepted EGG signals to be analyzed with 512-point FFT(FHT) and the signal to be sampled with a sampling frequency of 2 Hz (71, 72). This indicates that frequency transforms are to be performed on time segments with a length of 256 seconds (4.27 minutes). Frequency resolution in this case is 0.003906 Hz or 0.234 cpm. Obviously, in order to follow the dynamics of the frequency components in the whole recording, spectra from successive 4.27 min. intervals should be obtained. Kingma et al. (67) proposed to arrange these EGG spectra one behind another with a small shift, forming the so called "three dimensional" (magnitude/power-frequency-time) plots. This technique was later used by Van Der Schee et al. (68, 69) and became known as *running spectrum analysis*.

There are two ways of presenting successive spectra in a three dimensional plot:

- (a) normalize each spectrum separately to 100% in a given frequency window;
- (b) find the absolute maximum of all spectra and normalize it to 100%.

Both methods have advantages and disadvantages. When analyzing the frequency only, the first method is preferable if huge differences in the signal amplitudes are expected. On the other hand, when the differences in the amplitudes are to be investigated the second option should be available.

Instead of taking successive time intervals, it is possible to overlap them, e.g. if the first spectrum is obtained for the time interval (0-255 sec), the second could be calculated in the interval (128 - 383 sec) instead in (256 - 511 sec). This introduces a 50% overlap between the successive time segments. The overlap allows frequency dynamics of the signal to be followed better, but it also increases the number of spectra in the three dimensional plot.

A sample of a 1-hour three dimensional plot of a sine wave with an initial frequency of 0.05 Hz, which changed to 0.07 Hz after the first half hour of recording is shown on Fig.4.5.

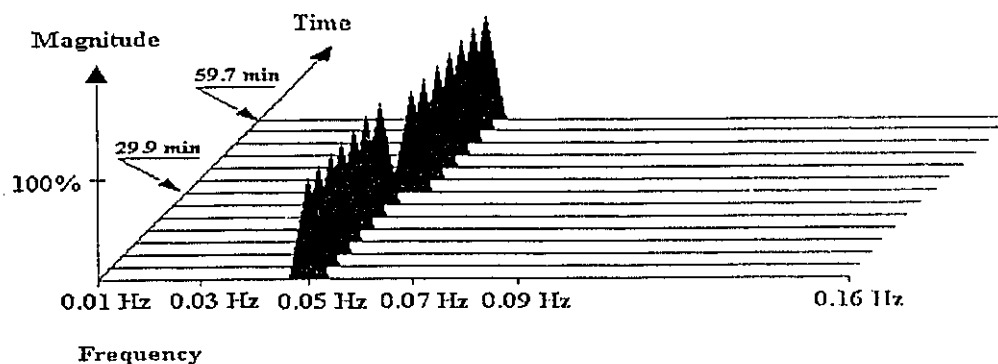


Figure 4.5. One-hour three dimensional plot of a sine wave signal which changes its frequency from 0.05 Hz to 0.07 Hz after the first half hour of recording. The frequency window is 0.01-0.16 Hz

Grey Scale and Contrast Plots.

Normalizing the absolute maximum of all spectra in the three dimensional plot to a 100% can be equivalent to assigning it a black color. On the contrary, white color could

then represent the absolute minimum in the three dimensional plot. All spectral magnitudes in between the two extremes can be represented by the levels of gray color. Thus, one of the dimensions in the three dimensional plot, the magnitude, can be eliminated. In the new two dimensional plot the magnitudes are represented as pixels with different levels of gray from white to black. This plot was first suggested by Van Der Schee et al. (68, 69) and was given the name "*gray scale plot*".

One convenient modification of the gray scale plot for the needs of EGG is the *contrast plot* (70), in which only two colors are present - black and white. When a given spectral component exceeds a predetermined magnitude level (specified in percents), it is represented in the plot with a black pixel. The pixels remain white if the spectral magnitude is below this level.

Time-Frequency Plots.

The spectra from Fig.4.5 are individually normalized to 100%. They explicitly show dominant peaks in the given frequency window. In the *time-frequency plot* (71), the maxima of the dominant peaks from each spectrum are arranged in a plot versus time and connected with lines, i.e. the amplitude information is completely eliminated (Fig. 4.6).

It is quite obvious that

- (a) time-frequency plots are two-dimensional;
- (b) they are built by points, each of which represents the frequency of the dominant peak in the corresponding spectrum;
- (c) since the spectra in the three dimensional plot represent successive time intervals, the points that build up the time frequency plot are shifted with this interval;
- (d) when overlap is introduced, the interval T_I between any two successive points in the time-frequency plot is given with:

$$T_I = [N/F_s].[(100 - OVL)/100] \quad [4.20]$$

where OVL is the percentage of overlap used.

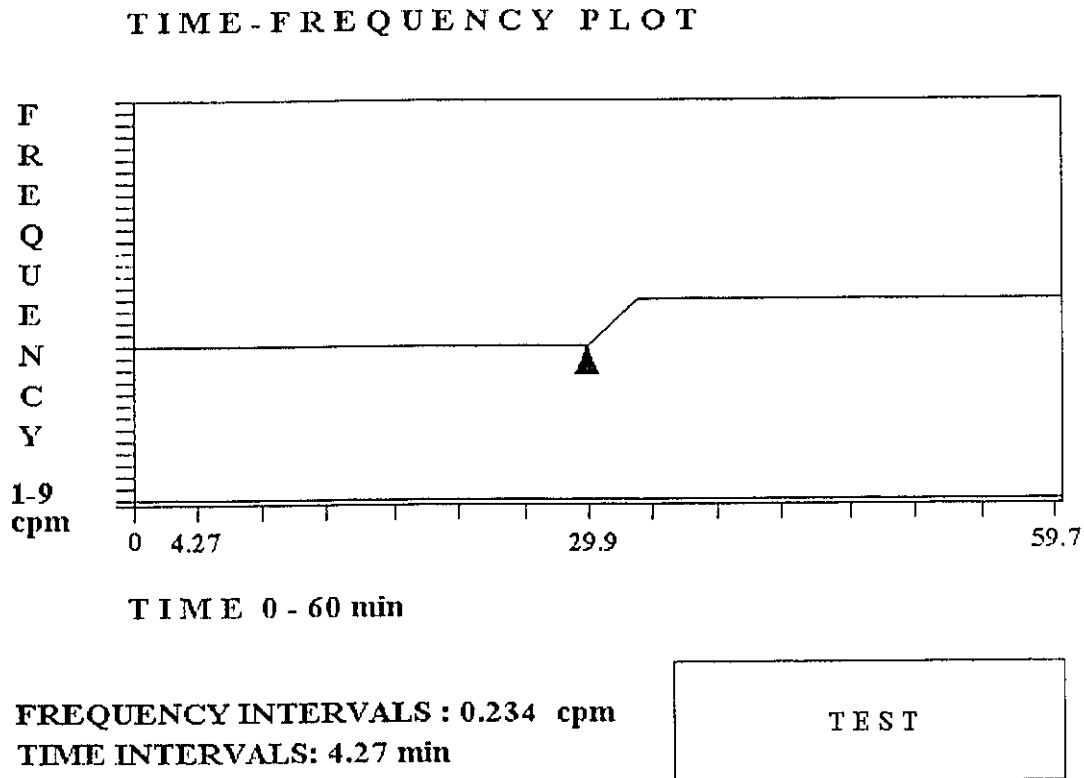


Figure 4.6. Time-frequency plot extracted from the three dimensional plot shown on Fig. 4.5. with frequency scale in cycles per minute (cpm). The moment of the change in frequency is clearly seen.

4.4.3. STATISTICAL EVALUATION OF TIME-FREQUENCY PLOTS.

For every signal interval Δt transformed into frequency domain, there is only one dominant frequency peak and respectively only one point in the time-frequency plot. If a signal with duration D_S is digitized with sampling interval T_S , the number of points in the time-frequency plot N_{tf} is given with:

$$N_{tf} = (\text{int})[(D_S / (N \cdot T_S)) / (1 - \text{OVL} / 100)] \quad [4.21]$$

where N is the number of points of the transform ($\Delta t = N.T_g$) and OVL is the percentage of overlap between the successive time intervals. The points are later arranged versus time and connected with lines to form the actual time-frequency plot. These points can be subjected to various methods of simple statistical evaluation (61, 72, 73). Mean value, variance and standard deviation, called by Challis and Kitney (61) "basic averages", will be used in this study. Mean value M_n is defined as (61):

$$M_n = (\sum F_i) / N_{tf}, \text{ cpm} \quad [4.22]$$

where F_i are the frequency values of the points in cycles per minute (cpm). The variance V_r can be calculated as:

$$V_r = \sum (F_i - M_n)^2 / N_{tf} = \sum F_i^2 / N_{tf} - M_n^2, \text{ cpm}^2 \quad [4.23]$$

The standard deviation SD is the square root of the variance and when assessing time-frequency plots is measured in cycles per minute (cpm), similar to the mean value (61, 72).

Another way of evaluating the points from the time-frequency plot is to build the so called "probability density function" (61, 73). This function measures the probability (in %) of one unknown process or function to have a given value. In the simplest case the probability density function (pdf) of a sine wave with a period of 20 seconds would be a single 100% line at a frequency of 3 cpm. However, if the period of the sine wave changes with the time, many different frequencies would be present and the pdf would become a curve. The probability Pr for the frequency of the sine wave f_w to belong to an interval of frequencies $F_a - F_b$ ($F_b > F_a$) can be given with (73):

$$\Pr(F_a < f_w < F_b) = S_{ab}/S_{total} \quad [4.24]$$

where S_{ab} is the area between the frequencies F_a and F_b , and S_{total} is the total area under the pdf curve. In general, pdf is an analog function. Challis and Kitney (61) point out that the narrower this function is, the more precise the analyzed process is.

The situation changes when for some reason slight changes in the process cannot be assessed by the analytical methods used, i.e. when the resolution of these methods is finite. If, for example, a frequency change of less than 0.024 cpm cannot be measured by the equipment, the pdf of the sine wave with a varying period becomes a stepwise function which could be considered discrete and looks more like a histogram.

The frequency resolution FR of a digital time-frequency plot is finite, and can be given with:

$$FR = f_s/N \quad [4.25]$$

where f_s is the sampling frequency and N is the number of points of the time-to-frequency transform. It is obvious that the pdf of the points of such a time-frequency plot will be a histogram. The width of each bar in this histogram will be equal to the frequency resolution of the time-frequency plot.

Similar statistical evaluations can be used to assess time shift and gradient plots.

4.5. DIGITAL FILTERING OF GEA.

4.5.1. FREQUENCY-SAMPLING FILTERS.

The theory of *frequency-sampling filters* is well described in the literature (63, 64). They can be designed directly in the frequency domain. The designer simply specifies the value one in the passband and zero in the stopband without providing any transition

band. Although this simple filter has a finite impulse response (FIR), i.e. its phase characteristic, is linear, its response may display significant ripple between frequency sample points. This difficulty can be minimized by providing a certain transition band, i.e. there by including transition points between the last unity value in the passband and the first zero value in the stopband. However, there is not a definite rule what the width of this transition band should be in a given case (64).

Frequency sampling filters with a programmable transition band based on the fast Hartley transform will be used in this study. The linearity of the phase characteristic of these filters make them also applicable for time shift studies of EGG.

4.5.2. ADAPTIVE FILTERS.

Although adaptive filtering was introduced in the early sixties, only recently has it been applied to canine GEA signals (74) and human (75) GEA signals. There has not been dramatic success in either subject.

Figure 4.7 shows the typical block-diagram of an adaptive filter as suggested by Widrow et al. (76).

Several simple equations can be written to describe this system (74):

$$z = s + n_0 - y \quad [4.26]$$

which after squaring gives

$$z^2 = s^2 + 2s.(n_0 - y) + (n_0 - y)^2 \quad [4.27]$$

Taking the expectation values (the power) at both sides and presuming that s is uncorrelated with n_0 and y , it can be shown that

$$\min E(z^2) = E(s^2) + \min E((n_0 - y)^2) \quad [4.28]$$

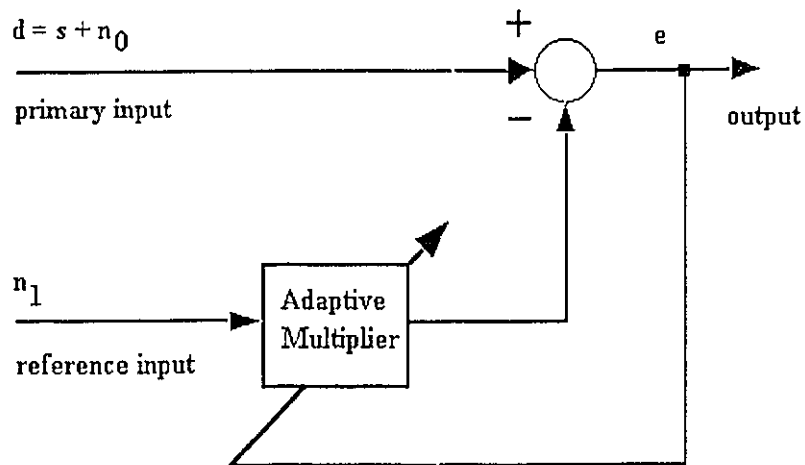


Figure 4.7. Block diagram of an adaptive filter. Recorded signal d is considered a superposition of the primary signal s and the noise n_0 , which are not correlated. The reference signal n_1 is a noise, correlated with n_0 . The objective of the filtering process is to extract the primary signal s .

Consequently, if the output signal power $E(z^2)$ is minimized the signal s will not be affected, but the noise will be eliminated. The minimization process, known as Widrow-Hoff least mean squares (LMS) algorithm (76) is based on the adaptive adjustment of the coefficients w , with which the reference noise n_1 is multiplied to produce the signal y .

Unfortunately, when recording GEA signals it is very difficult to find a pure source of noise. That is why the block-diagram from Fig. 4.7 has been modified first by Kentie et al.

(74) and later by others (75, 77). Instead of using two channels, they suggest using one channel from which the noise channel is derived by a band rejection of the EGG component (Fig. 4.8). This modification, however, is not quite legitimate, because the quality of the noise n_1 , and especially its relations to the signal s are now dependent on the quality of the band reject filter used. In that sense, converting the band reject filter into a bandpass filter and using it directly to eliminate the noise from signal d would have exactly the same result (10).

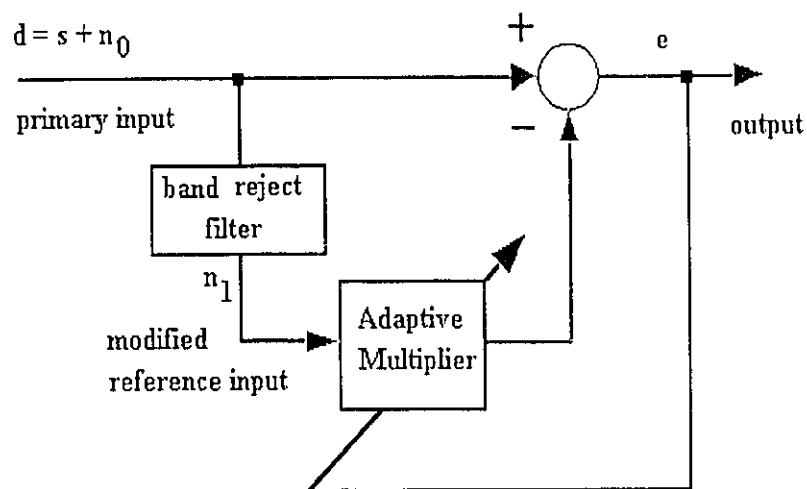


Figure 4.8. A modified adaptive filter for EGG. The noise n_1 is obtained from the recorded signal d using a band reject filter.

The only impact that the adaptive algorithm may have on the output signal is the unknown time shift that it would introduce. In general, this time shift would differ for

different EGG channels and it is not surprising that Chen et al.(41) discovered occasional large time shifts between different EGG channels after using this modified algorithm.

CHAPTER FIVE

ACCURACY OF EGG

5.1. INTRODUCTION.

In the last 10 years there have been several publications describing abnormalities in the gastric electrical activity (GEA) and cutaneous electrogastrogram (EGG) in a variety of clinical conditions (78 - 93). Unfortunately, the diagnostic value of EGG remains in question because although reportedly reliable in recognition of normal frequency and tachygastria, cutaneous recordings have not been shown to be accurate in assessing uncoupling and contractions (39, 42).

Ideally abnormalities of gastric electrical activity would first be recognized with implanted electrodes and the diagnostic value of cutaneous EGG be confirmed by simultaneous recording with both techniques. Unfortunately this is rarely possible. In the current study invasively obtained gastric electrical and mechanical activity were compared to EGG and evaluated the reliability and usefulness of the four major properties of the cutaneous signal i.e., frequency, amplitude, phase lag and wave form.

5.1.1. FREQUENCY.

The gastric slow wave frequency can occasionally be recognized visually in cutaneous recordings, but it is most reliably assessed using computer-aided running spectrum analysis (RSA). Such analysis depends upon wave shape. Invasive recordings obtained with short distance (2-8 mm) bipolar (SDB) electrodes produce signals with waveshapes that preclude recognition of the fundamental frequency with RSA. Spectral comparison of records obtained cutaneously with those obtained from implanted electrodes is therefore difficult if not impossible. A technique has been developed which allows internal recordings to be analyzed with the fast Hartley transform and compared directly with cutaneous EGG signals. A quantitative comparison of the frequency changes in internal and cutaneous gastric electrical activity was also done.

5.1.2. AMPLITUDE.

Increased signal amplitude is often attributed to the appearance of electrical response activity (ERA), (12) and it is therefore assumed to indicate the presence of contractile activity. A significant increase in the amplitude of cutaneous gastric signals has been observed postprandially (9, 11, 12). In this study we determined the reliability of the relationship between amplitude changes in cutaneous EGG and the occurrence of gastric contractions.

5.1.3. PHASE LAG.

The direction of spread of gastric electrical activity over the stomach determines the direction of propagation of contractions. Chen et al.(41) described phase lag (time shift) between different cutaneous EGG channels recorded from fasting and postprandial patients. In the present study the use of cutaneous electrodes to recognize phase lag is reexamined.

5.1.4. WAVE FORM.

Familoni et al. (39) suggested that the propagation direction could be determined from the wave form of the cutaneous EGG. If with a specified electrode configuration, the ascending portion (arm) of each wave was shorter than the descending arm propagation of the EGG wave was considered aboral. This concept has been reexamined.

5.2. METHODS.

5.2.1. SUBJECTS.

These studies were performed on one patient with surgically implanted and cutaneous electrodes, four volunteers with cutaneous electrodes, another four volunteers with an intraluminal pressure (ILP) recording tube and cutaneous electrodes, and four anaesthetized dogs with serosal electrodes, serosal force transducers (FT) and cutaneous electrodes. In two of the dogs an intraluminal distending balloon was introduced also. The clinical study was approved by the Ethics Committee of the University of Alberta Hospitals and informed written consent was obtained from each subject before the procedure. The animal study was approved by the University of Alberta Health Sciences Animal Welfare Committee.

The patient was a 42 year old female with a 10 year history of recurrent anorexia, nausea, vomiting, heartburn and weight loss. Three years earlier a vagotomy and pyloroplasty had been done for duodenal ulcer without improvement in her symptoms. Investigation revealed slow gastric emptying with no organic obstruction and gastroesophageal reflux. She underwent fundoplication and insertion of three sets (3 cm apart) of stainless steel wire bipolar electrodes (0.5 cm apart) into the serosa of the antrum at operation. The technique was previously described (10). The electrodes were removed nine days following operation. Four abdominal surface electrodes (Hewlett Packard 14445) were attached on the abdominal surface overlying the serosal electrodes. Three 2-hour recordings of serosal and cutaneous electrical activity of the patient in fasting state were performed on subsequent days. Five additional recordings of 1 hour fasting and 1 hour postprandial activity were also performed on subsequent days. A standard 500 Kcal meal containing 68g of CHO (52%), 24g of protein (19%) and 17g fats (29%) was ingested during a twenty-minute break between the fasting and postprandial recordings.

Four volunteers underwent recording of the cutaneous EGG for 1 hour fasting and 1 hour after the test meal. It was assumed that the lesser curvature begins at the Xiphisternum and ends at the point where the midclavicular line meets the costal margin. The greater curvature is situated to the left and inferior to that line depending on gastric distention. The most proximal electrode was placed 5 cm left of the Xiphisternum on the costal margin, and a row of 4 more electrodes (3 cm apart) was placed linearly between the first electrode and the junction of the midclavicular line with the right costal margin.

In four other volunteers a four-tube perfused intraluminal pressure monitoring assembly was introduced and positioned fluoroscopically in the gastric antrum. The recording assembly had four openings at 5 cm intervals from the distal tip. The tubes were perfused with water by an Arndorfer pump. Simultaneous 2-hour recordings of ILP and cutaneous EGG in the fasting state were obtained from each subject.

Four fasting dogs underwent a laparotomy under Pentotal anesthesia. Three sets of bipolar electrodes (0.5 cm apart) and force transducers were sutured to the antral serosal surface at 3 cm intervals. In two of the dogs a fundal gastrotomy was made and a 7 mm diameter tube with attached latex balloon for stomach distention placed into the antrum. Four cutaneous electrodes (3 cm apart) were placed on the shaved anterior abdominal wall.

In the dogs and the patient with implanted electrodes two types of recordings of serosal electrical activity were made. The usual SDB recordings from pairs of electrodes placed close together were obtained. In addition by using electrodes from different SDB pairs new pairs were obtained to give a long distance bipolar (LDB) recording. The increment in distance between internal serosal bipolar electrodes produced signals with similar waveshape and spectral characteristics as those obtained cutaneously. Spike activity clearly recognized in SDB channels could not be seen in LDB recordings. After amplification and filtering the data were sampled at a rate of 10 Hz and an analog-to-digital conversion made.

5.2.2. FREQUENCY.

To study gastric frequency 2-hour experiments were performed on the patient (2 LDB, 2 SDB and 2 cutaneous bipolar channels, fasting and postprandial state), 4 healthy volunteers (2 cutaneous bipolar channels, fasting and postprandial state) and four unconscious fasting dogs (2 SDB, 2 LDB and 2 cutaneous bipolar channels). The experiments on the patient were repeated on 5 consecutive days after the operation. For the LDB and cutaneous channels a time constant of 10 s (cut-off frequency of the high pass filter of 0.017 Hz) and cut-off frequency of 0.3 Hz of the low pass filter were used, while for the SDB channels these parameters were 0.3 s and 4 Hz respectively.

To determine the reliability of registration of rhythm changes in LDB and cutaneous channels in the time domain, periods from the SDB with more than 25% change in duration than the preceding period were compared to the same periods in LDB and cutaneous recordings.

When representing the frequency dynamics, best results were achieved by normalizing each spectrum in the power 3-D plot so that the fundamentals of all spectra had the same height. Power changes over time were therefore obscured, but the dynamics of the frequency peaks were clearly seen. Time-frequency plots of each channel were plotted as well using the methodology described in Chapter 4.

5.2.3. AMPLITUDE.

Three different experiments were performed to determine the relationship between antral contractions and cutaneous EGG amplitude changes.

A comparison was made between contractions noted in ILP recordings and increments in amplitude seen with cutaneous electrodes in 2-hour experiments with 4 healthy fasting volunteers (2 channels cutaneous EGG, 3 channels ILP). Recognizable

contractions in an ILP channel were defined when the recorded pressure waves exceeded 25% of the maximal pressure recorded during the whole experiment in this channel. Similarly, recognizable increments in each separate cutaneous EGG channel were defined when the amplitude exceeded 25% of the maximal recorded EGG amplitude in this particular channel.

In two fasting dogs (2 channels SDB, 2 channels LDB, 2 channels FT and 2 channels cutaneous EGG), contractions as demonstrated by serosal FT were compared with the changes in SDB, LDB and cutaneous EGG. The periods of spike bursts in SDB were also compared to contractions and amplitude changes in LDB and cutaneous EGG. Antral contractile activity was stimulated with 0.25 mg/kg Pentagastrin IV on four separate occasions. Twenty minutes after each Pentagastrin injection mechanical activity was blocked with 0.25 mg Glucagon. At the end of each experiment all antral contractile activity was blocked with 0.25 mg Atropine and 0.25 mg Glucagon. The antral balloon was then distended intermittently in stages after 200, 400 and 600 ml air were introduced. Each air inflation was done for approximately 20 seconds and the new air volume was maintained for 5 minutes. Four distentions were performed in each dog. Changes in cutaneous EGG amplitude were noted. The examined amplitudes were considered increased when they reached or exceeded the level of 25% from the maximum both for the EGG and the FT channels.

5.2.4. PHASE LAG.

In three 2-hour recordings from the patient in the fasting state, LDB and SDB serosal signals obtained from different areas of the stomach were compared with 4 channels cutaneous EGG, recorded from the orthogonal projections of those areas on the abdominal wall. Separate 2-hour experiments were also performed on 4 fasting dogs using a similar electrode configuration.

In four volunteers 4-channel cutaneous EGG was recorded for 2 hours (1 hour fasting and 1 subsequent hour postprandially) using the above cutaneous electrode configuration.

In all recordings from the patient, volunteers, and dogs the signal from the proximal electrode was compared to the signal from the distal one. It was pointed out previously (see Chapter 4) that with running cross-correlation analysis mean time shifts could be obtained. This approach was applied for 4.27 minute intervals and the obtained time shifts were arranged in a plot against time (time shift plot). The recordings were filtered (bandpass digital filter, 0.02-0.1 Hz) so that only the fundamental gastric component remained. The processing was done using the fast Hartley transform (FHT, 66) and the cross-correlation functions were successively obtained from the transform. The possibility for direct calculation of the cross-correlation function from the Hartley coefficients was mentioned by Bracewell (65, 66) and described in Chapter 4. It was found to be more convenient for the time shift study than the method proposed by Chen et al. (41). Recorded time shifts were defined as "significant" if they exceeded 2.5 s (approximately a quarter of the half-period of the signals).

5.2.5. WAVE FORM.

The wave form was studied in the same experiments that measured gastric frequency. A cut-off frequency of 0.3 Hz was used instead of 0.5 or 1 Hz as recommended before (41) and thus most of the respiration artifacts were avoided, preserving the first three harmonics of the signal. To assess the changes in the wave form both ascending and descending arms of each wave were compared by a computer program which utilized the gradient method described in the previous chapter. The study was done separately in the fasting and postprandial state for the humans and before and after gastric distentions in dogs.

5.3. RESULTS.

5.3.1. FREQUENCY.

There was good correlation between the different recording methods. A comparison of visually evident frequency changes recorded with cutaneous and implanted electrodes is given in Table 5.1. Intermittent irregularities in gastric electrical activity were recorded from the patient during the first postoperative day (Fig. 5.1).

A well-defined peak of the fundamental gastric frequency in the spectral range of 2.54-3.67 cycles per minute (cpm) was recognized after the application of the Fast Hartley Transform (FHT) on successive 4.27 minute intervals of human cutaneous recordings. Use of the FHT (instead of the FFT) increased both the speed of spectral procedures and conversion speed .

Table 5.1. *Recognition of changes in gastric electrical frequency by different recording methods.*

	LDB/SDB, %	EGG/SDB, %	EGG/LDB, %
Patient	93	87	83
Dog 1	95	88	84.5
Dog 2	89	83	79
Dog 3	93	82	80
Dog 4	91	85	82.5

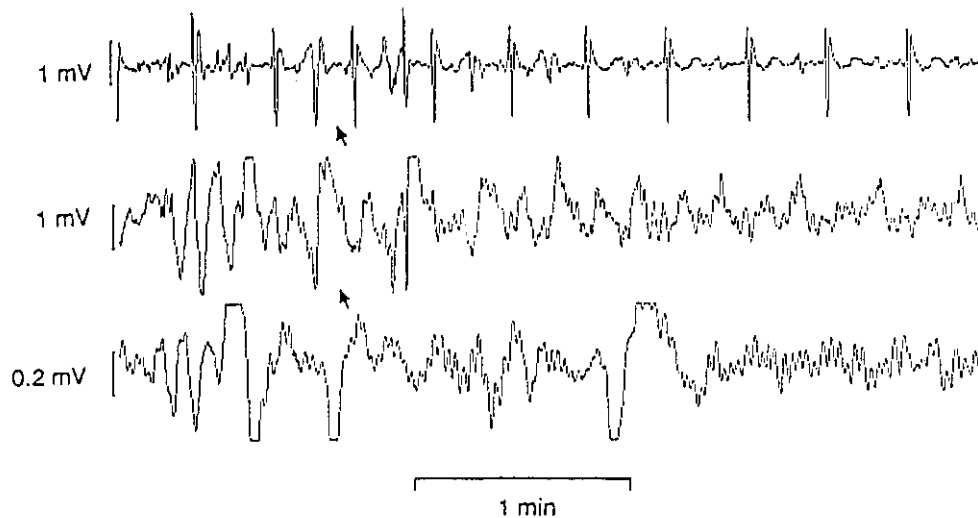


Figure 5.1. Gastric electrical signals obtained with SDB electrodes (top), LDB electrodes (center), and cutaneous electrodes (bottom) during the first postoperative day of the patient. Rhythm irregularities are clearly seen.

Computer frequency analysis could not be reliably applied to recordings obtained with electrodes implanted into the stomach in the usual manner i.e., short distance bipolar (SDB) recordings. The rapid bi-directional wave obtained in such studies yielded a broad frequency spectrum, in which the fundamental EGG component can be obscured. The use of pairs of implanted electrodes separated by several centimeters (long distance bipolar recordings, LDB) resulted in a signal that approximated a sine wave and resembled the cutaneous signal. This could be easily analyzed by the FHT. Comparison of frequency spectra obtained by implanted and cutaneous electrodes then became possible. Similar wave shapes and spectral characteristics were seen in LDB recordings and cutaneous EGG (Fig.5.2). Normalized 3-D plots were also very similar (Fig.5.3). The plots clearly showed postprandial frequency increments as reported before [9, 11, 12, 17, 45].

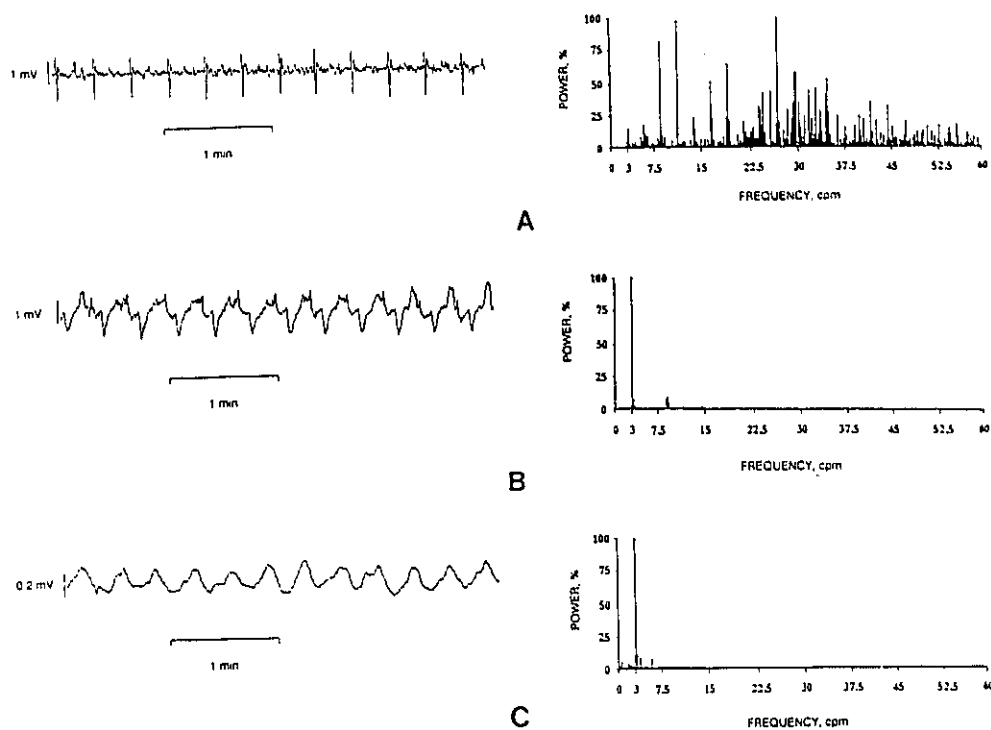


Figure 5.2. Human gastric electrical signals obtained with SDB electrodes (left, A), LDB electrodes (left, B) and cutaneous electrodes (left, C) and their respective power spectra (right, A-C).

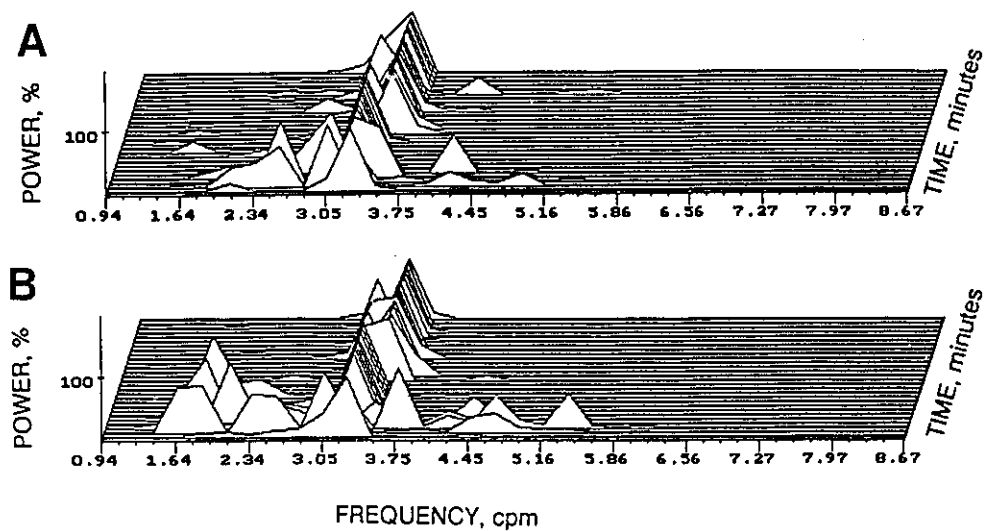


Figure 5.3. Two-hour (1 hour fasting and 1 hour postprandial) three-dimensional plots of LDB signal (A) and cutaneous EGG (B) of the patient. Power spectra are calculated from successive 4.27-minute intervals without overlapping. Postprandial increment in the frequency is seen in both channels.

5.3.2. AMPLITUDE.

The amplitude of electrical signals from internal electrodes varied with distance from the pylorus in the patient (0.6 - 2.2 mV) and dogs (0.4 - 2.0 mV). Cutaneous EGG were also of higher amplitude in electrodes near the pylorus in humans (0.05 - 0.52 mV) and dogs (0.01 - 0.45 mV). Force transducer amplitudes ranged from 0 to 0.54 N and intraluminal recordings ranged from 0 to 127 cm H₂O. In dogs and humans amplitude changes in cutaneous EGG did not reliably reflect gastric contractions. Only a minority of increased EGG signal amplitudes was associated with contractions and the majority of contractions was not associated with increased EGG amplitude (Fig.5.4, Fig.5.5).

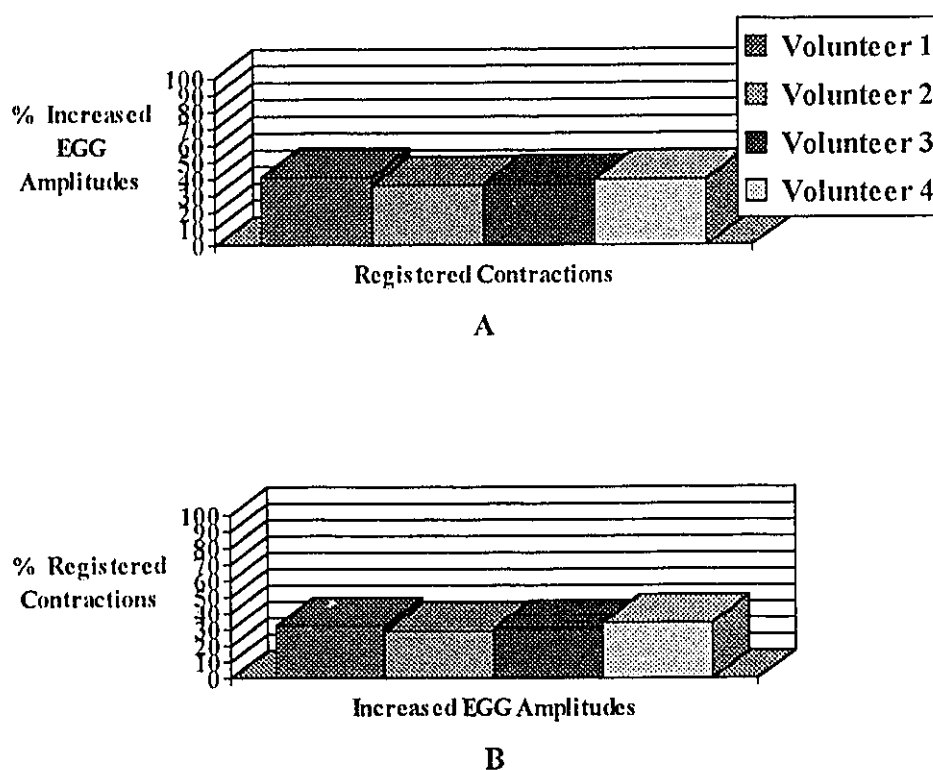


Figure 5.4. Relationship between gastric contractions and changes in EGG amplitude in normal volunteers: (A) incidence of increased EGG amplitudes during gastric contractions and (B) incidence of gastric contractions during increased EGG amplitudes.

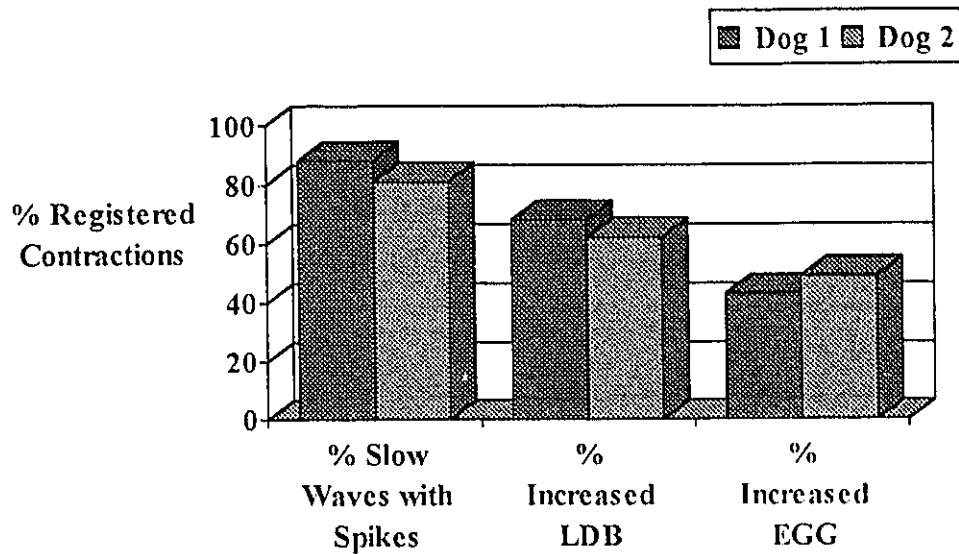


Figure 5.5. Incidence of gastric contractions when (Left) SDB channels displayed spikes; (Center) Increased signal amplitude was observed in LDB channels; and (Right) Increased signal amplitude was observed in EGG recordings.

Distention of the atonic canine stomach with a balloon increased the amplitude of EGG signals even when gastric contractile activity was completely abolished by Atropine and Glucagon (Fig. 5.6).

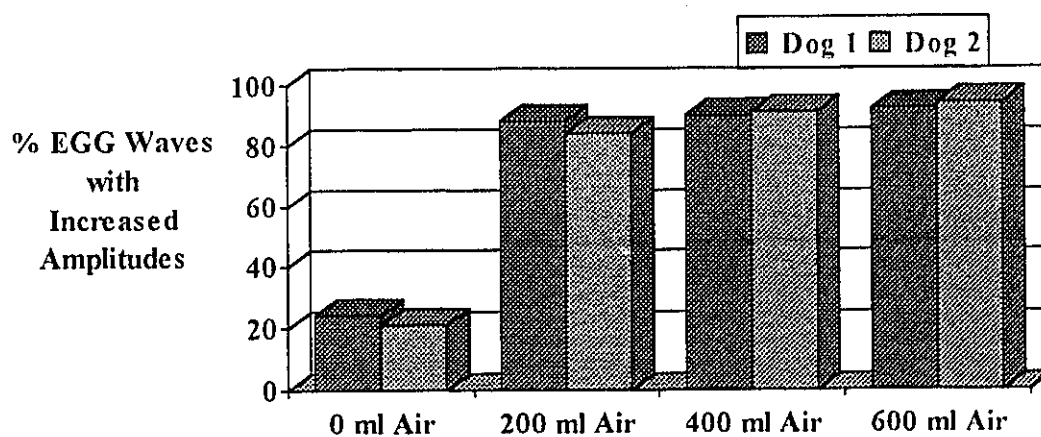


Figure 5.6. Effect of gastric distention on incidence of increased EGG signal amplitudes.

Most of the cutaneous EGG amplitudes increased significantly after air infiltration, while force transducer channels and signals recorded with internal electrodes did not change (Fig. 5.7).

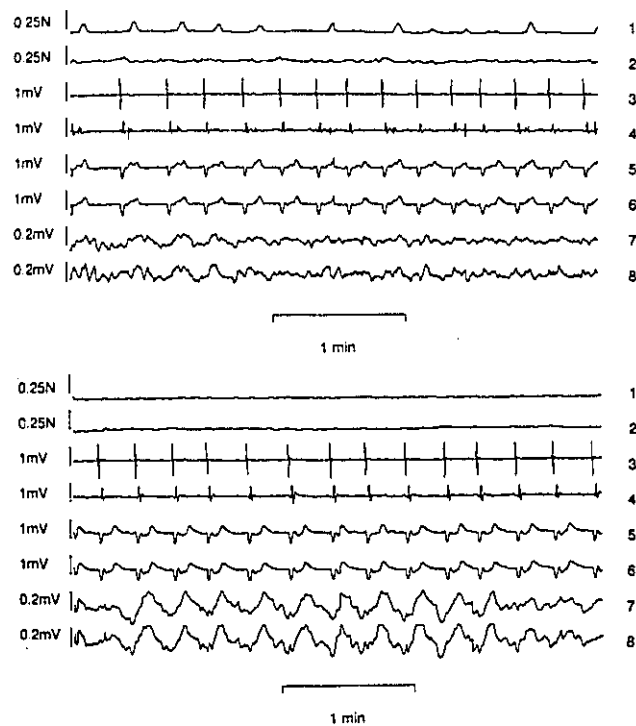


Figure 5.7. Signals recorded from nondistended (top) and distended (bottom) canine stomach with force transducers (1, 2), SDB electrodes (3, 4), LDB electrodes (5, 6) and cutaneous electrodes (7, 8). Gastric distention after blocking the mechanical activity with atropine and glucagon led to significant increment in the cutaneous but not internal recordings.

Figure 5.8 shows the change in EGG amplitude at the moment of gastric distention, while FT channels remain unchanged.

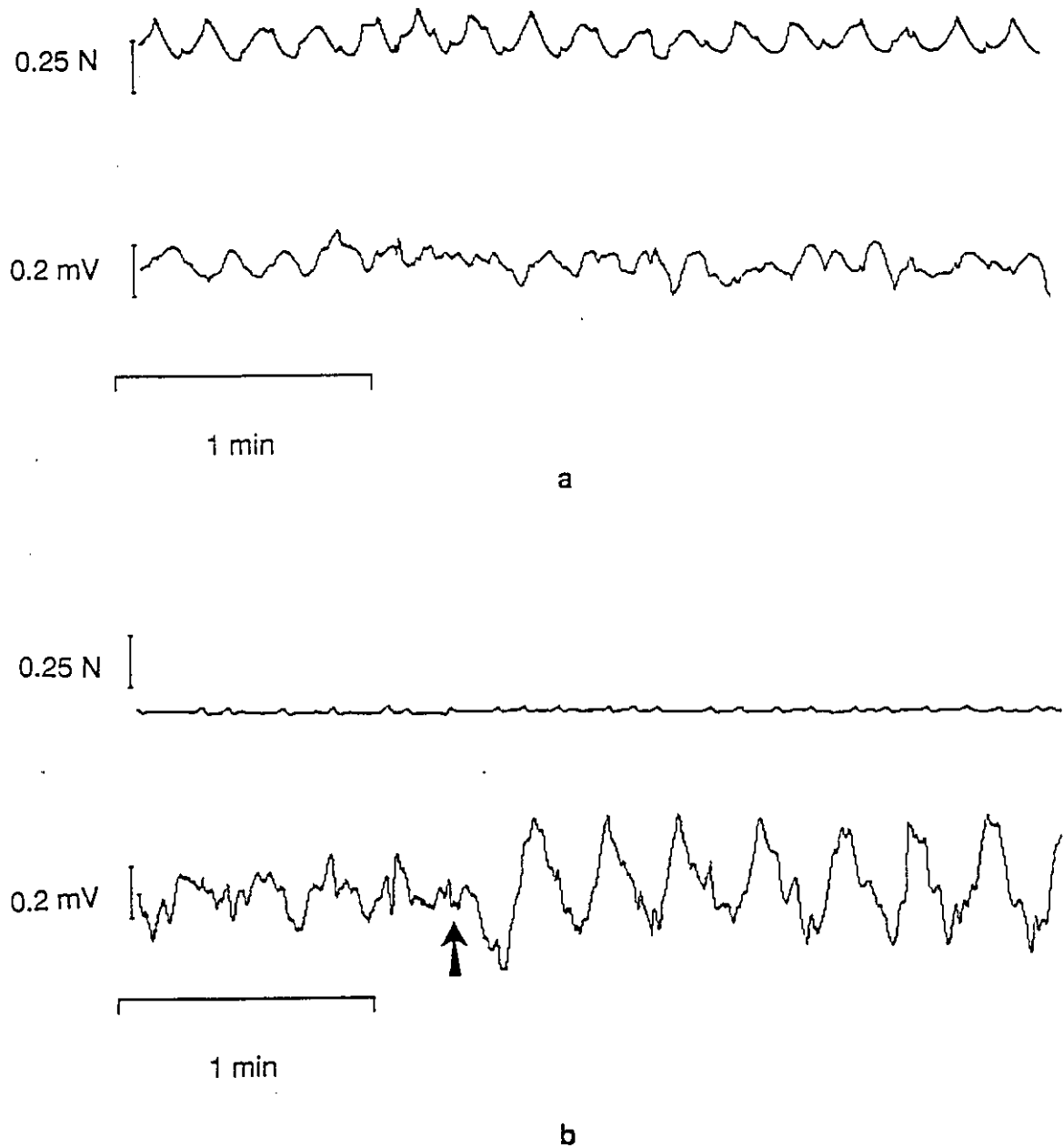


Figure 5.8. Mechanical activity of the stomach (top) and EGG (bottom) before any blocking of contractile activity (a) and after that (b). The moment of distention is marked with an arrow. A significant increase of EGG amplitude is clearly seen.

5.3.3. PHASE LAG.

In the patient with implanted and cutaneous electrodes time shift (phase lag) between the most distal and the most proximal implanted electrodes was consistently between 5 and 8 seconds. In cutaneous recordings, however, no time shift was recorded in 2 of the 6 recording hours (Fig.5.9). In the remaining 4 hours the time shift was very small ranging from 0.5 to 1.8 seconds.

The time shift obtained from the four volunteers was less consistent in the fasting state, probably due to the worse signal-to-noise ratio. After a test meal it became stable but remained close to 0.

The time shift obtained from internal electrodes in dogs varied from 3 to 7 seconds. Cutaneous recordings, however, revealed small but consistent time shift of 0.5 to 1.8 seconds for 64 % of the 8 hour recording time.

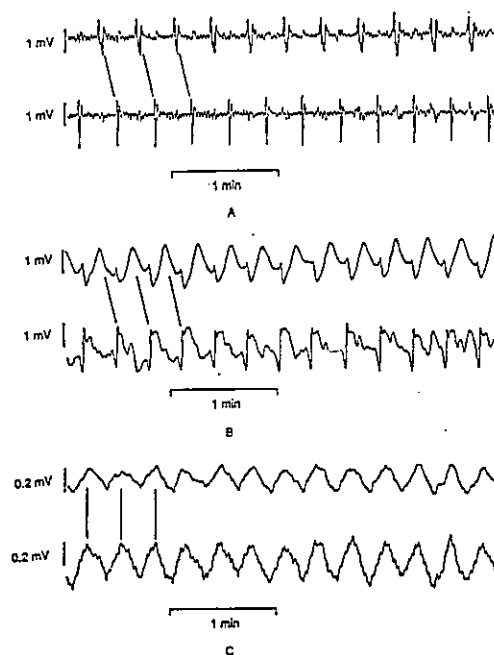


Figure 5.9. Time shifts between pairs of SDB (top), LDB (middle) and EGG (bottom) channels. SDB and LDB pairs were implanted in proximal and distal antrum. EGG electrodes were overlying the LDB ones.

5.3.4. WAVE FORM.

In the fasting state wave forms displayed small predominance of the descending arms or symmetry in all subjects. After feeding of the humans the descending arm in cutaneous waves dominated more evidently, but still this predominance was insignificant. Distention of the canine stomachs had little effect on the wave form of LDB signals, but slightly increased the preponderance of the descending arms in cutaneous EGG waves (Table 5.2).

Table 5.2. *Quantitative study of GEA Waveform.*

	Recording Method	State	Waves with Prolonged Ascending Arm, %	Waves with Prolonged Descending Arm, %	Symmetrical Waves
Patient	LDB	Fasting	24	64	12
	LDB	Fed	7	82	11
	EGG	Fasting	5	53	42
	EGG	Fed	2	62	36
Dogs	LDB	Fasting	0	82	18
	EGG	Fasting	0	80	20
Volunteers	EGG	Fasting	6	33	61
	EGG	Fed	4	55	41

The differences between the ascending and descending arms in all recordings were small and gradient plots in all measurements showed very little deviation from symmetry in favor of the descending arms (Fig.5.10).

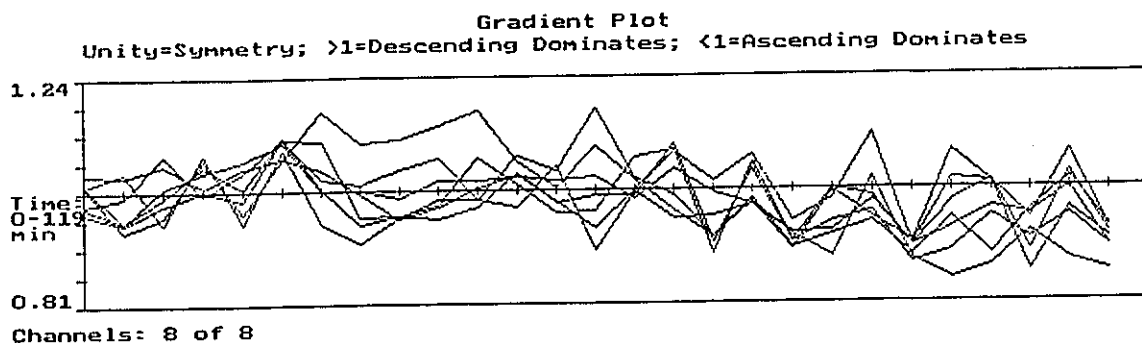


Figure 5.10. A typical gradient plot of multichannel EGG recorded from a volunteer. Only a slight dominance of the descending arms was noted.

5.4. DISCUSSION.

Each single gastric antral muscle cell undergoes periodic depolarizations and the muscular array simulates a series of relaxation oscillators i.e., higher frequency oscillators pull up lower frequency oscillators to the higher frequency. The highest frequency oscillator in man lies high in the greater curvature and periodically depolarizes 3 times per minute. Entraining all distal oscillators whose intrinsic frequency is lower to this frequency results in an aboral spreading wave of depolarization. Electrical response activity (ERA) which heralds contractions is superimposed upon electrical control activity (ECA) so the frequency and direction of propagation of ECA waves determines the frequency and direction of propagation of contractions.

Abnormalities in gastric electrical activity could have a profound effect on gastric motor function so the recent quickening of interest in the electrogastronomy is very

understandable. Using EGG, a large and growing number of clinical conditions have been associated with gastric electrical abnormalities. Before accepting these findings as "true bills", two vital questions demand answers:

1. Does the EGG accurately reflect gastric electrical activity?
2. Does the reported electrical abnormality have an effect on gastric motor function?

Most recorded EGG abnormalities have been changes in frequency, usually reported as bradygastria or tachygastria. Several authors have suggested that increments in EGG amplitude are associated with antral contractions (9, 11, 12, 45).

The present study clearly demonstrates that the amplitude of EGG signals can increase significantly when there are neither antral contractions nor spikes in the SDB channels. A changed or changing position of the antrum with respect to the skin electrodes is sufficient to cause increased amplitude in cutaneous EGG. Such changes could for example be the result of feeding or any other mechanical displacement, which leads to a change in the distance between the source of the electrical field in the stomach and the cutaneous electrodes.

Running cross-correlation analysis based on direct application of the FFT facilitated the study of time shift dynamics. Chen et al. (41) have reported occasional significant phase lags (or time shifts) between different sets of cutaneous electrodes. However we could not confirm these results. No significant (above 2.5 s) time shift were noted in the different sets of cutaneous electrodes. It is possible that the EGG signal is so integrated, that the actual time shifts recorded internally cannot be registered on the abdominal wall or they are very small.

Familoni et al.(39) suggested that oral propagation of gastric electrical signals would result in prolongation of the ascending arm of the waves. In this study the descending arm dominated in both internal LDB and cutaneous recordings in humans and dogs. After feeding or gastric distention this preponderance became more marked in cutaneous recordings, probably due to an improved signal-to-noise ratio. Preponderance

of the ascending arm of the waves was rarely observed. Unfortunately oral propagation of gastric slow waves was not seen during this study and the hypothesis suggested in (39), could not be directly tested.

Electrogastrography, although a very appealing non-invasive technique is not currently of clinical diagnostic value. There is insufficient evidence that 1) abnormalities in EGG are commonly present in patients with gastric motor dysfunction, and 2) cutaneous EGG can actually record gastric electrical abnormalities. Only gastric electrical frequency can be assessed with good reliability by EGG. Therefore, at the present time the information coded in gastric frequency determines the clinical value of EGG.

CHAPTER SIX

**DERIVATION OF AN OBJECTIVE METHOD
FOR CLINICAL STUDY OF EGG.**

6.1. INTRODUCTION.

Many authors (82-89, 92-94, 97, 103, 111) attempted to use electrogastrography for clinical assessment of gastric motility disorders. Unfortunately, only qualitative (and therefore subjective) methods of evaluation of the EGG were suggested. In this study an attempt is made to derive an objective quantitative method of evaluation of gastric electrical activity including EGG.

In order to establish the differences between normal and abnormal EGG patterns a study of normal volunteers was performed. The discussion in the previous chapters imply several important suggestions for the direction of the study:

- (a) the frequency of the EGG signals reliably represents gastric electrical frequency and at the present time it is the only parameter that can be used for clinical evaluation of EGG;
- (b) time-frequency plots obtained with or without overlap are a convenient way to represent dynamics of the dominant spectral component of EGG signals during the experiment;
- (c) gastric electrical activity in normal subjects is assumed to be regular and coupled, therefore frequencies recognized from different EGG channels should be ideally the same, but since the recordings are performed in vivo some minor deviations are expected;
- (d) overlap of the time intervals used in calculation of time-frequency plots can affect the stability of these plots.

6.2. METHODS.

This study was performed on 15 healthy volunteers (6 male and 9 female) without any history of gastrointestinal complaints for one hour in the fasting state and one consecutive hour postprandially with a short (15-20 min.) interruption for feeding. A standard 500 Kcal meal was given to the subjects for postprandial studies. To record the

EGG a row of five standard neonatal EKG monitoring electrodes numbered from 1 (most proximal) to 5 (most distal) was placed along the abdominal projection of the stomach axis on each subject. The distance between the centers of two electrodes in the row was 2.5 cm. Eight bipolar EGG channels were recorded using the same electrode combinations for all subjects. Table 6.1. shows the electrode combinations used. The electrode surface was kept constant.

Table 6.1. *Electrode combinations used for different EGG channels. Electrode 1 was the most proximal, Electrode 5 - the most distal.*

	Channel 1	Channel 2	Channel 3	Channel 4	Channel 5	Channel 6	Channel 7	Channel 8
Elec-								
trodes	1-2	2-3	3-4	4-5	1-3	2-4	1-4	1-5

The settings of the equipment were the same as in Chapter 5 (experiments with cutaneous electrodes). The signals were acquired with a 10 Hz sampling frequency. In off-line studies however, the sampling frequency was reduced to 2 Hz after digital filtering with sampling filters in the frequency band 0.02- 0.1 Hz, i.e. only the first one or two EGG frequency components were retained for further processing.

Separate time-frequency plots were obtained in the fasting and postprandial states from each subject. The plots were built from successive spectra obtained after 512-point FHT of 4.27 min. intervals of the recorded EGG signals. Plots obtained from different EGG channels were superimposed on the computer screen using different colors. The impact of 75% overlap on the time-frequency plots was investigated.

To evaluate quantitatively EGG, statistical evaluation of the points that built up each time-frequency plot was performed including calculation of the mean value, variance

and the standard deviation as well as computation of the probability density function of the frequencies present in the plots (see Chapter 4). It was assumed that the standard deviation was indicative of the level of stability of the time-frequency plot in a given EGG channel. Instability of the time-frequency plot could be caused by two factors:

- (a) irregularities in gastric electrical frequency;
- (b) external factors (noise, motion artifacts, etc).

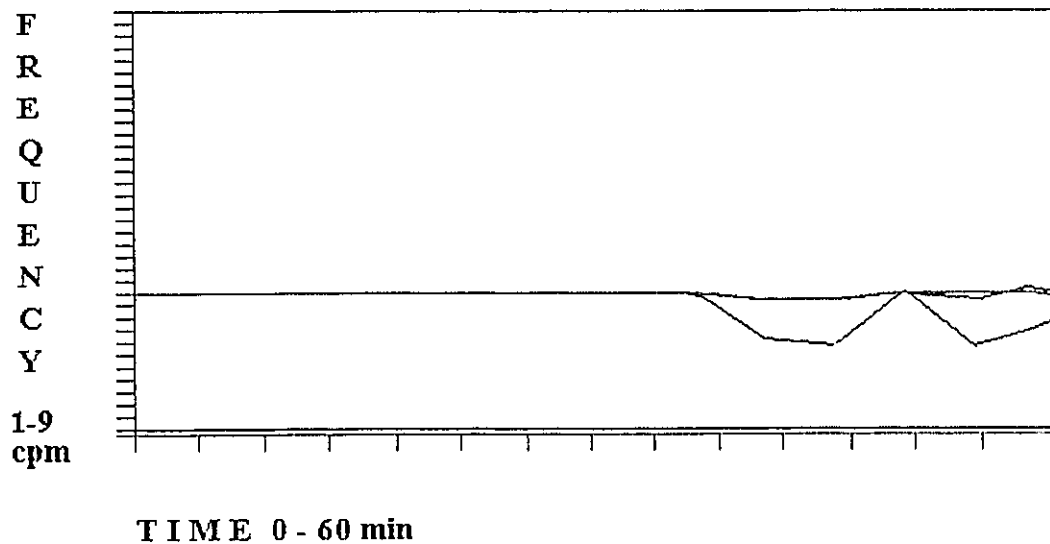
Keeping in mind that the probability density function (pdf) shows the distribution of the points that represent different EGG frequencies in the time-frequency plot, it is obvious that the maximum of this function for a given EGG channel would be at the frequency that is most often present in this channel during the whole test. If the pdf maxima derived from the time-frequency plots of different EGG channels coincide, the same frequency dominates in these channels. Lack of coincidence would indicate an absence of the same dominating frequency in different EGG channels.

6.3. RESULTS.

6.3.1. STATISTICAL EVALUATION OF TIME-FREQUENCY PLOTS.

Mean value, variance and standard deviation (called here basic averages) of the points that built up the time-frequency plots of different EGG channels were calculated to evaluate the stability of the dominant spectral component. The overall results from all volunteers showed that at least in three out of eight EGG channels the standard deviation of the dominant frequency component as assessed from the time-frequency plots was less than 0.450 cpm. These channels were qualified as stable. The frequency range as assessed by the mean frequency in the stable channels was in the range 2.5 - 3.75 cpm. Typical time-frequency plots obtained from a healthy volunteer and its statistical evaluation are shown on Fig. 6.1 and Table 6.2 respectively.

TIME - FREQUENCY PLOT



FREQUENCY INTERVALS : 0.23 cpm
 TIME INTERVALS: 4.27 min

PATIENT: X. H.
 DATE: 19.03.1993.

Figure 6.1. Typical time-frequency plots obtained for each EGG channel recorded from a healthy volunteer.

Table 6.2. Basic averages obtained from the time-frequency plot on Fig.6.1. Only one EGG channel showed standard deviation higher then 0.450 cpm.

	Ch. 1	Ch. 2	Ch. 3	Ch. 4	Ch. 5	Ch. 6	Ch. 7	Ch. 8
Mean Value [cpm]	3.030	3.013	3.013	3.013	2.645	3.013	3.013	3.013
Variance [cpm ²]	0.190	0.007	0.007	0.016	0.460	0.007	0.007	0.007
Standard								
Deviation [cpm]	0.436	0.085	0.085	0.085	0.678	0.085	0.085	0.085

Maxima of the probability density functions (pdf) obtained from the time frequency plots of the stable EGG channels coincided at the frequency of the dominant spectral component (Fig. 6.2).

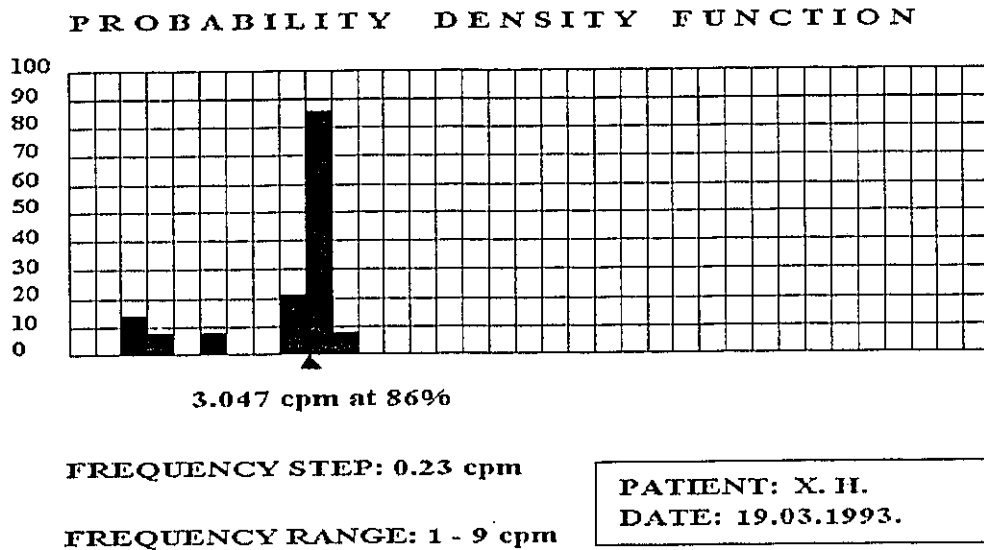


Figure 6.2. Probability density functions of the points that built up the time-frequency plots of Fig. 6.1. Maxima coincided at 3.047 cpm, but some other frequencies were also present.

6.3.2. IMPACT OF THE OVERLAP.

Introducing a 75% overlap of the time domain intervals when building time-frequency plots improved their stability (Fig.6.3), reduced the standard deviation (Table 6.3) and narrowed the probability density functions (Fig.6.4) in 8 out of 15 cases. In 3 out of 15 cases the overlap had a negative effect on the stability of the time-frequency plots, worsened the standard deviations and widened the probability density functions. In all these cases, however, at least three EGG channels exhibited standard deviations less than 0.450 cpm and the maxima of their probability density functions coincided. Four out of 15

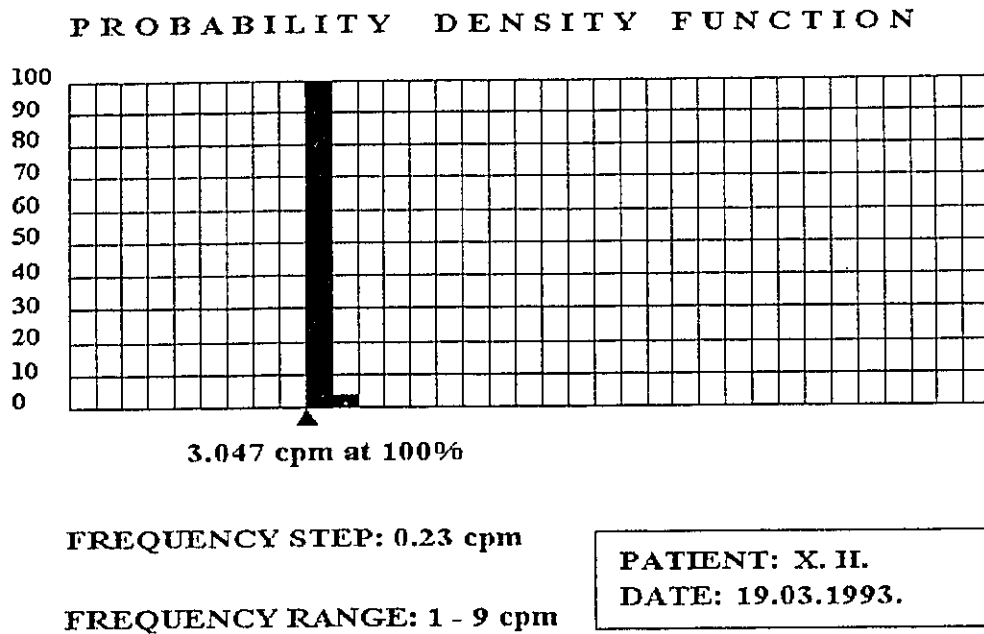


Figure 6.4. Probability density functions of the time-frequency plots obtained with 75% overlap were narrower than these shown on Fig. 6.2. Coincidence of their maxima was more evident.

6.3.3. CRITERION FOR STABILITY.

The above results indicated that a criterion for stability of the dominant frequency component as assessed from the time-frequency plots of different EGG channels could be established as follows:

The standard deviation of points that build up the time-frequency plots obtained with or without 75% overlap (whichever technique provided minimal standard deviation) should be less than 0.450 cpm in at least 3 out of 8 EGG channels recorded with standard disposable neonatal EKG electrodes positioned in a row collinear with the abdominal projection of the stomach axis.

An important question is how to assess stability when for different reasons fewer or more than 8 EGG channels are recorded. Of course, the first recommendation would be

to use the methodology described above and keep the number of channels at 8. When this is impossible the ratio between the number of stable channels and the total number of channels should be as close to $3/8$ as possible, keeping in mind that reducing the total number of channels worsens the precision of the suggested method.

Another relevant issue is whether it matters which three channels exhibit stable recordings. The model explicitly showed that cutaneous recordings are subjected to a strong integration. That is why, only minor differences between the EGG channels are to be expected, so it would be very difficult, if not impossible to relate some of the channels to distinct areas of the stomach. Therefore, all electrode combinations used at the present time should be regarded as equally informative.

6.3.4. CRITERION FOR COUPLING.

The assumption that EGG signals recorded with standard EKG electrodes are quite integrated, which was confirmed by the computer modeling in Chapter 2, implies that only minor differences (if any) should be expected in the EGG frequencies recorded from different channels. Of course, in the normal patient one should expect a complete coincidence of the maxima of the probability density functions obtained from the time-frequency plots. This was the case in this study. The criterion for electrical coupling was established as follows:

The maxima of the probability density functions of the points that build up the time-frequency plots of all stable EGG channels (as determined by the criterion for stability) should coincide at the same frequency (between 2.5 and 3.75 cpm).

The suggested criteria are not independent - poor stability of the time-frequency plots can jeopardize the coincidence of the maxima of the probability density functions, although relatively good coincidence was observed even when the standard deviations of some time-frequency plots were in the range of 0.6 - 0.7 cpm.

6.4. DISCUSSION.

In this chapter two quantitative criteria for normality were introduced. They were extracted from the results obtained from 15 healthy volunteers.

The first criterion determines the stability of the dominant spectral component of gastric electrical frequency as recognized from different EGG channels, i.e. it assesses cutaneously gastric irregularities or/and changes in gastric electrical frequency. Unfortunately, random motion artifacts, respiration, or any other external disturbances can mislead the investigator if they are consistent, with high amplitude and long duration. This is especially dangerous when patients with unexplained nausea and vomiting and anorexic patients are studied, because motion artifacts are usually related to their condition and are more or less inevitable. In these cases the recordings could be repeated several times with more careful preparation or they could be split in shorter recording intervals, which could be combined during the evaluation process.

The second criterion assesses the electrical coupling between different EGG channels. Despite the fact that EGG signals recorded with standard EKG electrodes appear to be strongly integrated, eventual uncoupling should manifest itself with differences in the frequency of dominant spectral components obtained from different EKG channels, i.e. the maxima of the probability density functions extracted from the time-frequency plots would not coincide in the normal frequency range of 2.5 - 3.75 cpm. This criterion can be considered dependent on the criterion for stability, because greater standard deviations inevitably indicate wobbling of the dominant spectral component and this would make the probability density function wider. Despite that, if the pdf maxima obtained from the time-frequency plots of different EGG channels coincide, the requirements of this criterion are met. Eventual elimination of some of the external factors for instability in EGG recordings (mainly motion and respiration artifacts) would allow an additional requirement to be established for the pdf maxima to be greater than a certain percentage value.

CHAPTER SEVEN

CLINICAL EGG STUDY

7.1. INTRODUCTION.

In the previous chapter the normal EGG was defined through the development of two objective quantitative criteria. In this chapter the usefulness of these criteria in differentiating normal from abnormal GEA in the clinical situation is assessed.

Several groups of patients were studied:

- (a) patients with implanted and cutaneous electrodes;
- (b) patients with partial gastric resection (gastrectomy);
- (c) ileus (postoperative) group of patients;
- (d) patients with idiopathic constipation;
- (e) patients with other gastrointestinal complaints.

Studies in the first group of patients allowed a direct comparison between internal and cutaneous signals. Indirect testing of the method was done in the second, third and fourth group of patients. Gastric electrical abnormalities are most likely to be present in patients with partial gastrectomy and in patients during the first postoperative days (ileus group). Constipated patients would be expected to have normal GEA.

7.2. POSSIBLE PATTERNS OF GASTRIC ELECTRICAL ABNORMALITIES RECOGNIZED BY THE EGG.

The two criteria introduced in chapter 6 combined with the established normal range of EGG frequency as recorded from volunteers indicate that six possible patterns of gastric electrical abnormalities might be recognized with the suggested method:

1. Irregular gastric electrical activity with normal electrical coupling of different parts of the stomach. The standard deviations of more than 6 out of 8 standard EGG channels should be higher than 0.450 cpm. The maxima of the probability density

functions of at least 3 out of 8 channels, however, must coincide in the normal frequency range of 2.5 - 3.75 cpm.

2. Irregular gastric electrical activity combined with electrical uncoupling of different parts of the stomach. The standard deviations fall out of the normal range, as described #1, and the maxima of the probability density functions of more than 6 out of 8 standard EGG channels do not coincide in the normal EGG frequency range.

3. Regular gastric electrical activity in the normal frequency range, but abnormal electrical coupling of different parts of the stomach. Gastric electrical frequency is in the normal range and remains stable (standard deviations less than 0.450 cpm) in at least 3 out of 8 EGG channels, but the maxima of the probability density functions of at least 6 out of 8 standard EGG channels do not coincide in the normal frequency range.

4. Regular gastric electrical activity outside the normal frequency range combined with normal electrical coupling. Gastric electrical frequency is outside the normal frequency range, but is stable in at least 3 out of 8 channels. The maxima of the probability density functions of at least 3 channels coincide, but outside the normal frequency range.

5. Irregular gastric electrical activity combined with normal electrical coupling, but outside the normal frequency range. Gastric electrical frequency is not stable in more than 6 out of 8 channels. The maxima of the probability density functions coincide, but outside the normal frequency range.

6. Regular gastric electrical activity outside the normal frequency range and abnormal electrical coupling. Gastric electrical frequency is outside the normal frequency range, but is stable in at least 3 out of 8 channels. The maxima of the probability density functions of at least 6 out of 8 channels do not coincide.

It should be made clear, that in certain occasions the registered frequency irregularities from EGG might be due to external factors, not actual gastric electrical frequency irregularities. These factors include sudden but consistent motion artifacts and poor signal-to-noise ratio in patients with very high body mass index (calculated as a ratio

between the height and the weight). In studies, where there was a suspicion of excessive motion artifacts, the tests were repeated. Elimination of the intervals with motion artifacts, or even interruption of the recording during these intervals (especially during periods of nausea and vomiting) could help also. When recording from obese patients repetition of the test would not help, because the high resistance of the abdominal fat is a factor which is difficult to eliminate. More careful preparation of the skin and higher gains of the amplifier can help in these situations.

7.3. SUBJECTS AND SETTINGS.

The study was performed on two postoperative patients (one male and one female) with suspected gastric motility disorders (6 one-hour recordings during the fasting state and 4 one-hour recordings during the postprandial state for five consecutive postoperative days), with implanted short distance bipolar (SDB), long distance bipolar (LDB) and cutaneous electrodes overlying the implanted pairs and 30 other patients with a variety of gastrointestinal complaints (1 hour in fasting state and one consecutive hour postprandially) with cutaneous electrodes only.

A standard 500 Kcal meal was given to the subjects for postprandial studies.

To record the EGG a row of five standard neonatal EKG monitoring electrodes was placed along the abdominal projection of the stomach axis on each subject. The distance between the centers of two electrodes in the row was 2.5 cm. Eight bipolar channels cutaneous EGG were recorded using the same electrode combinations as in the study of the 15 healthy volunteers. The electrode surface was kept constant.

The female patient with implanted electrodes was the 42-year-old woman whose medical history was discussed in the Chapter 5. The second patient with implanted electrodes was a 52-year-old male patient with a past history of pyloroplasty and vagotomy for peptic ulcer disease in 1965, who underwent fundoplication and

implantation of an electrode set similar to the one used on the female subject. The standard configuration of the EGG electrodes overlying the internal pairs was used. The duration of the tests was the same as in the study of the female patient.

The other patients were classified with respect to their major complaint or clinical condition into several groups (Table 7.1).

The settings of the equipment were the same as in the previous chapter. Body mass indexes, weight, pulse, maximal and minimal chest circumferences as well as the abdominal circumference were measured prior to the recordings.

Table 7.1. *Number of patients with identical or similar complaints.*

Patients Studied	Number
Previous Partial Gastrectomy	4
Post-Operative Ileus	3
Idiopathic Constipation	7
Other:	16
Unexplained Epigastric Pain	8
Unexplained Epigastric Pain and Distention	4
Simple Gastro-Esophageal Reflux	2
Unexplained Nausea and Vomiting	1
Post Obesity Surgery	1

7.4. RESULTS.

7.4.1. COMPARISON BETWEEN INTERNAL AND CUTANEOUS RECORDINGS IN THE TWO POSTOPERATIVE PATIENTS.

The female patient exhibited normal gastric electrical activity in records obtained with internal electrodes both in terms of frequency regularity and electrical coupling. A typical 4-minute tracing that illustrates these findings is shown on Fig. 7.1. When processed with the technique described in Chapter 4, the EGG recordings also displayed normal gastric electrical activity. Typical time-frequency plots of all channels, basic averages extracted from them and probability density functions are shown on Fig.7.2, Table 7.2 and Fig. 7.3 respectively. In order to be processed with the suggested method, SDB channels were filtered with a very narrow bandpass digital filter (0.03 - 0.08 Hz) because the first harmonic (which represents the period of the signal) of the signal was with very low power. Only this harmonic was left for further processing.

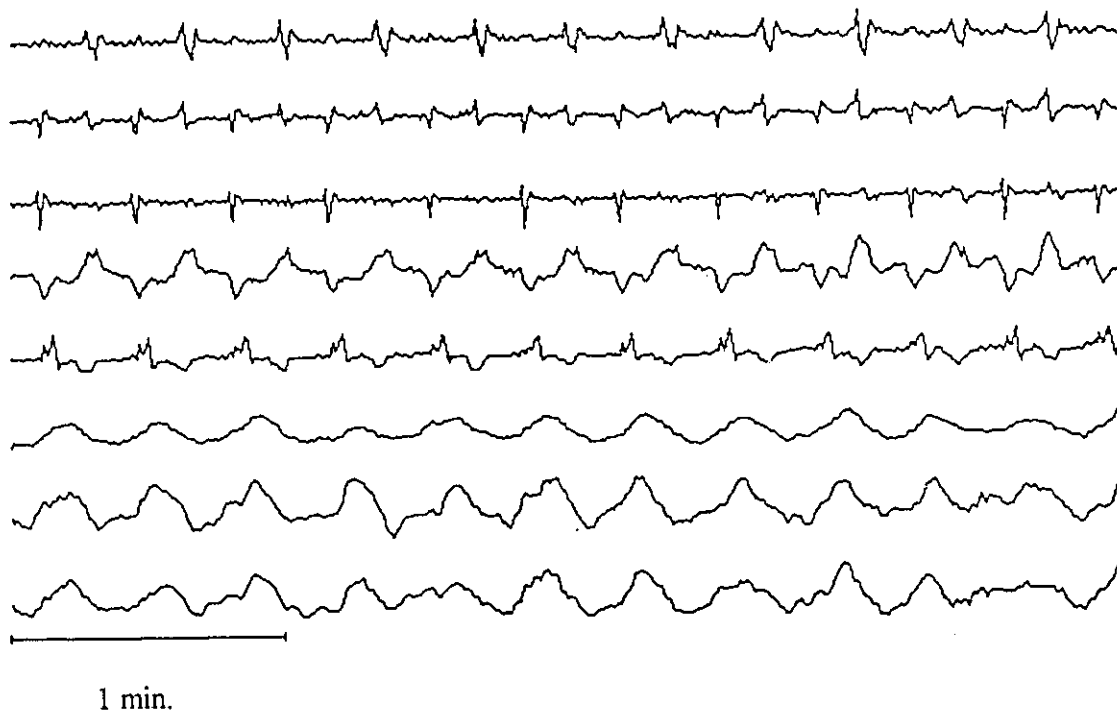
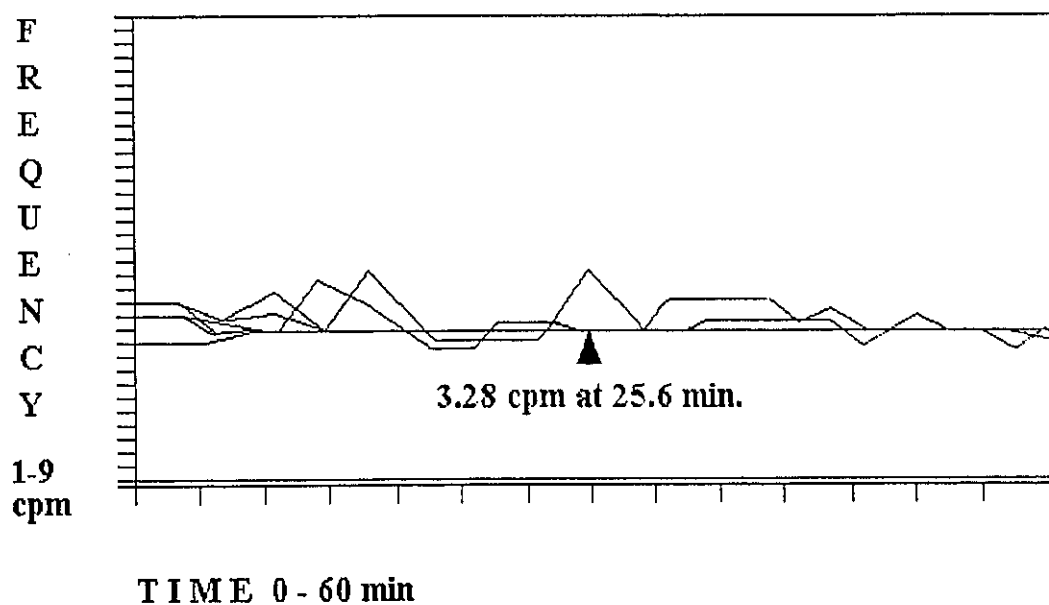


Figure 7.1. *Four-minute combined recording of SDB (1, 2 and 3), LDB (4 and 5) and EGG (6-8) channels from the female patient. Regular gastric frequency and electrical coupling were clearly seen.*

TIME-FREQUENCY PLOT



FREQUENCY INTERVALS : 0.23 cpm
 TIME INTERVALS: 4.27 min

PATIENT: B. W.
 DATE: 03.12.1990.

Figure 7.2. Typical time-frequency plots recorded from the female patient.

Table 7.2. Basic averages of the time-frequency plots from Fig. 7.2. Only one channel was out of the range of stability.

	Ch. 1	Ch. 2	Ch. 3	Ch. 4	Ch. 5	Ch. 6	Ch. 7	Ch. 8
Mean Value [cpm]	3.311	3.330	3.311	3.555	3.340	3.301	3.320	3.330
Variance [cpm ²]	0.006	0.158	0.006	0.309	0.025	0.004	0.018	0.019
Standard								
Deviation [cpm]	0.079	0.397	0.079	0.556	0.158	0.066	0.132	0.138

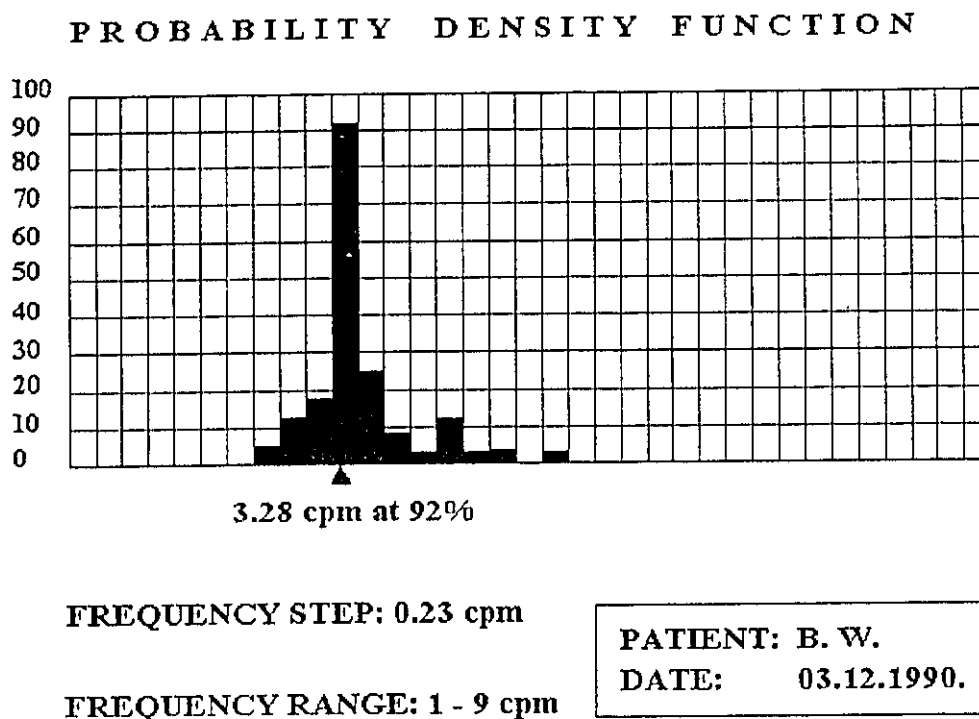


Figure 7.3. Probability density functions obtained from the time-frequency plot on Fig.7.2. All maxima coincided in the normal frequency range.

Only in one out of 8 recordings from the male subject did the implanted SDB electrode recordings show good coupling and few frequency irregularities. In this particular recording the EGG processed with the suggested technique showed good stability of the frequency in 2 out of 5 channels. Taking into consideration that the established criterion for stability was valid for 3 out of 8 EGG channels the above result does qualify as normal.

In the other seven recordings the implanted electrodes displayed abnormal GEA. Well defined and consistent frequency irregularities and electrical uncoupling were seen (Fig. 7.4). Simultaneous EGG recordings were also abnormal (Pattern 2) in all seven recordings. The two criteria for normality were not met (Fig.7.5, Table 7.3, Fig.7.6).

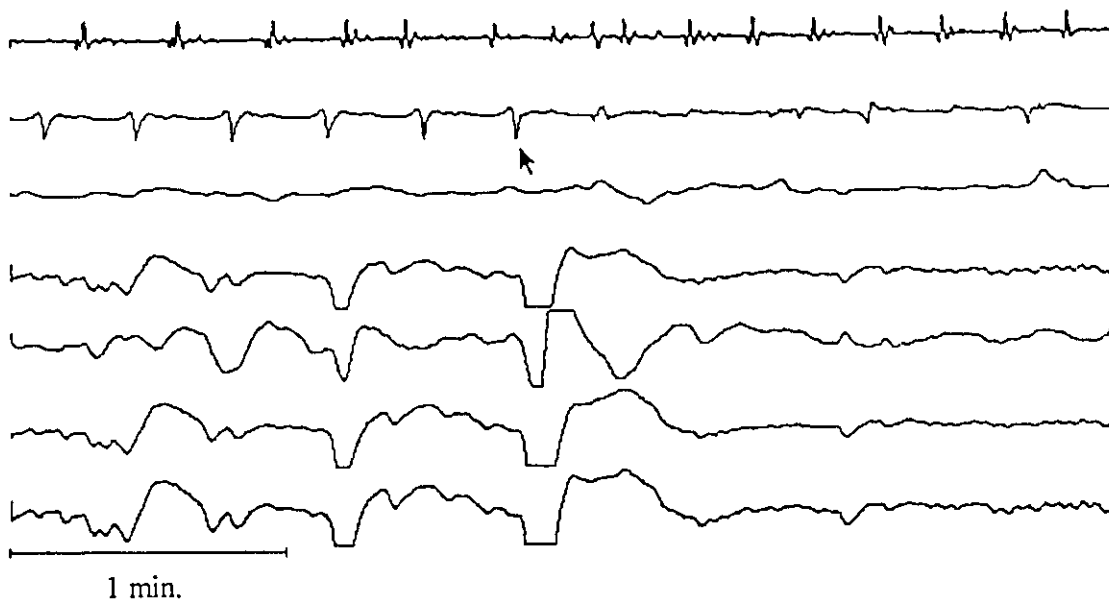


Figure 7.4. SDB channels recorded from the male patient showed consistent frequency irregularities as well as electrical uncoupling.

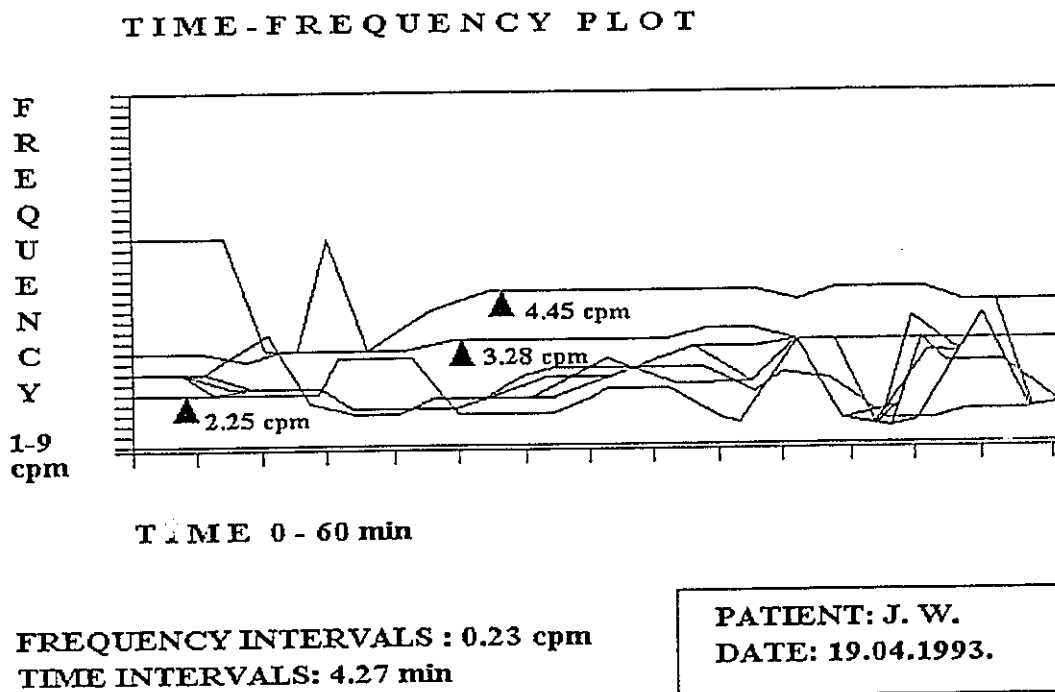
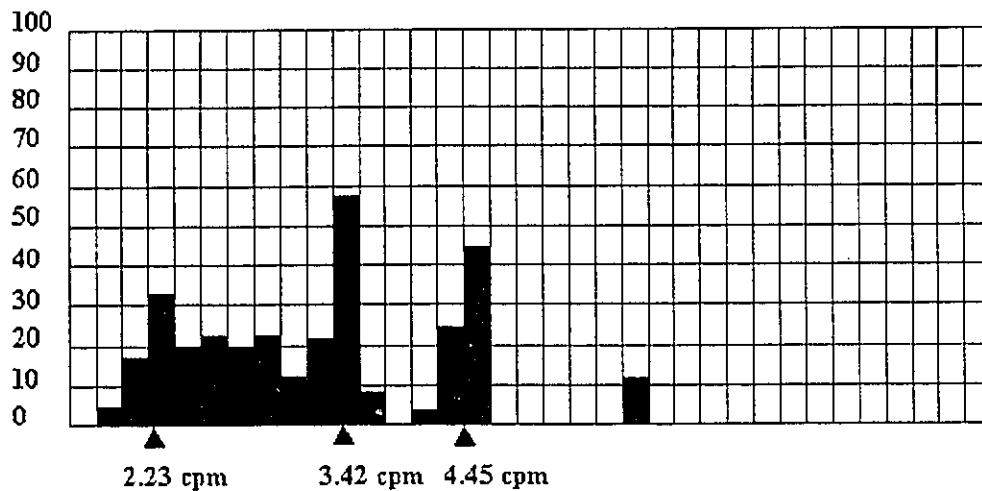


Figure 7.5. Typical time-frequency plots recorded from the male patient.

Table 7.3. Basic averages of the time-frequency plot on Fig.7.5. Standard deviations of all EGG channels were out of the normal range.

	Ch. 1	Ch. 2	Ch. 3	Ch. 4	Ch. 5	Ch. 6	Ch. 7	Ch. 8
Mean Value [cpm]	3.556	3.975	3.691	2.021	2.529	2.148	2.275	2.295
Variance [cpm ²]	0.308	0.408	0.995	0.185	0.821	0.333	0.532	0.501
Standard Deviation [cpm]	0.555	0.639	0.997	0.431	0.906	0.577	0.730	0.708

PROBABILITY DENSITY FUNCTION



FREQUENCY STEP: 0.23 cpm

FREQUENCY RANGE: 1 - 9 cpm

PATIENT: J. W.

DATE: 19.04.1993.

Figure 7.6. Probability density functions obtained from the time-frequency plot on Fig.7.5. The maxima did not coincide.

7.4.2. PATIENTS WITH PARTIAL GASTRECTOMY.

All four patients with partial gastrectomy (3 female and 1 male) exhibited abnormal EGG. One of the patients had a normal EGG in the fasting state, while the postprandial recording was abnormal. In one other patient the opposite was noted.

Two of the patients (one of them postprandially only) displayed unstable EGG frequency and different maxima of the probability density functions (abnormal pattern 2). One patient had regular EGG frequency and good electrical coupling both in fasting and postprandial states, but the mean value of the frequency was outside the normal range of 2.5 - 3.75 cpm seen in volunteers. This was defined earlier as an abnormal pattern 4. In one other fasting patient the EGG frequency was regular but very low (below 2.5 cpm), while the electrical coupling was abnormal, which was described as abnormal pattern 6. After feeding, the mean EGG frequency of this patient entered the normal range probably due to the postprandial increment of gastric frequency seen in some subjects. However, the pdf maxima coincided, which indicated improved electrical coupling and thus qualified the whole postprandial recording as normal.

7.4.3. ILEUS PATIENTS.

The three patients from this group underwent cutaneous recordings of GEA during the first 48 hours after a laparotomy. In all subjects the recordings clearly demonstrated abnormal EGG (pattern 2) both in the fasting and the postprandial states. In two of patients the tests were repeated to make sure that the results were not influenced by external noise factors. Because of the postoperative condition of the patients, the standard meal for the postprandial studies was replaced with liquids.

7.4.4. PATIENTS WITH IDIOPATHIC CONSTIPATION.

In the fasting state, all patients (1 male and 6 female) had normal EGGs. The male patient showed an abnormal EGG (pattern 2) after feeding, i.e. his EGG frequency was not stable in more than five channels, and the pdf maxima of the EGG channels did not coincide.

7.4.5. PATIENTS WITH OTHER GASTROINTESTINAL COMPLAINTS.

This group of patients was divided into four subgroups (see Table 7.1), each of which will be considered separately.

Patients with unexplained epigastric pain.

In this subgroup of 8 subjects, 6 were normal. One patient had abnormal EGG (pattern 2) only during the fasting state. One other patient displayed abnormal EGG (pattern 4; stable EGG frequency outside the normal frequency range and good electrical coupling) both in the fasting and postprandial states.

Patients with unexplained epigastric pain and distention.

Two out of four patients in this subgroup exhibited abnormal pattern 2 (irregular EGG frequency and electrical uncoupling). In one of them this was noted in fasting state only, while the postprandial recording was normal. The other two patients showed normal EGG pattern.

Patients with simple gastro-esophageal reflux.

One out of 2 patients displayed an abnormal EGG (pattern 6; stable EGG frequency outside the normal range and abnormal electrical coupling) in fasting state only. The postprandial recording from this patient, as well as the recordings from the other patient (both in fasting state and after feeding) were normal.

Patients with unexplained nausea and vomiting.

The only patient with this complaint showed an abnormal EGG (pattern 2) both in the fasting state and after feeding.

Patients with post obesity surgery.

This patient exhibited normal EGG both in fasting and posprandial states. The test was performed several months after the surgery.

7.5. STUDY OF THE ABNORMAL EGG PATTERNS.

7.5.1. ABNORMAL ELECTRICAL ACTIVITY - PATTERN 2.

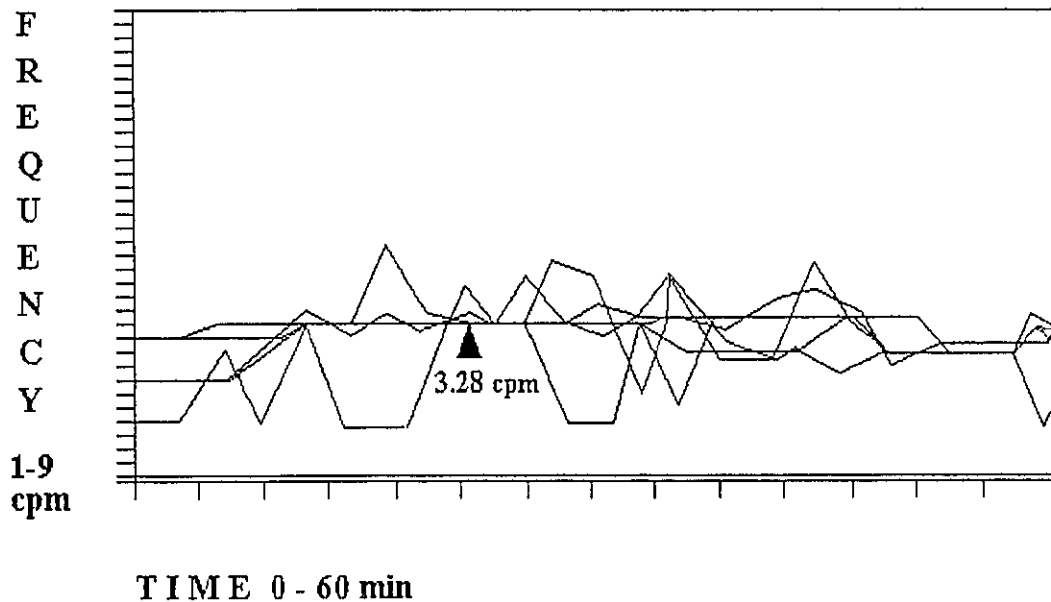
Table 7.4 shows the number of patients with similar complaints who had abnormal gastric electrical activity with the second defined pattern (irregular gastric electrical activity and abnormal electrical coupling). Altogether 12 out of 30 patients (40 % from the total number), exhibited this abnormal EGG pattern. In 3 of these cases the tests were repeated on a different day because of suspicion that external motion artifacts influenced the results. In all three cases, however, the new tests confirmed the findings.

Table 7.4. *Quantitative comparison between abnormal (Pattern 2) and total number of patients with identical or similar complaints.*

Complaint	Total Patients	Abnormal Patients (Pattern 2, fasting)	Abnormal Patients (Pattern 2, fed)	Abnormal Patients (Pattern 2, Total)
Previous Partial Gastrectomy	4	1	2	2
Ileus Patients	3	3	3	3
Idiopathic Constipation	7	0	1 (male)	1 (male)
Epigastric Pain	8	1	0	1
Epigastric Pain & Distention	4	1	2	3
Simple Gastro-esophageal reflux	2	0	0	0
Unexplained Nausea & Vomiting	1	1	1	1

Typical time-frequency plots, basic averages and probability density functions obtained from a patient with abnormal gastric electrical activity (Pattern 2) are shown on Fig. 7.7, Table 7.5 and Fig. 7.8 respectively. Time frequency plots were unstable. Standard deviations calculated from these plots were greater than 0.450 cpm in at least 6 out of 8 EGG channels. The maxima of the probability density functions did not coincide.

TIME-FREQUENCY PLOT



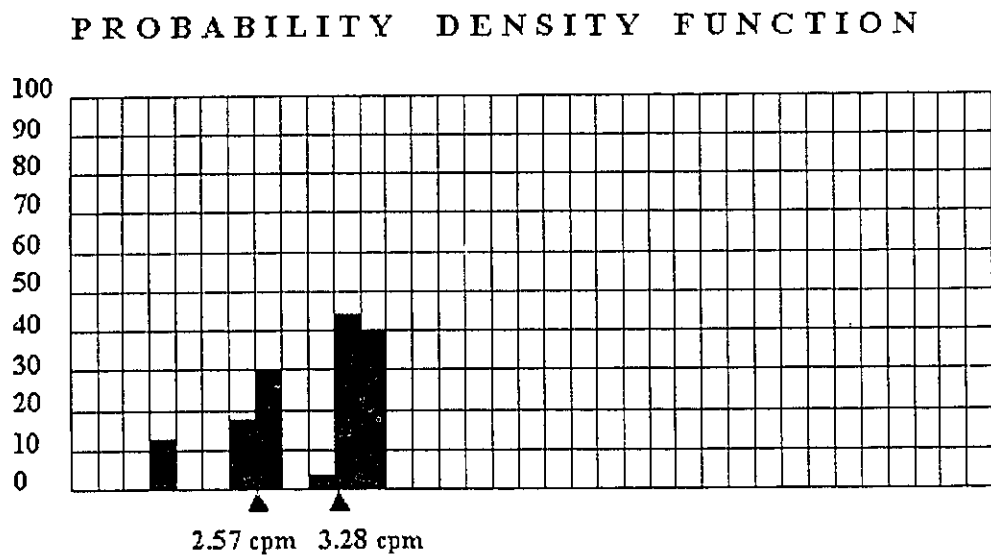
FREQUENCY INTERVALS : 0.23 cpm
TIME INTERVALS: 4.27 min

PATIENT: W. B.
DATE: 09.07.1993.

Figure 7.7. *Unstable time-frequency plots recorded from a patient with abnormal gastric electrical activity (Pattern 2).*

Table 7.5. Basic averages obtained from a patient with abnormal gastric electrical activity (Pattern 2).
Only 2 EGG channels were within the normal frequency range.

	Ch. 1	Ch. 2	Ch. 3	Ch. 4	Ch. 5	Ch. 6	Ch. 7	Ch. 8
Mean Value [cpm]	2.939	3.037	3.076	3.447	3.311	2.891	3.145	2.949
Variance [cpm ²]	0.616	0.217	0.804	0.657	0.068	0.400	0.152	0.406
Standard								
Deviation [cpm]	0.785	0.466	0.897	0.810	0.261	0.632	0.390	0.637



FREQUENCY STEP: 0.23 cpm

FREQUENCY RANGE: 1 - 9 cpm

PATIENT:	W. B.
DATE:	09.07.1993.

Figure 7.8. Probability density functions calculated from the time-frequency plots of different EGG channels. The maxima did not coincide in the normal frequency range.

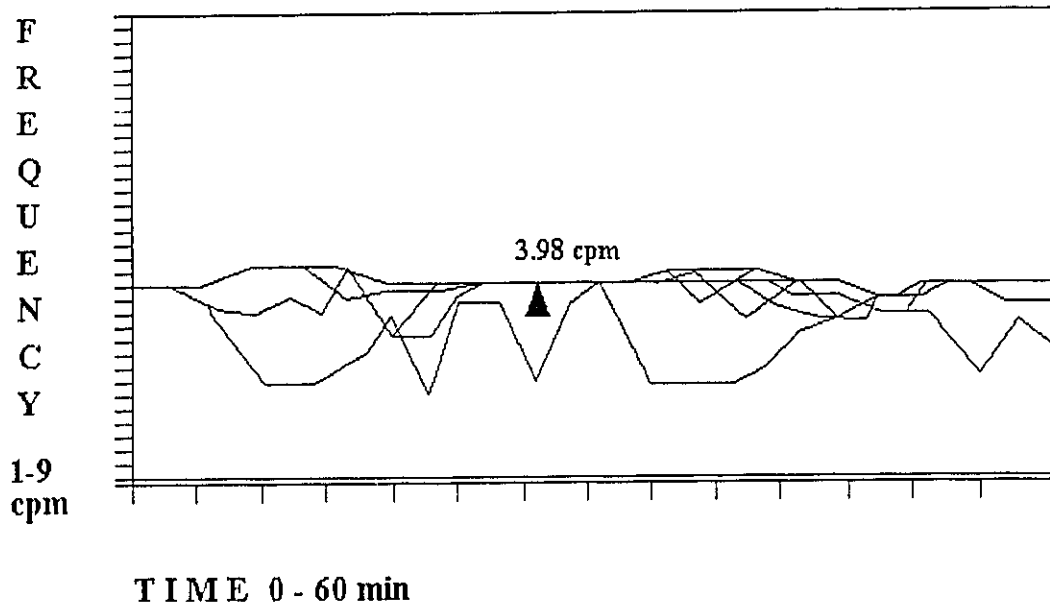
7.5.2. ABNORMAL ELECTRICAL ACTIVITY - PATTERN 4.

Table 7.6 shows the number of patients with similar complaints who exhibited abnormal gastric electrical activity with the fourth pattern - regular gastric electrical activity outside the normal frequency range combined with good electrical coupling of different parts of the stomach. This pattern was observed in 2 out of 30 patients (6.7 % from the total number). Typical time-frequency plots, basic averages and probability density functions are shown on Fig. 7.9, Table 7.7 and Fig. 7.10 respectively. Standard deviations calculated from the time-frequency plots in at least 3 out of 8 EGG channels were less than 0.450 cpm, but the maxima of the probability density functions coincided at frequency outside the normal frequency range.

Table 7.6. *Quantitative comparison between abnormal (Pattern 4) and total number of patients with identical or similar complaints.*

Complaint	Total Patients	Abnormal Patients (Pattern 4, fasting)	Abnormal Patients (Pattern 4, fed)	Abnormal Patients (Pattern 4, Total)
Previous Partial Gastrectomy	4	1	0	1
Epigastric Pain	1	1	1	1

TIME - FREQUENCY PLOT



FREQUENCY INTERVALS : 0.23 cpm
 TIME INTERVALS: 4.27 min

PATIENT: B. W.
 DATE: 08.06.1993.

Figure 7.9. Time-frequency plots recorded from patient with abnormal gastric electrical activity (Pattern 4).

Table 7.7. Basic averages obtained from a patient with abnormal gastric electrical activity (Pattern 4).

	Ch. 1	Ch. 2	Ch. 3	Ch. 4	Ch. 5	Ch. 6	Ch. 7	Ch. 8
Mean Value [cpm]	3.906	2.822	4.004	3.760	3.975	3.945	3.984	3.984
Variance [cpm ²]	0.051	0.657	0.057	0.122	0.036	0.089	0.053	0.053
Standard								
Deviation [cpm]	0.226	0.810	0.2 '9	0.349	0.189	0.299	0.229	0.229

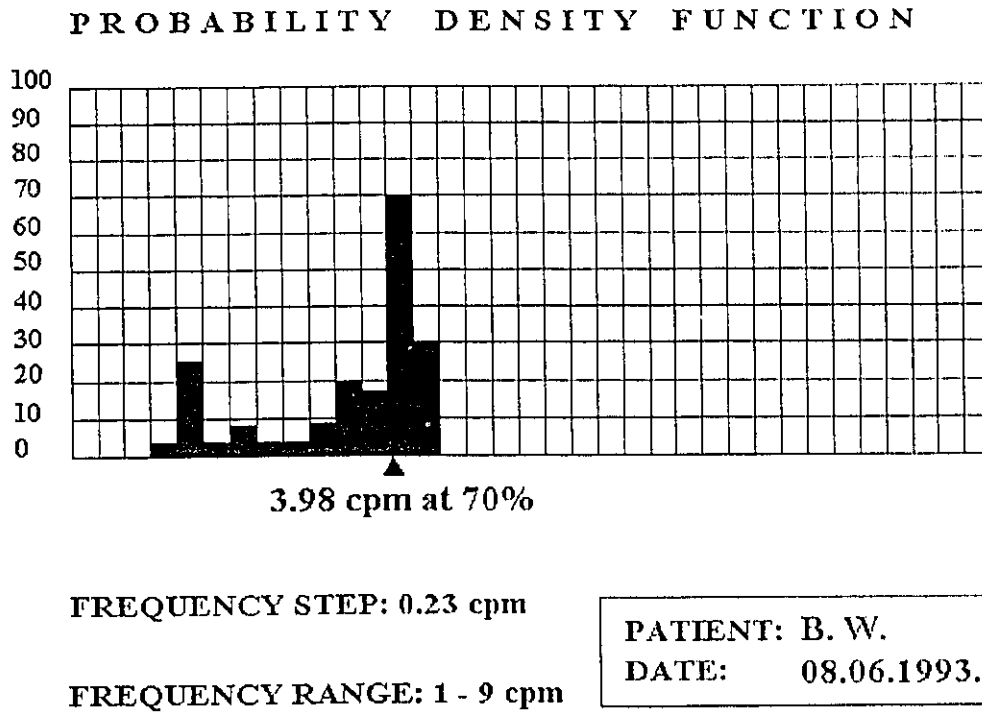


Figure 7.10. Probability density functions calculated from the time-frequency plot on Fig. 7.9. Note that the maxima coincided, but outside the normal frequency range.

7.5.3. ABNORMAL ELECTRICAL ACTIVITY - PATTERN 6.

Table 7.8 shows the number of patients with similar complaints who exhibited abnormal gastric electrical activity with the pattern 6 - regular gastric electrical activity outside the normal frequency range, but electrical uncoupling of different parts of the stomach. The pattern was observed in 2 out of 30 patients (6.7 % from the total number). Typical time-frequency plots, basic averages and probability density functions are shown on Fig. 7.11, Table 7.9 and Fig. 7.12 respectively. Stable frequency outside the normal range was registered, but the maxima of the probability density functions did not coincide in more than 2 EGG channels.

Table 7.8. *Quantitative comparison between abnormal (Pattern 6) and total number of patients with identical or similar complaints.*

Complaint	Total Patients	Abnormal Patients	Abnormal Patients	Abnormal Patients
		(Pattern 6, fasting)	(Pattern 6, fed)	(Pattern 6, Total)
Previous Partial Gastrectomy	4	1	0	1
Simple Gastro-esophageal Reflux	2	1	0	1

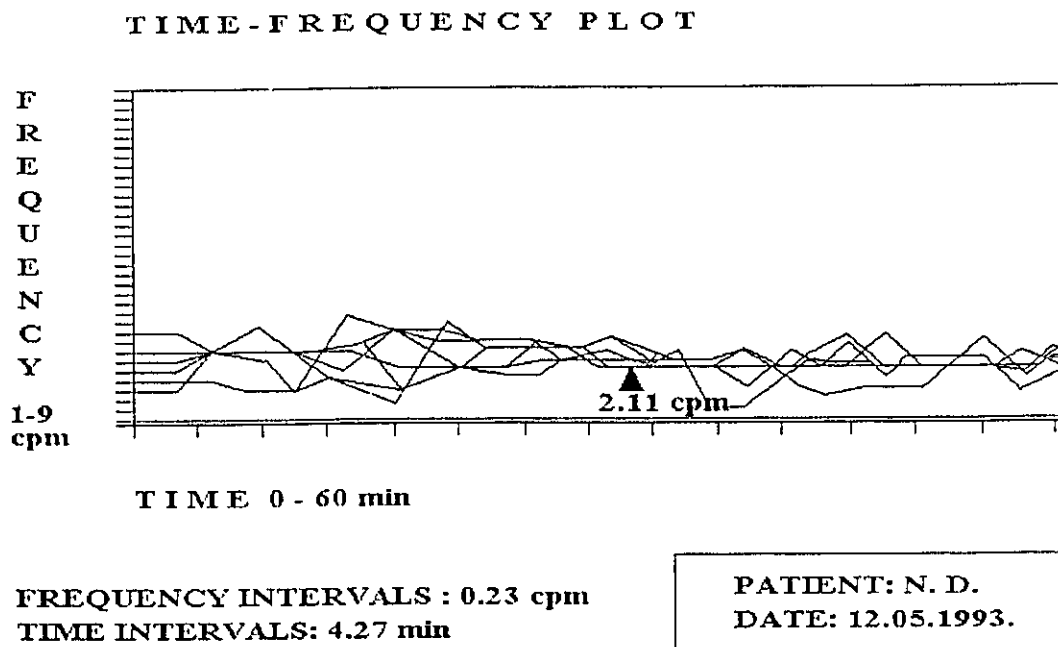
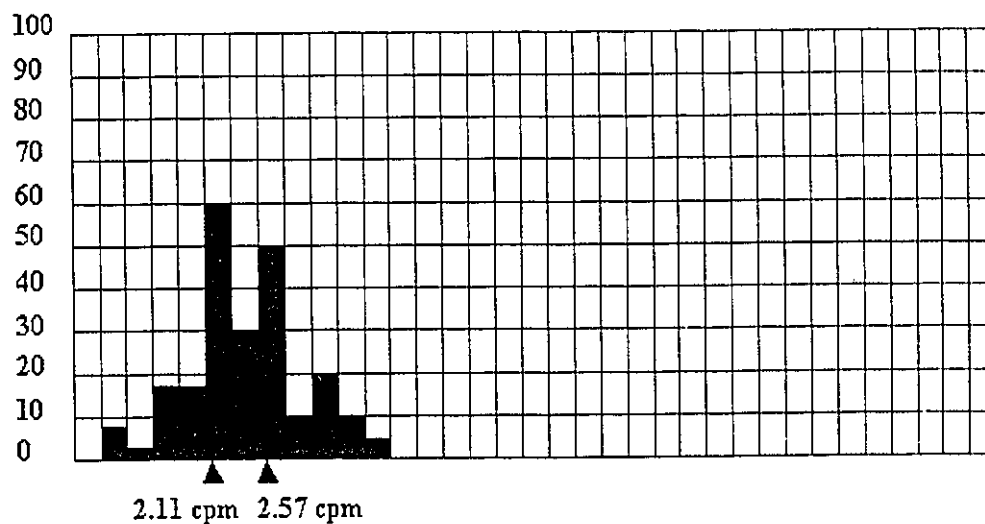


Figure 7.11. *Time-frequency plots recorded from patient with abnormal gastric electrical activity (Pattern 6).*

Table 7.9. Basic averages obtained from a patient with abnormal gastric electrical activity (Pattern 6).
More than 3 EGG channels exhibited stability, but outside the normal frequency range.

	Ch. 1	Ch. 2	Ch. 3	Ch. 4	Ch. 5	Ch. 6	Ch. 7	Ch. 8
Mean Value [cpm]	2.363	2.285	2.275	2.100	2.578	2.285	2.354	2.373
Variance [cpm ²]	0.143	0.374	0.184	0.251	0.191	0.183	0.122	0.121
Standard Deviation [cpm]	0.378	0.611	0.429	0.501	0.437	0.427	0.349	0.348

PROBABILITY DENSITY FUNCTION



FREQUENCY STEP: 0.23 cpm

FREQUENCY RANGE: 1 - 9 cpm

PATIENT: N. D.

DATE: 12.05.1993.

Figure 7.12. Probability density functions calculated from the time-frequency plots on Fig. 7.11. The maxima did not coincide well.

7.5.4. ABNORMAL ELECTRICAL ACTIVITY - OTHER PATTERNS.

Other abnormal patterns were not seen in any of the studied patients, although they were defined theoretically. Irregular gastric electrical activity but normal electrical coupling either inside or outside the normal frequency range (patterns 1 and 5) probably could not be recorded because of the possible inter relation between gastric electrical irregularities and uncoupling.

7.6. DISCUSSION.

In this study a method for extraction of valuable diagnostic information from cutaneous gastric electrical signals using current amplification and electrode techniques has been developed and tested. The objective was to transform electrogastrography (EGG) from a research tool into a useful clinical measurement based on an objective quantitative method.

The main advantage of the proposed method for evaluation of EGG is its potential to become more reliable with future technological development. More powerful amplification methods or better digital signal processing procedures, for example, could make the suggested criterion for stability even more precise by decreasing the standard deviation required to qualify an EGG channel as stable. Stomach distention after feeding could affect signal-to-noise ratio and thus the results of the analysis. The impact of postprandial distentions as well as the influence of other external noise factors on the quality of the recording could be minimized with the future developments in amplification technology.

Future studies could explore the extent of the discovered gastric electrical abnormalities. Work needs to be done to relate more reliably the abnormal patterns of EGG to certain clinical conditions. Clinical manifestation (if any) of the abnormal patterns

that were not clinically seen in this study could also be examined. One interesting issue is the interrelation between electrical uncoupling of different parts of the stomach and irregularities of gastric electrical frequency. The problem is whether these two entities manifest themselves independently, or does the appearance of one lead to the appearance of the other as well.

An important benefit of the proposed method is that it is realistic. It was clearly demonstrated that the most reliable EGG parameter is gastric electrical frequency. Its good level of stability in all normal subjects and unconscious dogs studied suggested that external artifacts do not drastically affect the recordings when the experiment is carried out carefully.

With the described method EGG makes its first steps towards reliable clinical applications. Similarly to electrocardiography in its early years, electrogastrography has the potential to become a routine clinical procedure in the near future.

REFERENCES

1. Alvarez W. C. Differences in rhythmicity and tone in different parts of the wall of the stomach. *Am. J. Physiol.*, 11:585-91, 1916.
2. Alvarez W. C. New methods of studying gastric peristalsis. *JAMA*, 79(16):1281-85, 1922.
3. Alvarez W. C. The electrogastrogram and what it shows. *JAMA*, 78(15):1116-18, 1922.
4. Alvarez W. C. and Mahoney L. J. Action current in stomach and intestine. *Am. J. Physiol.*, 58(3):477-82, 1922.
5. Alvarez W. C. and Mahoney L. J. The relations between gastric and duodenal peristalsis. *Am. J. Physiol.*, 64(2):371-76, 1923.
6. Luckhard A. B., Phillips H. T., Carlson A. J. Contributions to the physiology of the stomach. *Am. J. Physiol.*, 50:57-62, 1919.
7. Richter C. P. Action currents from the stomach. *Am. J. Physiol.*, 67:612-33, 1924.
8. Klein E. Gastric motility. *Arch. Surg.*, 12:571-75, 1926.
9. Geldof H. Electrogastrography. Clinical applications. Ph.D. Thesis. Erasmus University, Rotterdam, The Netherlands, 1987.
10. Kingma Y. J. The electrogastrogram and its analysis. *C.R.C. Critical Reviews in Biomedical Engineering*, 17 (2): 105-124, 1989.
11. Smout A. J. P. M., Van der Schee E. J., Grashuis J. L. What is measured in electrogastrography? *Dig. Dis. & Sci.*, 25:179-88, 1980.
12. Smout, A. J. P. M. Myoelectric activity of the stomach. *Gastroelectromyography and electrogastrography*. Delft University Press, Delft, The Netherlands, 1980.
13. Daniel E. E. and Chapman K. M. Electrical Activity of gastrointestinal tract as an indicator of mechanical activity. *Am. J. Dig. Dis.* 54: 54-102, 1963.
14. Papasova M. P. and Boev K. The slow potential and its relationship to the gastric smooth muscle contraction. In: *Physiology of Smooth Muscle*, ed. E. Bulbring and M. F. Shuba, Raven Press, N.Y., 209-16, 1978.

15. Pappasova M. P., Nagai T., Prosser C. L. Two component slow waves in smooth muscle of cat stomach. *Am. J. Physiol.*, 214:695-702, 1968.
16. Sarna S. K. Gastrointestinal electrical activity: terminology. *Gastroenterology*, 68:1631-35, 1975.
17. Abell T. L. and Malagelada J. - R. Electrogastrography. Current assessment and future perspectives. *Dig. Dis. Sci.*, 33:982-92, 1988.
18. Szurszewski J. H. Electrical basis for gastrointestinal motility. In: *Physiology of the Gastrointestinal Tract*, Vol 2., ed. L. R. Johnson, Raven Press, N. Y., 1435-66, 1981.
19. Gabella G. Structure of smooth muscle. In: *An Illustrated Guide to Gastrointestinal Motility*. Ed. D. Kumar and S. Gustavsson, J. Wiley & Sons, London, 1988.
20. Small V. J. and Sobieszek A. The contractile apparatus of smooth muscle. *Int. Rev. Cytol.*, 64:241-306, 1980.
21. Ohba M., Sakamoto Y., Tomita T. Effects of sodium, potassium and calcium ions on slow wave in circular muscle of guinea-pig stomach. *J. Physiol. (London)* 253: 505-16, 1977.
22. Weber J. and Kohatsu S. Pacemaker localization and electrical conduction patterns in the canine stomach. *Gastroenterology*, 59: 717-26, 1970.
23. Kelly K. A. and Code C. F. Canine gastric pacemaker. *Am. J. Physiol.* 220: 112-18, 1971.
24. Daniel E. E. and Sarna S. Generation and conduction of activity in smooth muscle. *Ann. R. Pharm.*, 18: 145 - 66, 1978.
25. Bauer A. J., Publicover N. G., Sanders K. M. Origin and spread of slow waves in canine gastric antral circular muscle. *Am. J. Physiol.*, 234: G800-6, 1985.
26. Code C. F. and Marlett J. A. The interdigestive myoelectrical complex of the stomach and small bowel of dogs. *J. Physiol.*, 246: 289-309, 1975.
27. Szurszewski J. H. A migrating electrical complex of the canine small intestine. *Am. J. Physiol.*, 217: 1757-63, 1969.

28. Geldof H., Van der Schee E. J., Grashuis J. L. Electrogastrographic characteristics of the interdigestive migrating complex in man. *Am. J. Physiol.*, 250: G165-G171, 1986.
29. Suckling E. E. *Bioelectricity*. McGraw Hill Inc., N.Y., 1961.
30. Rosenfalck P. Intra- and extracellular potential fields of active nerve and muscle fibers. A physico-mathematical analysis of different models. Akademisk Forlag, Copenhagen, 1969.
31. Mirrizzi N. and Scafoglieri U. Optimal direction of the electrogastrographic signal in man. *Med. Biol. Eng. & Comput.*, 21:385-89, 1983.
32. Mirrizzi N., Stella R., Scafoglieri U. A model of extracellular waveshape of the gastric electrical activity. *Med. Biol. Eng. & Comput.*, 23:33-37, 1985.
33. Mirrizzi N., Stella R., Scafoglieri U. Model to simulate the gastric electrical control activity on the stomach wall and on abdominal surface. *Ibid*, 24:157-163, 1986.
34. Sarna S. K., Daniel E. E., Kingma Y. J. Premature control potentials in the dog stomach and in the gastric computer model. *Am. J. Physiol.*, 222:1518-23, 1972.
35. Sarna S. K., Daniel E. E., Kingma Y. J. Effects of partial cuts on gastric electrical control activity and its computer model. *Ibid*, 223:332-40, 1972.
36. Sarna S. K., Daniel E. E., Kingma Y. J. Simulation of the electrical control activity of the stomach by an array of relaxation oscillators. *Amer. J. Dig. Dis.*, 17:299-310, 1972.
37. Linkens D. A., Khelfa M., Nicklin G. Multioscillator simulator for gastrointestinal electrical activity modelling. *Med. Biol. Eng. & Comput.*, 21: 591-8, 1983.
38. Plonsey R. and Barr R. C. *Bioelectricity. A quantitative approach*. Plenum Press, N. Y., 1988.
39. FAMILONI B. O., KINGMA Y. J., BOWES K. L. Study of transcutaneous and intraluminal measurement of gastric electrical activity in humans. *Med. Biol. Eng. & Comput.*, 25:397-402, 1987.

40. Hamilton J. W., Bellahsene B. E., Reichelder M., Webster J. G., Bass P. Human electrogastrograms: comparison of surface and mucosal recordings. *Dig. Dis. Sci.*, 31:33-9, 1986.
41. Chen J., Vandewalle J., Sansen W., Van Cutsem E., Vantrappen G., Janssens J. Observation of the propagation direction of human electrogastric activity from cutaneous recordings. *Med. Biol. Eng. & Comput.*, 27:538-42, 1989.
42. Mintchev M. P., Kingma Y. J., Bowes K. L. Accuracy of cutaneous recordings of gastric electrical activity. *Gastroenterology*, 104:1273-80, 1993.
43. Familoni B. O., Bowes K. L., Kingma Y. J., Cote K. R. Can transcutaneous recordings detect gastric electrical abnormalities? *Gut*, 32:141-6, 1991.
44. Barnett R., Ziegler M. R. *College Mathematics*. Dellen Publ. Company, San Francisco, C., 1984.
45. Chen J. and McCallum R. W. Electrogastrography: measurement, analysis and prospective applications. *Med. Biol. Eng. & Comput.*, 29:339-50, 1991.
46. Jung W. G. *IC Op-Amp Cookbook*. Howard W. Sams & Co., Indianapolis, IN, 1986.
47. Graeme J. G., Tobey G.E., Huelsman L. P. (Editors). *Operational Amplifiers*. McGraw Hill, N.Y., 1971.
48. Offner F. *Electronics for Biologists*. McGraw Hill, N.Y., 1967.
49. Metting Van Rijn A. C., Peper A., Grimbergen C. A. High-quality recording of bioelectric events. Part 1. *Med. Biol. Eng. & Comput.*, 28: 389-97, 1990.
50. Huhta J. G., Webster J.G. 60 Hz interference in electrocardiography. *IEEE Trans. Biomed. Eng.*, BME-20, 91-101, 1973.
51. Metting Van Rijn A. C., Peper A., Grimbergen C. A. High-quality recording of bioelectric events. Part 2. *Med. Biol. Eng. & Comput.*, 29: 433-40, 1991.
52. Lenhart J.M. *A Study on Silver-Silver Chloride Electrodes*. M.Eng. Thesis, University of Alberta, Department of Electrical Engineering, Edmonton, Canada, 1980.

53. Van Heuningen R., Goovaerts H. G., De Vries F. R. A low noise isolated amplifier system for electrophysiological measurements: basic considerations and design. *Ibid*, 22:77-85, 1984.
54. Jacobson B., Webster J. G. *Medicine and Clinical Engineering*. Prentice-Hall Inc., N.J., 1977.
55. Levkov C. Amplification of biosignals by body potential driving. *Ibid*, 20:248-50, 1982.
56. Burr-Brown Integrated Circuits Reference Guide. Volumes 1 and 2. 1991-93.
57. Publicover N. G., Sanders K. M. Myogenic regulation of propagation in gastric smooth muscle. *Am. J. Physiol.*, 234: G512-20, 1985.
58. Bass P. and Wiley J. N. Contractile force transducer for recording muscle activity in unanesthetized animals. *J. App. Physiol.*, 32:567-70, 1972.
59. Kingma Y. J., Van der Schee E. J., Grashuis J. L. Implantable transducer for sensing contractions of the stomach wall and intestine. In: *Proc.Int.Conf. on Biomedical Transducers (Biocapt)*, Paris, Tome 1: 69-74, 1975.
60. Gustavson S. and Tucker R. Manometry. In: *An Illustrated Guide to Gastrointestinal Motility*. Ed. D. Kumar and S. Gustavsson, J. Wiley & Sons, London, 1988.
61. Challis R. E. and Kitney R. I. Biomedical signal processing (in four parts). Part 1. Time domain methods. *Ibid*, 28:509-24, 1990.
62. Challis R. E. and Kitney R. I. Biomedical signal processing (in four parts). Part 2. The frequency transforms and their interrelationships. *Ibid*, 28:509-24, 1990.
63. Oppenheim A. V. and Schafer R. W. *Digital signal processing*. Prentice-Hall, N. J., 1975.
64. Stanley W.D., Dougherty G.R., Dougherty R. *Digital Signal Processing*. Prentice Hall, Reston, VA, 1984.
65. Bracewell R. N. *The Hartley transform*. Oxford University Press, N. Y., 1986.
66. Bracewell R. N. The fast Hartley transform. *Proc. of IEEE*, 72:1010-15, 1984.

67. Kingma Y. J., Chambers M. M., Bowes K. L., Bannister C. Interpretation of computer processed electrical signals from the gastro-intestinal tract. In: Proc. of 14th Hawaii Int. Conf. on System Sci., Honolulu, Hawaii, 1981.
68. Van der Schee E. J., Smout A. J. P. M., Grashuis J. L. Application of running spectrum analysis to electrogastrographic signals recorded from dog and man. In: Motility of the Digestive Tract, ed. M. Wienbeck, Raven Press, N. Y. 1982.
69. Van der Schee E. J. and Grashuis J. L. Running spectrum analysis as an aid in the representation and interpretation of electrogastrographic signals. *Med. Biol. Eng. & Comput.*, 25:57-62, 1987.
70. Mintchev M. P. and Bowes K. L. Capabilities and limitations of electrogastrograms. In: *Electrogastrography. Theory and Applications*. Eds. J. Chen and R. W. McCallum, Raven Press (in print).
71. Mintchev M.P., Kingma Y. J., Bowes K. L.. Use of Hartley Transform in the Analysis of Surface Electrogastrographic Signals. In: Proc.of 17-th Canadian Medical & Biological Engineering Society Int.Conference, Banff, Canada, May 1991.
72. Hays W. L. *Statistics*. CBS College Publ., N.Y., 1981.
73. Brown, B.W., Hollander M. *Statistics. A Biomedical Introduction*. John Wiley & Sons, N.Y., 1977.
74. Kentie M. A., Van der Schee E. J., Grashuis J. L., Smout A. J. P. M. Adaptive filtering of canine electrogastrographic signals. Parts 1 and 2. *Med. Biol. Eng. & Comput.*, 19:759-69, 1981.
75. Chen J., Vandewalle J., Sansen W., Vantrappen G., Janssens J. Adaptive method for cancellation of respiratory artefact in electrogastric measurements. *Ibid*, 27:57-63, 1989.
76. Widrow B., Glover J.R., McCool J.M., Kaunitz J., Williams C.S., Hearn R.H., Ziedler J.R., Dong E.J., Goodlin R.C. Adaptive noise cancellation: principles and applications. *Proc.IEEE*, 63:1692-1716.

77. Rude R.G. Adaptive Filtering Applied to Gastric Electrical Activity. M.Sc. Thesis, University of Alberta, Department of Electrical Engineering, Edmonton, Canada, 1987.
78. Stanghellini, V. and Corinaldesi R. Gastrointestinal motility disorders. Stomach and Duodenum. In: Illustrated Guide to Gastrointestinal Motility. ed. D. Kumar and S. Gustavsson. John Wiley & Sons, London, 1988.
79. Kelly K. A. Surgical treatment of gastric and small intestinal motility disorders. In: Physiology, Diagnosis & Therapy in GI Motility Disorders, ed. M. C. Champion and R. W. McCallum, 191-200, The MEDICINE Publishing Foundation, Oxford, 1987.
80. McCallum R. W. Diagnosis of gastric motility disorders. *Ibid*, 61-79, 1988.
81. Champion M. C. Treatment of gastric motility disorders. *Ibid*, 165-75, 1988.
82. Geldof H., Van der Schee E. J., Van Blankenstein M., Smout A. J., Akkermans L. M. Effects of highly selective vagotomy on gastric myoelectrical activity. An electrogastrographic study. *Dig. Dis. Sci.*, 35(8): 969-75, 1990.
83. Vantrappen G., Coremans G., Janssens J., Mantides A., Vanden Borre F. Inversion of the slow wave gradient in symptomatic patients with Roux-en-Y anastomoses. *Gastroenterology*, 101(5):1282-8, 1991.
84. Pezzolla F., Riezzo G., Maselli M. A., Giorgio I. Gastric electrical dysrhythmia following cholecystectomy in humans. *Digestion*, 49(3):134-9, 1991.
85. Clevers G. J., Smout A. J., Van der Schee E. J., Akkermans L. M. Myo-electrical and motor activity of the stomach in the first days after abdominal surgery: evaluation by electrogastrography and impedance gastrography. *J. Gastroenterol. Hepatol.*, 6:253-9, 1991.
86. Coehlo J. C., Pupo C. A., Campos A. C., Moss Jr. A. A. Electromyographic activity of the gastrointestinal tract following cholecystectomy. *World J. Surg.*, 14:523-7, 1990.
87. Hocking M. P., Harrison W. D., Sninsky C. A. Gastric dysrhythmias following pylorus-preserving pancreaticoduodenectomy. Possible mechanism for early delayed gastric emptying. *Dig. Dis. Sci.*, 35: 1226-30, 1990.

88. Schaap H. M., Smout A. J., Akkermans L. M. Myoelectrical activity of the Billroth II gastric remnant. *Gut*, 31:984-8, 1990.
89. Geldof H., Van der Schee E. J., Smout A. J. P. M., Van de Merwe J. P., Van Blankenstein M., Grashuis J. L. Myoelectrical activity of the stomach in gastric ulcer patients: An electrogastrographic study. *J. Gastroint. Motil.*, 1:122-30, 1989.
90. Miller L. J., Malagelada J. R., Longstreth G. F., Go V. L. W. Dysfunctions of the stomach with gastric ulceration. *Dig. Dis. Sci.*, 25:857-64, 1980.
91. Malagelada J. R. Gastric, pancreatic and biliary responses to a meal. In: *Physiology of Gastrointestinal Tract*. ed. L. R. Johnson, Raven Press, N. Y., 1981.
92. Pfister C. J., Hamilton J. W., Nagel N., Bass P., Webster J. G., Tompkins W. J. Use of spectral analysis in the detection of frequency differences in the electrogastrograms of normal and diabetic subjects. *IEEE Trans. on BME*, 35:935-41, 1988.
93. Koch K. L., Stern R. M., Stewart W. R., Vasey M. W. Gastric emptying and gastric myoelectrical activity in patients with diabetic gastroparesis: effect of long-term Domperidone treatment. *Am. J. Gastroenterol.*, 84:1069-1075, 1989.
94. Malagelada J. R., Camilleri M., Stanghellini V. *Manometric diagnosis of gastrointestinal motility disorders*. Georg Thieme Verlag, Stuttgart, 1986.
95. Ercolani M., Baldaro B., Trombini G. Effects of two tasks and two levels of difficulty upon surface electrogastrograms. *Percept. Mot. Skills*, 69:99-110, 1989.
96. Hu S., Stern R. M., Koch K. L. Electrical acustimulation relievesvection-induced motion sickness. *Gastroenterol.*, 102:1854-8, 1992.
97. Hu S., Stern R. M., Vasey M. W., Koch K. L. Motion sickness and gastric myoelectric activity as a function of speed of rotation of a circularvection drum. *Aviat. Space Environ. Med.*, 60:411-4, 1989.
98. Robinson P. H. Gastric function in eating disorders. *Ann. N. Y. Acad. Sci.*, 575:456-64, 1989.

99. Sz mukler G. I., Young G. P., Lichtenstein M., Andrews J. T. A serial study of gastric emptying in anorexia nervosa and bulimia. *Aust. N. Z. J. Med.*, 20:220-5, 1990.
100. Hutson W. R., Wald A. Gastric emptying in patients with bulimia nervosa and anorexia nervosa. *Am. J. Gastroenterol.*, 85:41-6, 1990.
101. Robinson P. H. Perceptivity and paraceptivity during measurement of gastric emptying in anorexia and bulimia nervosa. *Br. J. Psychiatry*, 154:400-5, 1989.
102. Dubois A., Gross H. A., Ebert M. H., Castell D. O. Altered gastric emptying and secretion in primary anorexia nervosa. *Gastroenterol.*, 77:319-23, 1979.
103. Cucchiara S., Riezzo G., Minella R., Pezzolla F., Giorgio I., Auricchio S. Electrogastrography in non-ulcer dyspepsia. *Arch. Dis. Child.* 67:613-7, 1992.
104. Cucchiara S., Minella R., Riezzo G., Vallone G., Vallone P., Castellone F. Reversal of gastric electrical dysrhythmias by cisapride in children with functional dyspepsia. *Dig. Dis. Sci.*, 37:11136-40, 1992.
105. Wengrower D., Zaltzman S., Karmeli F., Goldin E. Idiopathic gastroparesis in patients with unexplained nausea and vomiting. *Dig. Dis. Sci.*, 36:1255-8, 1991.
106. Kerlin P. Postprandial antral hypomotility in patients with idiopathic nausea and vomiting. *Gut*, 30:54-9, 1989.
107. Abell T. L., Chung H., Kim M. D., Malagelada M. D. Idiopathic cyclic nausea and vomiting - a disorder of gastrointestinal motility? *Mayo Clin. Proc.*, 63: 1169-75, 1988.
108. Barkakati N. *The Waite Group's TurboC Bible*. SAMS, 1990.
109. Mintchev M. P., Kingma Y. J., K. L. Bowes. Differential surface electrogastrogram - myth or reality? *Gastroenterology (Abstract)*, 103:1399, 1992.
110. Malagelada J. R. Pathophysiological response to meal in the Zollinger-Ellison syndrome. 1. Paradoxical postprandial inhibition of gastric secretion. *Gut*, 19: 284-9, 1978.
111. Geldof H., Van der Schee E. J., Grashuis J. L. Electrogastrographic characteristics of interdigestive migrating complex in humans. *Am. J. Physiol.*, 250:G165-71, 1986.

APPENDIX

